Durham University

Durham E-Theses

Tension stiffening effects in reinforced concrete members

Scott, R. H.

How to cite:

Scott, R. H. (1985) *Tension stiffening effects in reinforced concrete members*, Durham theses, Durham University. Available at Durham E-Theses Online: http://etheses.dur.ac.uk/6803/

Use policy

The full-text may be used and/or reproduced, and given to third parties in any format or medium, without prior permission or charge, for personal research or study, educational, or not-for-profit purposes provided that:

- a full bibliographic reference is made to the original source
- a link is made to the metadata record in Durham E-Theses
- the full-text is not changed in any way

The full-text must not be sold in any format or medium without the formal permission of the copyright holders.

Please consult the full Durham E-Theses policy for further details.

Academic Support Office, The Palatine Centre, Durham University, Stockton Road, Durham, DH1 3LE
e-mail: e-theses.admin@durham.ac.uk Tel: +44 0191 334 6107
http://etheses.dur.ac.uk

TENSION STIFFENING EFFECTS IN REINFORCED CONCRETE MEMBERS

R.H. Scott

BSc(Eng) MSc DIC
CEng MICE MIStructE

A Thesis submitted for the Degree of PhD in the Faculty of Science, University of Durham

July 1985

The copyright of this thesis rests with the author. No quotation from it should be published without his prior written consent and information derived from it should be acknowledged.

28. JAN. 1986

To the

Memory

of my

Father

ABSTRACT

This thesis is in two parts which are related by the common theme of tension stiffening.

Part I develops the concept of a stress-strain envelope to model the behaviour of the concrete in tension below the neutral axis of a reinforced concrete beam. This is substantiated by an analysis of the data from fourteen test beams. The envelope concept is then applied to the calculation of the moment-curvature relationships for these beams, which are also compared with the test results.

Part II presents an experimental investigation of the longitudinal reinforcement strain distributions in reinforced concrete tension members. Test results for fourteen specimens having various cross-sections and reinforcement types are presented, with the reinforcement strains being measured by strain gauging the reinforcement internally. The comprehensive analysis of the test results includes specific design recommendations concerning bond stresses at working loads. Suggestions are made for further work.

ACKNOWLEDGEMENTS

I should like to thank my colleague Dr. P.A.T. Gill for the help, support and experience that contributed to the success of the work described in Part II, in which he was my co-worker. Also, my thanks go to my Supervisor, Professor G.R. Higginson for all his good advice and assistance ever since I joined the Department. I should also like to acknowledge the contributions of other colleagues, in particular Dr. A. Unsworth for many helpful conversations and Mr. D.E. Willis for his assistance with the experimental work.

I am extremely grateful for the technical support given by Mr. W.C. Roscamp and all his colleagues. Not only is their workmanship appreciated, but also their willingness and good humour. In particular I wish to thank Mr. B.P. Scurr for his assistance during all my time in the Department, and Mr. T.D. Harrison for the meticulous quality of his strain gauging work.

The data used in Part I came from beam tests undertaken at the Cement and Concrete Association and my thanks go to Dr. W.B. Cranston for his permission to publish it and to Mr. D.M. Speirs for all his patient help. Also at the C & CA, I thank Dr. A.W. Beeby for his useful comments.

I am pleased to acknowledge the financial support given by the Science and Engineering Research Council for the work described in Part II.

This thesis has been typed by Miss L.A. Graham with much care and patience. However, it would probably never have been written at all without the steadfast and unwavering support of my wife, to whom I owe a particular debt of gratitude.

DECLARATION

No material in this thesis has previously been submitted for a degree in this or any other university.

The work in Part I is my own, while that in Part II was undertaken jointly with my colleague Dr. P.A.T. Gill. The regulations of the university accordingly require me to define my involvement in the Part II work.

I initiated the work and was then joined by Dr. Gill for its subsequent development. Testing was performed jointly as was a part of the data collation. Analysis of the results and the development of the design recommendations were my own work. I also wrote all the computer software.

STATEMENT OF COPYRIGHT

The copyright of this thesis rests with the author. No quotations from it should be published without his prior written consent and information derived from it should be acknowledged.

CONTENTS

LIST OF FIGURES

Page

NOTATION

B - Beam
T - Tension Specimen

A_s	Area of tension reinforcement (B&T)
A'_s	Area of compression reinforcement (B)
$a_1 \ldots a_n$	Points on stress-strain envelope (B)
B	Bond influence length (T)
b	Breadth of section (B)
C	Cover (T)
d	Effective depth (B)
d'	Cover to centre of compression reinforcement (B)
E	Young's modulus (B)
E_c	Young's modulus for concrete in compression (B)
E_{ct}	Young's modulus for concrete in tension (B)
E_s	Young's modulus for steel (B&T)
E'_s	Modified Young's modulus for steel (B)
E_1	Young's modulus for concrete at first major crack (B)
E_2	Young's modulus for concrete at last major crack (B)
$(EA)_{cr}$	Stiffness of cracked section (T)
$(EA)_u$	Stiffness of uncracked section (T)
EI	Flexural stiffness (B)
$(EI)_{cr}$	Flexural stiffness of cracked section (B)

$(EI)_u$	Flexural stiffness in uncracked section (B)
e	Raw strain value (T)
e_{bf}	Bottom face strain (B)
e_c	Concrete compressive strain at top face at cracked section (B)
e_{cc}	Concrete compressive strain at top face (B)
e_{cm}	Mean concrete compressive strain at top face (B)
e_{ct}	Eccentricity of F_{ct} relative to neutral axis (B)
e_f	Reinforcement strain at first effective crack (T)
e_l	Reinforcement strain at last crack (T)
e_{penult}	Reinforcement strain at penultimate crack (T)
e_s	Strain in tension reinforcement assuming no tension stiffening (B)
e_{sc}	Strain in compression reinforcement (B)
e_{sm}	Mean strain in tension reinforcement (B)
e_{st}	Strain in tension reinforcement (B)
e_t	Concrete ultimate tensile strain (B)
e_{t1}	Bottom face strain when first major crack forms (B)
e_{t2}	Bottom face strain when last major crack forms (B)
e_x	Raw strain value to left of e(T)
e_y	Raw strain value to right of e(T)
e_1	Recalculated strain value (T)
δ_e	Change in strain (T)
F_{cc}	Force in concrete in compression (B)

F_{ct}	Force in concrete in tension (B)
F_{sc}	Force in compression reinforcement (B)
F_{st}	Force in tension reinforcement (B)
F_1	Factor (B)
F_2	Factor (B)
f_b	Bond stress (T)
f_{bf}	Bottom face stress (B)
f_{bi}	Initial bond stress when crack forms (T)
f_c	Concrete ultimate compressive strength (B)
f'_c	Concrete cylinder strength (B)
f_{cc}	Top face concrete stress (B)
f_r	Modulus of rupture of concrete (B)
f_s	Steel stress assuming no tension stiffening (B)
f_{sc}	Stress in compression reinforcement (B)
f_{scr}	Value of f_s at the appearance of the first flexural crack (B)
f_{st}	Stress in tension reinforcement (B&T)
f_{sti}	Initial stress in tension reinforcement when crack forms (T)
f_t	Concrete indirect cylinder strength (B&T)
f_{t1}	Bottom face concrete stress at which first major crack forms (B)
f_{t2}	Bottom face concrete stress at which last major crack forms (B)
f_y	Steel yield stress (B)
δF	Error in force calculation (B)
h	Overall depth (B)

h_{rt}	Parameter in rectangular-triangular stress block (B)
I	Second moment of area (B)
I_{cr}	Second moment of area of cracked section (B)
I_{eff}	Effective second moment of area (B)
I_g	Second moment of area of gross concrete section (B)
I_u	Second moment of area of uncracked section (B)
I_1	Second moment of area at first major crack (B)
I_2	Second moment of area at last major crack (B)
K	Loading arrangement constant (B)
k	Deflection equation constant (B)
L	Span (B)
M	Bending moment (B)
M'	Modified bending moment (B)
M_{cc}	Moment of F_{cc} about neutral axis (B)
M_{cr}	Cracking moment (B)
M_{ct}	Moment of F_{ct} about neutral axis (B)
M_{sc}	Moment of F_{sc}, about neutral axis (B)
$M_{s\ell}$	Service load bending moment (B)
M_{st}	Moment of F_{st} about neutral axis (B)
M_1	Bending moment at first major crack (B)
M_2	Bending moment at last major crack (B)
m	Power in Branson's method (B)

δM	Error in bending moment calculation (B)
n_{av}	Average neutral axis factor (B)
P_f	Load to cause effective first crack (T)
R	Radius of curvature (B)
δT	Change in tensile force (T)
u	Rod perimeter (T)
W	Total load on span (B)
x	Neutral axis depth (B)
x_b	Distance from neutral axis to bottom face (B)
x_d	Distance from neutral axis to centre of tesion reinforcement (B)
δx	Small distance along tension reinforcement (T)
y_1	Distance from neutral axis to bottom face at first major crack (B)
y_2	Distance from neutral axis to bottom face at last major crack (B)
z	Lever arm (B)
β	Factor representing the efficiency of concrete in resisting tension (B)
δ	Deflection (B)
δ_1	CEB deflection at first crack (B)
δ_2	CEB deflection after cracking (B)
δ_3	CEB deflection (B)

θ	Rod diameter (T)
ϕ	Curvature (B)
ϕ_{eff}	Effective curvature (B)
ψ	Modifying factor

1. INTRODUCTION

The author joined the Department of Engineering at the University of Durham in October 1978 after spending eight years with a Consultant (Oscar Faber & Partners) and two years with a Local Authority (London Borough of Brent). During this time he was closely involved with the design of a large number of reinforced concrete structures ranging from schools and office buildings through to large industrial complexes such as cement works.

Throughout this period, a recurring problem was that of accurately predicting the deflections of reinforced concrete beams. This was made difficult by the complex post-cracking interaction between the concrete and the reinforcement in the tensile zone below the neutral axis. On coming to Durham this problem was studied further and the importance of tension stiffening, the contribution of the tensile concrete to the stiffness of a reinforced concrete member, was soon recognised. From this study, two substantial areas of investigation emerged which are reported in the two parts of this thesis.

Part I presents a procedure for the calculation of the moment-curvature relationship for reinforced concrete beams. The main feature of the procedure is the model it uses for the behaviour of the concrete in tension. This is substantiated by a comprehensive analysis of existing test data.

In contrast, Part II presents an experimental investigation of the longitudinal reinforcement strains in reinforced concrete tension members using an internal strain gauging technique to measure the reinforcement strains. The need for this work arose as a result of problems encountered during the moment-curvature investigation. It has proved to be a particularly fruitful area of research.

Part I

THE SHORT-TERM MOMENT-CURVATURE RELATIONSHIP FOR REINFORCED CONCRETE BEAMS

2. BACKGROUND

The Simple Theory of Bending dictates that for a beam formed of a homogeneous, isotropic, material, the bending moment, M, and curvature ϕ at any section along its length are related by the expression

$$M = EI\,\phi \qquad (2.1)$$

where E = Young's modulus of the beam material

I = Second moment of area of the beam section.

Also, by definition

$$\phi = \frac{1}{R} \qquad (2.2)$$

where R = radius of curvature at the section being considered.

The product EI is commonly referred to as the flexural stiffness of the beam section, or when the discussion centres solely on bending, simply "the stiffness".

The deflection δ at a point along a beam of span L may be expresed in the form

$$\delta = \frac{kWL^3}{EI} \qquad (2.3)$$

where K =a constant dependent on the type of loading and end restraint.

W = total load on span

This indicates that a prerequisite in deflection calculations is an accurate assessment of member stiffness (EI). This is straightforward when considering beams which comply with the Simple Theory. However, reinforced concrete beams are behaviourly much more complicated due to the complex material properties of the concrete itself and the indeterminate nature of the bond characteristic at the concrete/reinforcement interface. One of the major influences on the stiffness of a reinforced concrete beam is the behaviour of the concrete in the tension zone below the neutral axis. Concrete cracks at relatively low tensile stresses and typically a crack pattern similar to that shown in Fig.2.1 is formed. The strain in the tension reinforcement peaks where it crosses a crack, and declines away from the crack as load is shared with the surrounding concrete due to the action of bond.

As a result, the stiffness of the beam varies along its length even in a zone of constant bending moment. It is a minimum at the crack positions, whilst between the cracks it increases due to the contribution of the concrete in tension. This contribution of the tensile concrete to the stiffness of a reinforced concrete member is the well-known phenomenon called Tension Stiffening.

A corollary of the above is that the requirement of the Simple Theory of Bending that plane sections should remain plane does not hold locally for a reinforced concrete beam. But a reasonably linear strain distribution over the

depth of the section is obtained provided that the strains are measured over gauge lengths large enough to even out the effects of cracking. It has thus become usual to apply equation (2.1) to a reinforced concrete beam when large gauge lengths are being considered. However the stiffness term (EI) now varies along the span.

This approach yields the typical short-term moment-curvature relationship shown in Fig. 2.2. As a comparison, the hypothetical curve obtained by ignoring completely the contribution of the tensile concrete has also been shown.

The difference between these two curves is due to the effects of tension stiffening and it increases as the amount of tensile reinforcement is reduced. Accurate deflection calculations require that beam stiffnesses be obtained from the experimental curve and consequently considerable research effort has been directed to the problem of representing it mathematically. Typically this involves developing an expression for EI which incorporates tension stiffening.

Part I of this Thesis is concerned with the development of a new mathematical model for the moment-curvature relationship for rectangular, reinforced concrete beams. It is restricted to short-term loadings and retains the concept of average, linear, strain distributions introduced above. The method is extremely flexible and is very suitable for programming on a small computer.

A literature survey now follows to establish a basis for the work to be described.

3. PREVIOUS WORK

3.1 Introduction

This section presents a historical survey of the literature pertaining to the mathematical modelling of the moment-curvature relationship for rectangular reinforced concrete beams. In many ways this amounts to a survey of the different procedures advanced for the calculation of flexural stiffness, since this is the crucial parameter in the problem. However, the treatments are not all confined to this approach and their diversity reflects the range of thinking and attitudes which the topic has attracted.

It would be unwise to claim that this review is exhaustive, particularly as the treatment is largely confined to English language publications. However, it is extensive, nevertheless, and the author considers that it does represent a fair and balanced picture of what has been achieved in this field.

3.2 The Modelling Procedures

3.2.1 The Simple Rectangular Section

This must have been the earliest method used to calculate the stiffness of a reinforced concrete beam section. The second moment of area, I is calculated using the well-known expression for a simple rectangle

$$I = \frac{bh^3}{12} \qquad (3.1)$$

where b is the breadth of the section and h the overall depth. I is then multiplied by the Young's modulus for the concrete (E_c) to obtain the flexural stiffness of the section.

Equation (3.1) considers only the geometrical properties of the section and ignores completely the contribution of the reinforcement. The concrete is assumed to have the same properties in tension as in compression, and no allowance is made for the effects of cracking.

This is obviously too simplistic an approach to have remained in general use. Even so, a refinement of it, to be described next, still has a place in modern practice.

3.2.2 The Uncracked Section

This approach develops the previous procedure by replacing the areas of the tensile and compressive reinforcement with their respective equivalent concrete areas (Fig. 3.1) to produce what is known as the uncracked, transformed section. It is treated in all the standard texts (e.g. (1)) to yield

$$I_u = \frac{bh^3}{12} + bh\left(x - \frac{h}{2}\right)^2 + \frac{E_s}{E_c}A_s'\,(x - d')^2 + \frac{E_s}{E_c}A_s\,(d - x)^2 \qquad (3.2)$$

where

I_u = Second moment of area of the uncracked section.

b = Section breadth

h = Overall section depth

x = Neutral axis depth

E_s = Young's modulus for steel (tension and compression)

E_c = Young's modulus for concrete in compression

A'_s = Area of compression reinforcement

d' = Cover to centre of compression reinforcement

A_s = Area of tension reinforcement

d = Effective depth

The neutral axis depth (x) may be calculated from the expression

$$A_c \left(x - \frac{h}{2}\right) + \frac{E_s}{E_c} A'_s (x - d') = \frac{E_s}{E_c} A_s (d - x) \qquad (3.3)$$

The flexural stiffness is given by the product $E_c I_u$.

This method is accurate only over the small region of the moment-curvature relationship before the onset of cracking, but it still provides the best model for this early part of the moment-curvature relationship.

3.2.3 <u>The Cracked Section</u>

This is a well known procedure whose origins go back to at least 1914 (2). It assumes that the concrete is cracked up to the neutral axis and that no tensile stresses

exist in the concrete below it. This is considered to be the case everywhere along the beam.

The areas of the tensile and compressive reinforcement are replaced by their respective equivalent concrete areas to form the cracked, transformed section (Fig. 3.2). Again, it is dealt with in all the standard texts (eg (1)) and gives

$$\frac{I_{cr}}{bd^3} = \frac{1}{3}\left[\frac{x}{d}\right]^3 + \frac{E_s}{E_c}\frac{A_s}{bd}\left\{1 - \frac{x}{d}\right\}^2 + \frac{E_s}{E_c}\frac{A'_s}{bd}\left\{\frac{x}{d} - \frac{d'}{d}\right\}^2 \qquad (3.4)$$

where I_{cr} is the second moment of area of the cracked section.

x is calculated from the expression

$$\frac{x}{d} = -\frac{E_s}{E_c}\left\{\frac{A_s}{bd} + \frac{A'_s}{bd}\right\} + \left[\left\{\frac{E_s}{E_c}\left(\frac{A_s}{bd} + \frac{A'_s}{bd}\right)\right\}^2 + \frac{2E_s}{E_c}\left(\frac{A_s}{bd} + \frac{A'_s\, d'}{bd^2}\right)\right]^{1/2} \qquad (3.5)$$

This time, flexural stiffness = $E_c I_{cr}$

This approach yields the "no-tension" moment-curvature relationship shown in Fig. 2.2. It gives a poor model for the experimental curve since tension stiffening effects are ignored completely. Equations (3.4) and (3.5) are based on an elastic analysis and are thus not applicable once the tension reinforcement yields.

Present use of the cracked section is largely confined to the estimation of relative stiffnesses in strength calculations (for example when designing continuous beams or structural frames). For deflection calculations under working loads it can lead to errors in the order of 100%. (Section 3.3).

Ignoring tension stiffening completely makes the resulting moment-curvature relationship for the cracked section a lower bound for the other methods to be discussed. This provides a useful datum when making comparisons, as will be seen later.

3.2.4 Swain : 1924

Swain (3) developed an alternative expression to equation (3.4) for calculating the flexural stiffness of the fully cracked section, $(EI)_{cr}$

Referring to Fig. 3.3:

$$\phi = \frac{e_s}{(d-x)} = \frac{M}{(EI)_{cr}} \qquad (3.6)$$

when e_s is the strain in the tension reinforment assumming no tension stiffening

Substituting $M = f_s A_s z$

and $e_s = \frac{f_s}{E_s}$

gives

$$(EI)_{cr} = E_s A_s (d - x) z \qquad (3.7)$$

where

f_s = tensile reinforcement stress corresponding to e_s

z = lever arm

x and z have to be calculated using an elastic analysis.

Although pronounced as being useful by ACI Committee 435 in 1966 (4) this method does not appear to have found general favour. However, like the work of Murashev (see below) it is frequently referred to in the American literature.

3.2.5 Murashev : 1940

Murashev's method (5)* is an interesting early use of an approach which will recur later. This is to use the properties of the cracked, transformed section as a basis, but then to enhance one or more of its parameters, usually empirically, in order to allow for tension stiffening effects. In Murashev's case, the second moment of area is based directly on the cracked, transformed section, and it is the steel modulus (E_s) which is modified by a factor Ψ to give:-

$$E'_s = \frac{E_s}{\Psi} \text{ where } \Psi \leqslant 1.0 \qquad (3.8)$$

---

* In Russian. Reported in English by ACI Committee 435 (4).

$$\text{and } \Psi = 1 - \frac{2}{3}\left\{\frac{M_{cr}}{M_{s\ell}}\right\}^2 \qquad (3.9)$$

where

E'_s = Modified Young's modulus for steel

M_{cr} = Cracking moment

$M_{s\ell}$ = Service load bending moment

It was suggested that

$$M_{cr} = \frac{f_r I}{(h/2)} \qquad (3.10)$$

where f_r is the modulus of rupture of the concrete and I and h refer to the gross concrete section (neglecting steel reinforcement).

This approach is interesting historically, but does not appear to have been widely used, at least in the West.

3.2.6 Yu and Winter : 1960

Yu and Winter (6) proposed two methods for calculating the stiffness of a reinforced concrete beam.

Method A : Use the cracked, transformed section at mid-span (I_{cr}).

Method B : To allow for tension stiffening, apply a correction factor to give I_{eff} where

$$I_{eff} = I_{cr} \Big/ \left\{1 - \frac{bM'}{M_{s\ell}}\right\} \qquad (3.11)$$

M' is defined as:

$$M' = 0.1\,(f_c)^{2/3}\, h(h-x) \qquad (3.12)$$

where f_c is the ultimate compressive strength of the concrete.

The derivation of equations (3.11) & (3.12) follows an elastic theory approach and includes an allowance for the contributory effect of the tensile concrete based on a triangular stress distribution. The factor of 0.1 in equation (3.12) was determined empirically. Comparisons with test data indicated that Method B provided better results than Method A. This has proved to be an influential approach which is referred to frequently in the literature.

3.2.7 ACI Code : 1963

The 1963 ACI code (7) recommendations regarding stiffness were as follows:-

(i) For $\frac{A_s f_y}{bd} \leq 500$ the second moment of area should be based on the gross section.

(ii) For $\frac{A_s f_y}{bd} > 500$ the second moment of area should be based on the cracked, transformed section.

The expression $A_s f_y/bd$ has to be calculated in Imperial units, where f_y is the yield stress of the steel.

This approach recognises the strong influence that the amount of tensile reinforcement has on the stiffness of a reinforced concrete beam. However, its method of dealing with it is rather too straightforward.

3.2.8 Branson : 1963

Branson (8) sought an expression for the effective second moment of area (I_{eff}) at any particular cross-section of a reinforced concrete beam which would satisfy the following boundary conditions:-

1. When $M = M_{cr}$ then $I_{eff} = I_u$.
2. When $M >> M_{cr}$ then $I_{eff} \rightarrow I_{cr}$.

He accordingly proposed that

$$I_{eff} = I_u - [I_u - I_{cr}] \left(1 - \left[\frac{M_{cr}}{M}\right]^m\right) \qquad (3.13)$$

where m was an unknown power.

Replacing I_u with I_g, the second moment of area of the gross concrete section neglecting the effect of reinforcement, and re-arranging yielded

$$I_{eff} = \left[\left\{\frac{M_{cr}}{M}\right\}^m\right] I_g + \left[1 - \left\{\frac{M_{cr}}{M}\right\}^m\right] I_{cr} \qquad (3.14)$$

The power m was determined numerically from a sizeable number of test results that included both rectangular beams (simply supported and continuous) and T-beams (simply supported). Branson recommended m = 3 if an average value of I_{eff} was required over the entire length of a uniformly loaded simply supported beam, and m = 4 if I_{eff} was required at a particular section.

This has proved to be an important method and it is the approach adopted by the current (1977 83) ACI Code (9). It

is only applicable however for $M \geq M_{cr}$. If $M < M_{cr}$, then $I_{eff} = I_g$.

3.2.9 CEB : 1964

The CEB (Comité Europeen du Béton) surprisingly does not give specific recommendations regarding the calculation of flexural stiffnesses in its 1978 Model Code for Concrete Structures (10). However, some interesting points arise from its earlier comments regarding the calculation of deflections (11).

In 1964 the CEB recommended that the deflections of reinforced concrete beams should be computed in two parts (see Fig. 3.4): δ_1, the deflection attained at the time the first crack appears and δ_2, the deflection after cracking. A further quantity δ_3 is also calculated and the actual deflection of the beam is taken as the lesser of $(\delta_1 + \delta_2)$ or δ_3 where

$$\delta_1 = \frac{KL^2 M_{cr}}{E_c I_g} \qquad (3.15)$$

$$\delta_2 = \frac{KL^2 (M - M_{cr})}{0.75\, E_s A_s d^2 \left[1 - \frac{2A_s f_y}{bdf'_c}\right]\left[1 - \frac{2}{3}\frac{A_s}{bd}\frac{f_y}{f'_c}\right]} \qquad (3.16)$$

$$\delta_3 = \frac{KL^2 M}{E_s A_s d^2 \left[1 - \frac{2A_s f_y}{bdf'_c}\right]\left[1 - \frac{2}{3}\frac{A_s}{bd}\frac{f_y}{f'_c}\right]} \qquad (3.17)$$

where

f_y = yield stress of steel

f'_c = concrete cylinder strength

K = constant dependent on loading arrangement

δ_3 is effectively the deflection obtained if no tension stiffening is assumed and Beeby has pointed out (12) that the term

$$0.75 E_s A_s d^2 \left[1 - \frac{2A_s f_y}{bdf'_c}\right]\left[1 - \frac{2}{3}\frac{A_s}{bd}\frac{f_y}{f'_c}\right] \qquad (3.18)$$

in the expression for δ_2 is the gradient of the post cracking region of the moment-curvature relationship.

3.2.10 CP110 : 1972

CP110, the British Standard Code of Practice for the Structural Use of Concrete (13) prescribes two sets of assumptions for use when calculating beam curvatures (Clause A.2.2) which also influence the stiffness of the section. These can be summarised as follows:-

(1) Up to the onset of cracking the stiffness associated with the uncracked transformed section is to be used.

(2) After cracking, the stiffness is to be calculated by assuming that the stress distribution in the concrete in tension is triangular, having a value of zero at the neutral axis and a value at the centroid of the tension steel of 1 N/mm^2 (for short-term

loadings). The reinforcement, whether in tension or compression is to be assumed to be elastic, as is the concrete in compression.

This latter set of assumptions gives the stress and strain distributions shown in Fig.3.5 and yields the following expression for the effective second moment of area (14)

$$\frac{I_{eff}}{bd^3} = \frac{1}{3}\left[\frac{x}{d}\right]^3 + \frac{E_s}{E_c}\frac{A_s}{bd}\left[1 - \frac{x}{d}\right]^2$$

$$+ \frac{E_s}{E_c}\frac{A'_s}{bd}\left[\frac{x}{d} - \frac{d'}{d}\right]^2 + \frac{1}{3}\frac{E_{ct}}{E_c}\left[\frac{h}{d} - \frac{x}{d}\right]^3 \qquad (3.19)$$

where E_{ct} is the Young's modulus for the concrete in tension.

Use of equation (3.19) requires the calculation of x, the neutral axis depth. A rigorous approach to this would yield an immensely elaborate expression. Consequently the approximation of using the neutral axis depth for the cracked section has been recommended by Kong and Evans (1).

The terms Partially Cracked Section and Pseudo Cracked Section have been used by Kong and Evans (1) and Hughes (14) respectively to describe this approach.

3.2.11 Rao and Subrahmanyam : 1973

A research committee convened by the Institution of Civil Engineers to advise on the ultimate load design of reinforced concrete structures reported in 1962 (15) that the moment-curvature relationship for a reinforced concrete beam passes through three phases: an uncracked phase, then a cracked phase and finally an inelastic phase. They initially gave a tri-linear form to the moment-curvature relationship but then went on to suggest that a bi-linear approximation was acceptable, at least for strength calculations (Fig. 3.6).

Rao and Subrahmanyam (16) proposed a development of the tri-linear approach in which the segments need not be straight. This they called the Tri-Segmental Moment-Curvature Relationship and described it as follows:-

Stage I: Before cracking the moment-curvature relationship is calculated using the properties of the uncracked section based on elastic theory.

Stage II: After cracking effective curvatures are calculated using the expression

$$\phi_{eff} = \frac{e_{cm} + e_{sm}}{d} \qquad (3.20)$$

where

ϕ_{eff} = effective curvature

e_{cm} = mean concrete compressive strain in the top fibre

e_{sm} = mean strain in the tensile reinforcement.

Stage III: After yield of the tensile reinforcement

$$\phi_{eff} = \frac{e_c + e_s}{d} \qquad (3.21)$$

where

e_c = top fibre concrete strain at a cracked section

e_s = steel strain at a crack.

In Stage II, e_{cm} is calculated assuming the section to be fully cracked. e_{sm} will be smaller than e_s, the reinforcement strain at a cracked section so Rao and Subrahmanyam recommended that

$$e_{sm} = e_s - 0.18 \left[\frac{f_{scr}}{f_s}\right] \frac{f_r}{E_s} \frac{bd}{A_s} \qquad (3.22)$$

where

f_s = stress in steel at a cracked section

f_{scr} = value of f_s at the appearance of the first flexural crack.

This expression allows for an effective concrete area in tension. The constant 0.18 was obtained empirically from test results.

In Stage III it is assumed that the difference between e_s and e_{sm} is negligible.

Once the curvature appropriate to a particular applied moment has been determined, then the stiffness of the section follows directly.

3.2.12 Tsimbikakis : 1975

As with other methods, Tsimbikakis (17) has proposed that the stiffness of the uncracked section be used up to the onset of cracking. Beyond this point effective curvatures, allowing for tension stiffening are calculated using the expression

$$\phi_{eff} = \frac{f_s}{\beta E_s (1-n_{av})d} \qquad (3.23)$$

where

β = factor expressing the efficiency of the concrete in resisting tension

n_{av} = average neutral axis factor.

Elastic theory is used to derive equation(3.23) and graphs are provided in reference (17) for the determination of β and n_{av}.

3.3 Discussion

It is interesting to observe how attitudes have changed towards the calculation of beam stiffnesses. For instance, the two extremes of the uncracked and cracked EI have both found favour at different times. In 1947 the Portland Cement Association in a widely followed bulletin (18) recommended the use of the uncracked EI and suggested that the effects of the steel should be ignored completely.

This, in effect, recommended the use of the simple rectangular section to calculate stiffness. It was satisfactory in the context of the fairly deep, lightly reinforced and hence not too severely cracked sections which often prevailed at the time. However as beams became shallower and steel strengths increased, higher working stresses and greater cracking were experienced with the result that deflections were considerably underestimated.

The other extreme of the cracked section was being recommended as far back as 1931 by Myrlea (19) acting in the capacity of chairman of ACI Committee 307. This was later incorporated into the 1963 ACI Code (7) in an attempt to guard against underestimating the deflections of shallow beams.

The cracked section always overestimates deflections as it ignores tension stiffening completely. The degree of error depends on the steel percentage and increases as the steel percentage decreases. Beeby (12) has reported that with beams having 0.75% tension reinforcement, the error in the calculated deflections at working loads will be in the order of 100%.

All the other approaches outlined in the foregoing review recognise that the real post-cracking behaviour of a reinforced concrete beam lies between the two extremes of the cracked and uncracked sections and attempt to model it accordingly. With the exception of CP110, they adopt approaches which are basically empirical but share a common

desire to incorporate the influence of tension stiffening.

Their underlying principles are generally sound but the CEB method is open to criticism because of its use of the steel yield stress and concrete compressive strength as two of its parameters. As Beeby has noted (12) the former is inappropriate, since in general, deflections are calculated for load levels which are well below the value which would cause the steel to yield, while the latter causes the effect of concrete strength on the section properties to be grossly overestimated since a change in cube strength has a comparatively small effect on member stiffness.

The 1966 report of ACI Committee 435 (4) included a review of the then current methods for calculating deflections and deemed the methods of Yu and Winter (6), the 1963 ACI Code (7) and Branson (8) to be the most satisfactory. Of these it was considered that the methods of Yu and Winter and Branson were somewhat more accurate. Branson's method is rather the more cumbersome to use of the two, but nevertheless this is the one that was adopted in the 1977 ACI Code (9).

The CP110 approach (13) is interesting because of the way in which it deals with the problem at source, by suggesting how the behaviour of the tensile concrete should be modelled rather than by presenting a formula for the direct calculation of stiffness or deflection. This recognition that the calculation of member stiffness is

directly dependent upon the properties of the constituent materials is obviously appealing but it does lead to some complexity in the ensuing calculations. The origin of the value of $1N/mm^2$ used in defining the stress distribution in the tensile concrete is obscure.

Rao and Subrahmanyam (16) present the most sophisticated empirical approach that has appeared to date due to their use of a tri-segmental approximation. Either because of, or in spite of this, it does not appear to have been widely adopted.

A comparison of the moment-curvature relationships generated by the more significant methods discussed appears in Fig.3.7. The experimental curve shown is for a beam having 0.44% tension reinforcement tested at the Cement and Concrete Association and described in reference (20). A low percentage beam was selected because it would exhibit a high degree of tension stiffening and thus aid the clarity of the diagram. However, the comments to be made are quite general.

The inappropriateness of using the uncracked, transformed section to model anything but the pre-cracking behaviour of the beam is obvious, and the lower bound which the cracked, transformed section constitutes is also well illustrated. The "tension at crack only" curve illustrates the theoretical effect obtained by including the small

contribution of the tensile concrete at the cracked section. It is of little practical use and is only included out of interest.

The only approach which applies over the full range of the moment-curvature relationship, including that part where the tensile reinforcement has yielded, is that of Rao and Subrahmanyam. The remaining approaches are applicable over the elastic range only. Rao and Subrahmanyam's method underestimates the effect of tension stiffening quite markedly. The others produce substantially similar curves which are approximately parallel to that for the cracked, transformed section. Consequently they too generally underestimate the tension stiffening effect, but meet the experimental curve approximately when the onset of yield occurs in the tensile reinforcement.

None of these methods represents the true form of the experimental moment-curvature relationship because their empirical nature is too inflexible to deal with the changing form of the experimental curve. How to resolve this problem is the challenge that will now be considered.

4. ANALYSIS OF A REINFORCED CONCRETE BEAM SECTION

4.1 Introduction

A prerequisite in any investigation of the moment-curvature relationship for R.C. beams is the ability to analyse a beam section quickly and accurately. It soon became apparent that this would be best achieved by a purpose-written computer program.

A program was written for rectangular sections, dealing with both the uncracked and cracked sections and including provision for the effects of compression reinforcement. It assumed a linear strain distribution across the section and allowed non-linear stress-strain relationships to be used for the concrete (in compression) and the reinforcement (in tension and compression). Concrete in tension could be ignored completely, but if included the stress-strain relationship was assumed to be linear as it was anticipated that the data would never be sufficiently accurate to require a non-linear approach. This has indeed been the case. (A later variant of the program, which did permit a non-linear relationship for the tensile concrete, received very little use.)

The program proved to be very effective and useful. It will now be described in some detail since it became an important tool in the work to be described later.

4.2 Program Input

The following data was input to the program.

1. The section geometry and reinforcement areas.
2. The stress-strain data for the concrete and reinforcement. The continuous curves were linearized as shown in Fig. 4.1. This was found to be a convenient way of dealing with experimental data which would not normally be amenable to a continuous single curve mathematical representation. Up to fifty data points were permitted.
3. A list of the required solution parameters. The program would analyse the section subject to any one of the following being specified: applied bending moment, top (compressive) face strain, bottom (tensile) face strain, or strain in the tensile reinforcement. Any number of parameters could be specified in any order during a single run of the program.

4.3 Program Output

The program first listed the stress-strain data and geometrical properties of the section and then output the following data for each solution parameter:-

Strains: Top face of concrete (e_{cc})

Reinforcement in compression (e_{sc})

Reinforcement in tension (e_{st})

Bottom face of concrete (e_{bf})

Stresses: Top face of concrete (f_{cc})

Reinforcement in compression (f_{sc})

Reinforcement in tension (f_{st})

Bottom face of concrete (f_{bf}) (Zero if concrete in tension was being ignored)

Neutral Axis Depth (x)

Depth in tension below the neutral axis (Zero if concrete in tension was being ignored).

Lever arm (z)

Applied Bending Moment

Curvature

Flexural Stiffness (EI)

Forces: Concrete in compression (F_{cc})

Reinforcement in compression (F_{sc})

Concrete in tension (F_{ct})

(Zero if concrete in tension was being ignored).

Reinforcement in tension (F_{st})

Check-sum of all the forces (should be zero)

Moments of the above forces about the neutral axis (M_{cc}, M_{sc}, M_{ct}, M_{st} respectively)

Eccentricity of F_{cc} relative to neutral axis

Eccentricity of F_{ct} relative to neutral axis.

The program nomenclature is summarized in Fig. 4.2 (f_t and e_t are respectively the ultimate stress and strain for the tensile concrete).

4.4 Program Details

The problem reduced to that of finding a strain distribution across the section which satisfied two conditions:

1. The forces acting on the section must be in equilibrium.

$$F_{cc} + F_{sc} = F_{st} + F_{ct} \qquad (4.1)$$

2. The specified value of the solution parameter must be achieved.

A double iteration procedure was devised which is illustrated in Fig. 4.3.

An initial value of e_{st} was selected and e_{cc} then adjusted until a force balance was achieved (equation 4.1.), with F_{cc} being calculated by numerical integration of the stress distribution for the concrete in compression. In practice an exact balance was not sought as this could lead to numerical instability resulting from the very fine adjustments that had to be made to e_{cc}. Instead a quantity δF was calculated which expressed the percentage difference between the tensile and compressive forces

$$\delta F = \frac{(F_{st} + F_{ct} - F_{cc} - F_{sc}) \times 100}{(F_{st} + F_{ct})} \qquad (4.2)$$

Accepting any value of δF within the range ± 0.001 (i.e. achieving a force balance of $\pm 1/1000$ of 1% or better) achieved a good compromise between accuracy, stability and computation time. When δF was outside this range then the sign of δF indicated if an upward or downward adjustment of e_{cc} was required.

The magnitude of e_{bf} determined whether the section was cracked or uncracked for the particular strain distribution being considered. In the latter situation all the concrete below the neutral axis could, if desired, be included in the force calculation while in the former case the tensile concrete was either ignored completely (the usual situation) or, at the discretion of the user, the rather artificial and in practice rarely used process of including for a small triangular area of tensile concrete was undertaken (Fig. 4.2).

Adjustments were made to both F_{cc} and F_{ct} to compensate for the concrete areas occupied by the compressive and tensile reinforcement respectively.

Having obtained a force balance, the program then calculated the value this gave to the solution parameter (M, e_{cc}, e_{bf} or e_{st}) and expressed this once more as a percentage difference. For example, when solving for an applied moment, the quantity

$$\delta M = \frac{(M_{calculated} - M_{prescribed})}{M_{prescribed}} \times 100 \qquad (4.3)$$

would be calculated.

Again for reasons of numerical stability an acceptable range of ±0.001 was allowed for this difference. In general the value would be outside this range requiring that e_{st} be adjusted and the whole force balance procedure repeated to yield an improved value of the solution parameter.

This double iteration procedure continued until a solution within the prescribed limits was obtained whereupon a full set of data was output. Typically around 20 adjustments to e_{st} were made, each requiring about 20 adjustments to e_{cc}.

4.5 Example

Suppose the beam section shown in Fig. 4.4 is to be analysed for an applied bending moment of 20.0 kNm. The stress-strain relationships to be used are also shown in Fig. 4.4, already linearised.

The program first tries e_{st} = 100 microstrain and after 29 iterations achieves a force balance when e_{cc} = 49.65 microstrain with an error of +0.0001%. This yields δM = -68.28% indicating that the calculated moment is too small. Next e_{st} = 200 microstrain is tried which gives δM = -36.55%, then e_{st} = 300 microstrain which gives δM = -4.89%, and then e_{st} = 400 microstrain which gives δM = +26.57%. (e_{cc} is now 201.03 microstrain).

e_{st} has now been established to be in the range 300 < e_{st} < 400 microstrain. e_{st} = 350 microstrain is found to be too large as is the following attempt of e_{st} = 325 microstrain.

Next follow e_{st} = 312.50 microstrain (too small) 318.75 microstrain (too large) 314.06 microstrain (too small), and 314.84 microstrain (again too small). δM has now been reduced to -0.21% for this last case.

This iteration procedure continues until, after a total of 17 attempts, a solution within the specified tolerance is at last obtained when e_{st} = 315.51 microstrain. e_{cc} is now 157.23 microstrain and δM = - 0.0007%. The actual value of the calculated bending moment is 19.99986000 kNm which is very close to the 20.0 kNm specified.

The full output for this example is shown in Fig. 4.5 as item 1. As further examples the results for e_{st} being specified as 1000 microstrain (item 2) and e_{cc} being specified as 800 microstrain (item 3) are also shown.

Details of this program and its developments are to be published (21).

5. A MODEL FOR THE BEHAVIOUR OF THE CONCRETE IN TENSION

5.1 Introduction

We come now to our main concern of how to develop an improved mathematical model for the moment-curvature relationship for reinforced concrete beams within the context of averaged strain distributions already introduced.

The behaviour of a reinforced concrete beam stems from the behaviour of its constituent materials, steel and concrete. The modelling of a beam's behaviour requires an interpretation of the behaviour of these materials within the context of averaged strains.

In the compression zone it has been the custom to assume, not unreasonably, that there is little variation between the strain distributions at any cross-section in a zone of constant bending moment (Rao and Subrahmanyam (16)). No special averaging technique is thus required to determine what are already effectively the average strains. A more complicated situation exists in the tension zone however due to the effects of cracking. Strains in the tension reinforcement are at a maximum at the cracks and at a minimum approximately midway between the cracks with their average values lying somewhere between these two extremes.

With the tensile concrete, the problem has two aspects. Firstly, very little is actually proven about how the strain distributions in the tensile concrete vary from section to section between the major cracks. Secondly,

tensile stresses exist in the concrete even when the reinforcement strains are considerably above the commonly held value for concrete tensile failure of around 100 microstrain. This must be so since tension stiffening effects are still present, albeit much reduced, even when the tension reinforcement yields.

The key to the moment-curvature problem is to find a satisfactory way of modelling the behaviour of the tensile concrete. Once this has been achieved, then the complete solution of the problem will be shown to follow directly.

As a starting point, it is helpful to reconsider the approach adopted by CP110 in rather more detail as this provides a useful insight into the problem.

5.2 The CP110 Approach

CP110 averages the stress distributions in the tensile concrete by adopting the approach shown in Fig. 5.1a. A linear stress distribution is assumed with a prescribed value of 1 N/mm^2 at the level of the tension reinforcement. This is a fixed value which applies for all strains.

A consequence of this approach is that the stress-strain relationship for the tensile concrete as modelled by CP110 is always changing, with the Young's modulus decreasing as load is increased. This is illustrated in Fig. 5.1b where a number of these stress-strain relationships have been plotted up to the prescribed stress of 1 N/mm^2.

Now, points a_1, a_2 .... a_n in Fig. 5.1b form a stress-strain envelope, shown dotted. The envelope is, in fact, a stress-strain relationship for the concrete in tension at the level of the tension reinforcement. Since the stress is constant at 1 N/mm^2, it is strain independent.

Thus CP110 models the behaviour of the tensile concrete by defining a stress-strain envelope and then using it in conjunction with a linear stress-distribution in the tensile concrete that has a value of zero at the neutral axis.

This is an extremely useful way of viewing the problem which can be generalised as follows:-

1. A stress-strain envelope is defined to describe the behaviour of the tensile concrete at some convenient level on the beam cross-section (which for CP110 is the level of the tensile reinforcement).
2. In conjunction with the above, the form of the stress distribution in the tensile concrete is defined, (which for CP110 is linear). In the general case this may well change as load is increased.

CP110 fails to achieve a good representation of the moment-curvature relationship because the parameters it adopts are insufficiently sophisticated. We shall now consider how they can be developed.

5.3 Development of the Partially Cracked Section

Let us consider how the tensile stress in the concrete at the bottom (tensile) face of a beam varies as the applied moment is increased from zero to its ultimate value. Clark and Speirs (20) have reported the following model, which retains the concept of averaged concrete tensile stresses. It is illustrated in Fig. 5.2.

Initially the stress increases linearly with respect to strain until the first major crack forms at a stress f_{t1} and a strain e_{t1}. Increasing the moment initiates further major cracks and the stresses and strains continue to increase, but the former do so at a decreasing rate. This continues until the last major crack forms at a stress f_{t2} and a strain e_{t2}. Further increase in moment results in a continuing increase in strain, but the stress now falls owing to the breakdown of the bond between the tension reinforcement and the surrounding concrete. Effectively this means that the reinforcement carries an ever greater share of the tensile force in the beam.

It is likely that $f_{t1} < f_t < f_{t2}$ where f_t is the ultimate tensile strength of the concrete, and Clark and Speirs suggested values for f_{t1} and f_{t2} of $0.9\ f_t$ and $1.1\ f_t$ respectively. However, although they undertook a substantial investigation of the tension stiffening phenomenon in reinforced concrete beams and slabs (20) they did not attempt to justify this hypothesis experimentally.

Now Fig. 5.2 can also be used as a stress-strain envelope, this time relating stress to strain at the bottom face of the section rather than at the level of the tension reinforcement as was the case with Fig. 5.1b. However to use it as such, the forms of the tensile stress distributions in the concrete at all stages of loading have to be known, and these may well not be the simple linear distributions adopted by CP110.

Since this approach is a more sophisticated model for the behaviour of the concrete in tension, its use should lead to an improved representation of the moment-curvature relationship.

Experimental evidence to support Fig. 5.2 and to determine the form of the stress distribution for the concrete in tension was thus sought.

6. TESTING AND PRELIMINARY ANALYSIS OF RESULTS

6.1 Details of Test Beams

The results of 14 beam tests were kindly made available by the Cement and Concrete Association. The beams were all nominally 3.5 m long and 200 mm wide with depths varying from 200 mm to 500 mm. Tension reinforcement percentages varied from 0.44% to 1.99% and the reinforcement used was GKN Torbar. Cover to the centre of the tension reinforcement was nominally 35mm and nominal top steel was also provided in each of the beams. Fig. 6.1 summarises the dimensions of the specimens.

The beams were all tested in a four point bending arrangement which gave a constant moment zone of 1200 mm and two shear spars of 1000 mm each (Fig. 6.2). Longitudinal surface strains in the constant moment zone were measured at each load stage by using a grid of Demec points having gauge lengths of 200 mm. The layout of the Demec points is shown in Fig. 6.2 and it enabled strains to be determined over a total gauge length of 1000 mm so as to even out the effects of cracking.

Associated with each beam, control specimens were tested to obtain the ultimate compressive strength, indirect tensile strength, and compressive stress-strain relationship for the concrete. The tensile stress-strain relationships

for specimens of the reinforcement were also found. Results for the concrete control specimens are summarised in Fig. 6.3.

A detailed description of the test beams has been reported in reference 20.

6.2 Preliminary Analysis of Results

6.2.1 Regression Line Analyses

The test data was supplied to the author in the form of raw Demec readings as this was the most basic way in which it could be presented.

A computer program was written which converted the Demec readings (about 4000 in total) into strain values, and then performed a linear regression line (least squares) analysis to obtain the following strain distributions across the depth of the section:-

(i) For each individual column of Demecs.

(ii) For the centre three columns of Demecs taken together. (i.e. 600 mm gauge length overall).

(iii) For all five columns of Demecs taken together. (i.e. 1000 mm gauge length overall).

These combinations enabled a comparison to be obtained between the strain distributions at five locations along the beam ((i) above) and the average strain distributions of (ii) and (iii). The average strain distributions would also be used in the subsequent analysis. It was thought that

approach (iii) would provide the best average strain values since it had the greatest overall gauge length of 1000 mm. However (ii) was included out of interest to observe those differences, if any, which resulted from the shorter, 600 mm gauge length. It also provided a check on (iii) as the outermost Demec points were close to the loading points, which might distort the readings.

From each regression line, the following values were calculated:-

Top (compression) face strain.

Strain at the level of each line of Demec points.

Strain at the level of the tension reinforcement.

Bottom (tension) face strain.

Flexural stiffness.

Curvature.

A typical page of output from the regression line program is shown in Fig. 6.4.

6.2.2 Discussion of the Regression Line Analyses

Some interesting points emerged from the regression line analyses.

Before the first crack formed, there was close agreement between the individual regression lines. This was as would be hoped, but was reassuring to observe nevertheless.

As the cracks formed there were marked differences between the individual regression lines for zones which contained a crack (or cracks) and those which did not.

These differences became more marked still as load was increased.

Approaches (ii) and (iii) were generally in good agreement during the early stages of loading, although with some beams there were quite marked divergencies once all the major cracks had formed. These will be discussed in more detail later. However, as will also become apparent later, it is this early phase, where the correlations were good, that is crucial, and so it seemed only necessary to use the five column results in the ensuing analysis.

Correlation between the actual measured strains and the equivalent values calculated from the regression lines was good and justified the assumption of linear strain distributions across the section.

7. DETAILED ANALYSIS OF RESULTS

7.1 Introduction

The average strain distributions given by the regression line analyses formed the basis for the further analysis now to be described. The analysis was performed by computer using software purpose written by the author.

Data was handled on a beam-by-beam basis and the first part of the input was concerned with basic section data (depth, breadth, reinforcement areas and covers) followed by the stress-strain relationships for the steel and concrete in the linearised form described earlier. Then, for each load stage in turn, values of applied moment, curvature, and strain at one level on the section (which could be the strain in either the tensile or compressive reinforcement or the strain on the bottom face) were input. The curvature and strain value were obtained from the "five column" average of the regression line analysis, and provided sufficient data to define the average strain distribution across the section.

In the final version of this program, the analysis of this data was extremely comprehensive. However, this was the result of two distinct phases in the analytical process and it is convenient to treat these separately.

7.2 Calculation of Forces, Moments and Eccentricities

The first phase of the analysis was to calculate for each beam at every load stage the stresses in the tensile

and compressive reinforcement and the stress distribution in the concrete in compression. This was easily done by relating the stress-strain data to the average strain distributions.

The program then used this information to calculate the forces in the reinforcement in tension (F_{st}), the reinforcement in compression (F_{sc}) and the concrete in compression (F_{cc}). Calculation of F_{cc} involved numerical integration of the non-linear stress distributions across the concrete in compression.

Next the moments of F_{st}, F_{sc} and F_{cc} about the neutral axis were calculated (M_{st}, M_{sc} and M_{cc} respectively). It was now simple to calculate the average force in the concrete in tension (F_{ct}), the moment of this force about the neutral axis (M_{ct}) and the eccentricity of this force relative to the neutral axis (e_{ct}).

$$F_{ct} = F_{cc} + F_{sc} - F_{st} \qquad (7.1)$$

$$M_{ct} = \text{Applied Moment} - M_{cc} - M_{sc} - M_{st} \qquad (7.2)$$

$$e_{ct} = M_{ct}/F_{ct} \qquad (7.3)$$

It was originally hoped that the shape of the average stress distributions across the concrete in tension would be determined by examining how e_{ct} varied as the beams were loaded. It was obviously desirable that the form of the

average stress distribution in the tensile concrete should emerge from the data rather than having to be imposed upon it.

Regretably this was not possible since the variation of e_{ct} was too scattered for any reliable conclusions to be drawn. Consequently it was decided to effectively reverse the procedure by selecting some simple forms for the stress distribution in the tensile concrete and see how well they fitted the data. This was phase 2 of the analysis.

7.3 Trial Stress Distributions for the Concrete in Tension

In view of the scatter in the results just referred to, it was decided that simple shapes only should be used as trial stress distributions. Consequently triangular, rectangular and rectangular-triangular shapes were selected (Fig.7.1). The triangle seemed an obvious one to try and a precedent had already been set for its use in Appendix A of CP110. The rectangle was likely to be less appropriate but was included because of its use, again by CP110, as the equivalent rectangular stress block for concrete in compression, and there might be some sense in keeping to a consistent approach when dealing with the concrete in tension. The rectangular-triangular shape was slightly more complicated but had the virtue of biasing the stresses towards the bottom of the section and giving a zone of constant stress around the reinforcement. It was thought that this might provide the truest simple representation of the real situation.

The bottom face stress, f_{bf}, was calculated for all three shapes at every load stage and a correction was made each time for the area occupied by the tensile reinforcement. For the triangular and rectangular shapes this was particularly simple since the depth in tension was readily obtainable from the strain distribution across the section. However, two values of f_{bf} were obtained for both shapes each time since F_{ct} and M_{ct} could be used as independent bases for the calculation.

Triangle:-

$$f_{bf} = \frac{2F_{ct}\, x_b}{(x_b^2 b - 2 A_{st}\, x_d)} \qquad (7.4)$$

or $$f_{bf} = \frac{3 M_{ct}\, x_b}{(x_b^3 b - 3 A_{st} x_d^2)} \qquad (7.5)$$

Rectangle:-

$$f_{bf} = \frac{F_{ct}}{(x_b b - A_{st})} \qquad (7.6)$$

or $$f_{bf} = \frac{2 M_{ct}}{(x_b^2 b - 2 A_{st}\, x_d)} \qquad (7.7)$$

where x_b = Distance from neutral axis to bottom face

x_d =Distance from neutral axis to centre of tension reinforcement.

For the rectangular-triangular shape, there were two unknowns, f_{bf} and h_{rt} (see Fig. 7.1). These were calculated from the expressions

$$F_{ct} = \frac{b}{2} (2x_b - h_{rt}) f_{bf} - A_{st} f_{bf} \qquad (7.8)$$

$$M_{ct} = \frac{b\, h_{rt}^{\,2} f_{bf}}{3} + \frac{(x_b^{\,2} - h_{rt}^{\,2}) b\, f_{bf}}{2} - A_{st}\, x_d\, f_{bf} \qquad (7.9)$$

for $h_{rt} \leq x_d$.

For $h_{rt} > x_d$ the last term in both equations was multiplied by x_d/h_{rt}.

Thus both F_{ct} and M_{ct} were required in order to calculate one value of f_{bf}. Equations (7.8) and (7.9) were only valid for $x_b/2 < h_{rt} < 2x_{b/3}$ (approximately, due to the influence of the area of the tensile reinforcement).

In practice an iterative procedure was adopted to solve equations (7.8) and (7.9) because it was not known in advance if h_{rt} was greater or smaller than x_d, although the former, of course, was likely to be an undesirable solution.

Results for the rectangular-triangular stress distribution were scattered and thus this had to be regarded as an inappropriate shape, or at least one that was not supported by the data. Regrettably, it could not be preceeded with.

Results for both the triangular and the rectangular stress distributions looked more encouraging and so plots of f_{bf}/f_t against e_{bf}, the corresponding bottom face strain, were made for each beam for both shapes. The normalization with respect to f_t, the indirect tensile strength of the concrete for the beam being considered, facilitated comparison. These curves are shown in Figs. 7.2.1 to 7.2.14.

Both shapes gave curves that consistently had the general form postulated in Fig. 5.2. However, the values of f_{bf}/f_t for the rectangular stress-block were always well below 1.0, implying that the concrete never came near to its ultimate tensile strength. This was considered to be an incorrect representation of the real behaviour, so this shape also was not proceeded with.

The curves for the triangular stress-block were much more promising in that they showed f_{bf} rising rapidly to around f_t and then decreasing less steeply thereafter. There were exceptions, such as Beam 1 which exhibited a rapid stress decrease and Beams 2, 10 & 11 which showed little or no decrease at all, but taken overall they appeared to provide experimental evidence consistent with the envelope concept outlined in Fig. 5.2. It was decided to proceed with this approach and see if sensible parameters could be developed for its description.

7.4 Evaluation of Envelope Parameters

The load stages at which the first and last cracks formed were determined for each beam by plotting curves of applied moment against Demec reading for each of the five Demec gauge lengths on the bottom row of each beam. Abrupt changes in the slopes of these curves indicated the formation of cracks. Once the load stages at which the first and last cracks formed in a particular beam had been identified, then the results of the regression line analysis of the Demec readings (See Section 6.2.1) gave the appropriate values of e_{t1} and e_{t2}. Stresses f_{t1} and f_{t2} were then obtained from the analysis described in section 7.3. The values of e_{t1}, e_{t2}, f_{t1} and f_{t2} for all the beams are listed in Fig. 7.3.

Averaging all the beams gave values of 0.80 f_t for f_{t1} and 1.06 f_t for f_{t2} with standard deviations of 0.23 f_t and 0.11 f_t respectively. These are in good agreement with the corresponding values of 0.9 f_t and 1.1 f_t suggested by Clark and Speirs.

e_{t1} was expected to be close to the ultimate tensile strain of the concrete. An average of 89.3 microstrain was obtained with a standard deviation of 43.0 microstrain. This standard deviation was undesirably high and was caused in part by the use of discrete load stages in the testing of the beams. Since at least some of the cracks undoubtedly formed between load stages, then the approach adopted yielded lower bounds to the values of e_{t1} (and e_{t2} for the

same reason). Finer load increments would have allowed a more accurate identification of e_{t1} with a probable reduction in the standard deviation.

e_{t2} increased as the percentage of tensile reinforcement decreased (reinforcement percentages in the test beams ranged from 1.99% to 0.44%). A relationship between e_{t1} and e_{t2} was sought.

Now

$$f_{t1} = E_1 e_{t1} = \frac{M_1 y_1}{I_1} \qquad (7.10)$$

$$f_{t2} = E_2 e_{t2} = \frac{M_2 y_2}{I_2} \qquad (7.11)$$

where E_1, E_2, M_1, M_2, y_1, y_2, I_1, I_2 are the Young's moduli for the concrete, bending moments, distances from the neutral axis to the tensile face of the beam and second moments of area of the whole beam section for the first and last major cracks respectively. The relationships are approximate as it was assumed that the concrete had the same value of Young's modulus in tension as in compression.

Thus

$$\frac{e_{t2}}{e_{t1}} = \frac{M_2}{M_1}\,\frac{y_2}{y_1}\,\frac{E_1 I_1}{E_2 I_2} \qquad (7.12)$$

Now, $E_1 I_1$ is approximately equal to $(EI)_u$, the flexural stiffness of the uncracked section. $E_2 I_2$ can be expressed as $F_1 \times (EI)_{cr}$ where $(EI)_{cr}$ is the flexural

stiffness of the fully cracked section and F_1 is a factor to be determined.

Substitution into equation 7.12 gives

$$\frac{e_{t2}}{e_{t1}} = \frac{M_2}{M_1}\,\frac{y_2}{y_1}\,\frac{1}{F_1}\,\frac{(EI)_u}{(EI)_{cr}} \qquad (7.13)$$

or

$$\frac{e_{t2}}{e_{t1}} = F_2\,\frac{(EI)_u}{(EI)_{cr}} \qquad (7.14)$$

where

$$F_2 = \frac{M_2}{M_1}\,\frac{y_2}{y_1}\,\frac{1}{F_1} \qquad (7.15)$$

Referring to equation (7.14), e_{t2}/e_{t1} was plotted against $(EI)_u/(EI)_{cr}$ using all the test beams except numbers 7 and 8 (Fig. 7.4). These two were omitted as they yielded points which were very scattered, beam 7 being very high and beam 8 being very low. The cause of this was believed to be experimental. These beams had the lowest reinforcement percentages (0.44% and 0.45% respectively) as a result of which the last major cracks formed at comparatively high strains by which time the load increaments were becoming quite large. This made an accurate determination of e_{t2} difficult for the reasons outlined earlier.

Inspection of the twelve points plotted suggested that it would not be unreasonable to assume a linear relationship between e_{t2}/e_{t1} and $(EI)_u/(EI)_{cr}$ even though there was some scatter of the results. This meant that F_2 in equation

(7.14) was a constant. A linear regression analysis yielded $F_2 = 0.99$ with an intercept of -0.013 (e_{t2}/e_{t1}) on the ordinate.

For comparison, values of F_2 were worked out individually for each beam using the results of the analyses described earlier to evaluate the terms in equation (7.15). These gave a root-mean-square average of 1.13 for F_2. The agreement was considered to be good bearing in mind the experimental problems with work of this nature.

7.5 Envelope Parameters for Design

The suggested relationship between f_{bf}/f_t and e_{bf} is shown in Fig 7.5. The experimental evidence supported the shape postulated in Fig. 5.2 but was insufficiently detailed to allow the exact form of the curve to be determined. However approximating it to three straight lines seemed reasonable. The first two of these, up to the peak stress of $1.1\ f_t$ were in close agreement with the experimental curves of Figs. 7.2.1 to 7.2.14, but the third line representing the descending part of the curve was inevitably more conjectural. The experimental evidence was too scattered to enable a mathematical fit to be attempted so the rather more arbitary approach of assuming that tension stiffening effects ceased when e_{bf} reached 2500 microstrain was adopted. This corresponds approximately to the strain at which high yield reinforcement reaches its full yield stress and thus seemed a not unreasonable assumption. The other parameters were as discussed earlier with e_{t1} taken as

100 microstrain and F_2 taken as 1.0 to give e_{t2} = 100 x $(EI)_u/(EI)_{cr}$. In addition values of 0.8 f_t and 1.1 f_{t2} were adopted for f_{t1} and f_{t2} respectively.

It was appreciated that this linearisation of the descending part of the curve could lead to an overestimation of the tension stiffening effect in a number of cases. However the author was loath to experiment with alternative representations as the selection of a more sophisticated curve could only be done on a rather random basis. Consequently it was decided to investigate the moment curvature relationships that would be generated using the stress-strain envelope of Fig. 7.5.

7.6 Curve Modelling Examples

The computer program described in Section 4 was developed to accomodate the stress-strain envelope of Fig. 7.5 and a linear stress distribution across the concrete in tension. It was then used to calculate the moment curvature relationships for the fourteen test beams. These are illustrated in Figs. 7.6.1 to 7.6.14 where they are compared with the experimental points obtained from the analyses of the Demec data.

Results from both the three column and five column analyses (see section 6.2.1) were plotted. As indicated earlier, they were in close agreement in the early stages of loading, where the values of f_{t1}, f_{t2}, e_{t1} and e_{t2} were evaluated, but in a number of instances diverged later.

This was probably due to varying rates of crack widening along a specimen and illustrates the difficulty of obtaining an absolute moment-curvature relationship for a particular beam. The "no tension" curves were included to give each beam a theoretical lower bound, which was nevertheless crossed by the experimental curves for beam 1. The reason for this was not clear, but was possibly due to early yielding of the reinforcement across one (or more) of the cracks. This was also a beam with a high reinforcement percentage (1.91%) which made it particularly awkward to test. It was interesting to note the increased effects of tension stiffening as the reinforcement percentage was reduced.

The calculated curves generally modelled the experimental behaviour well. They were sensitive both to variations in the reinforcement percentage and to the non-linear nature of the steel stress-strain curves at strains above 1500 microstrain. Beams 1 and 5 had the poorest agreement between the experimental and calculated curves. The problems with beam 1 have already been indicated. The reasons for the discrepancies in the case of beam 5 are not clear.

There may be an overestimation of the tension stiffening effect as modelled by the calculated curves, but based on the available evidence it would appear to be slight.

Reference to Fig. 3.7 will indicate that current procedures all underestimate the contribution of tension stiffening, some quite considerably. Curves for the current procedures have not been included in Figs. 7.6.1 to 7.6.14 for reasons of clarity, but since the relative relationships of Fig. 3.7 are applicable for all reinforcement percentages, it is the author's opinion that the model developed in this thesis has been demonstrated to be an advance over those methods which are currently in use. A decription of it has been published in the Proceedings, Part 2, of the Institution of Civil Engineers (22).

7.7 Developments

While working on the material of Part I the author became increasingly curious as to what the longitudinal strain distributions in the tensile reinforcement of a beam really were and decided that this was a problem worthy of further investigation. The behaviour of the tension zone of a beam was modelled by testing a series of simple tension specimens in the laboratory. Electric resistance strain gauges were used to measure the reinforcement strains. It is these tests, with their use of a specially developed technique for measuring reinforcement strains, which are described in Part II of this thesis. This work was funded by a grant from the Science and Engineering Research Council.

Part II

REINFORCEMENT STRAIN DISTRIBUTIONS IN REINFORCED CONCRETE TENSION SPECIMENS

8. THE STRAIN GAUGING TECHNIQUE

8.1 Previous Work

A number of procedures have been developed over the years for measuring longitudinal reinforcement strains. An indirect approach is to interpolate from surface strain measurements made either with a Demec gauge or with surface mounted strain gauges, but this is obviously approximate since it is difficult to perform the interpolation with any real degree of confidence or accuracy. However, the Demec gauge can yield very useful data when used carefully and for this reason it has been widely adopted for a whole range of strain measuring applications. A drawback is that since a gauge length of 200 mm is typically used, the readings give average rather than local strain values. Gauges with shorter gauge lengths are available but these have reduced sensitivity and accuracy. For example, reducing the gauge length from 200 mm to 50 mm (which is still large in real terms) and assuming an accuracy in reading of ±1 division means a reduction in sensitivity from ±8 microstrain to ±20 microstrain with a corresponding loss of accuracy. Nevertheless, gluing Demecs studs to the surface of a concrete specimen is straightforward which is more than can be said for the alternative of mounting strain gauges directly onto a concrete surface, an operation well known for its awkwardness even when big gauges are used. Consequently the use of surface mounted strain gauges is

comparatively rare. A hybrid method mounts the gauges on short steel beams which then locate into pairs of Demec studs but this then gives the large gauge length problem already encountered.

Another method is to fix pins to the reinforcement which then project through to the surface of the concrete in specially formed ducts. Strain measurements are taken at the surface using a Demec gauge. This is an awkward method to perform in practice and the pins have to be kept short to avoid flexing and consequent loss of accuracy. In addition it too yields average, not localised, strain values.

The use of electric resistance strain gauges to measure reinforcement strains is obviously attractive since the data they yield is both more localised and an order of magnitude more sensitive than Demec readings. However, bonding strain gauges to the surface of the reinforcement degrades the bond characteristic between the rod and the surrounding concrete, and the lead wires are also a disturbance as they have to be taken out through the concrete to the sides or ends of the specimen.

A partial solution to these problems is to install both the gauges and the wiring in a groove milled in the surface of the reinforcement. This works reasonably satisfactorily if only a few gauges are used but it still results in a rod surface which is different from the prototype. This problem becomes worse as the number of

strain gauges to be installed increases and for this reason this procedure is unsuitable for large scale gauging operations.

To get round this difficulty, the author devised a technique which involves installing the strain gauges in a milled duct running longitudinally through the centre of the reinforcement, the lead wires being taken along the duct and out of the ends of the rod. This leaves the steel/concrete interface completely undisturbed and, as will be shown later, a large number of gauges can be installed in quite a small duct. Detailed and reliable measurements of reinforcement strains are obtained with no disturbance of the surrounding concrete.

Although the author devised this method working independently, it was subsequently found to have been used by others, starting with the work of Mains in 1951 (23). Mains used it to study reinforcement strain distributions in beams and his work and results are most interesting, not least for their insight into the strain gauging techniques of nearly 35 years ago. However, since then there have been considerable advances in concrete mix design and reinforcement quality as well as a remarkable miniaturization of the strain gauges themselves. Strain gauge instrumentation has of course advanced very dramatically in only the last few years and this trend can be expected to continue.

Mains' work seems to be unique in that he studied the reinforcement strain distributions all along a beam and thus obtained a general picture of the behaviour from first loading through to the yield of the tension reinforcement. Subsequent workers have concerned themselves with studying more localised problems with particular emphasis on investigating bond stress-slip relationships . This trend seems to have started with Nilson in 1971 (24), who considerably refined the technqiue, and continues to the present time (25). The specimens used tend to be small.

Although Mains' work was remarkable in its day, it was felt that the technical advances of 35 years made another general investigation of reinforcement strains worthwhile in order to further the understanding of the tension stiffening phenomenon. As has already been intimated, it was decided that as it was the behaviour of the concrete in tension below the neutral axis that was of prime interest, the problem could be rationalised to that of testing simple tension specimens rather than complete beams. This was obviously a compromise as effects caused by the flexing of the compression zone were to be ignored. However, the simplification of the experimental technique which this approach affords has made it attractive to other investigators also (26).

Reinforcement strains were to be measured by a further development of the internal strain gauging technique that would take advantage of current strain gauging and strain

measurement technology to increase considerably the number of gauges that could be installed in a rod. As already stated, the conceptual ideas behind this approach were developed by the author working independently, but he readily acknowledges the previous work of Mains et al in this field.

A description of how each strain gauged rod was manufactured now follows.

8.2 Rod Manufacture

Each strain gauged rod was formed by milling two reinforcing rods down to a half round and then machining a longitudinal groove in each to accommodate the strain gauges and their wiring (Figs. 8.1 and 8.2). After installation of the gauges the two halves were glued together so that outwardly they had the appearance of a normal reinforcing rod, but with the lead wires coming out at the ends. Both mild and high yield (Torbar) steel reinforcement was used, and the rods were all 2.6 m long and either 12 mm or 20 mm diameter. With the former the groove in each half of the rod was 5 mm wide and 2.5 mm deep, while with the latter it was 7 mm wide and 3.5 mm deep. The easing of the duct size in the 20 mm rods was done not to allow more strain gauges to be installed, but rather to give more room for the strain gauge installation procedure itself.

The feasibility of this technique was demonstrated in a final year undergraduate project supervised by the author (27) and this early work was later published (28). The

technique was developed to the stage where 84 strain gauges, each connected with three lead wires, were installed in a duct of overall size 5 mm x 5 mm. This is believed to be a unique development of this strain measurement procedure.

8.3 Bonding and Protection

The strain gauges were installed using an cyanoacrylic adhesive and protected with a polyurethane varnish. Considerable care was needed in organising and successively bonding down the lead wires as these were added, starting at each end and working towards the middle. Finally the two halves of the rod were bonded together with an epoxy resin which also filled any remaining spaces in the duct.

The gauge installation was designed to be completely waterproof and it withstood the rigours of concreting without difficulty. Long-term performance in a fully saturated environment was not fully assessed since the specimens were cured under damp hessian rather than by total immersion in a curing tank.

8.4 Wiring

The space available in the duct was severely limited which necessitated using very small diameter lead wires. A two wire, common dummy, installation was tried at first but gave problems with stability since the small lead wires were necessarily about four metres long and so had significant electrical resistance when used with the 120 ohm gauges employed. These stability problems (thought to be thermal)

were cured by changing to a three wire common dummy arrangement. This required even smaller lead wires, but this was now acceptable since the three-wire system effectively eliminated all lead wire resistance.

8.5 System Reliability

After the inevitable learning period with the early rods, the reliability of the strain gauge installations became very good with a gauge failure rate during installation of only 1 to 2%. This excellent perfomance was due largely to the meticulous care of the project's technician, Mr. T.D. Harrison.

Occasionally a few gauges would fail during a test when high strain levels were reached, particularly in the region of cracks in the concrete, but this was only to be expected.

9. SPECIMEN DETAILS

9.1 Specimen Dimensions

The main test series consisted of thirteen specimens all 1500 mm long with square, uniform cross-sections ranging from 70 mm x 70 mm up to 200 mm x 200 mm (Fig. 9.1). They were reinforced with either 12 mm or 20 mm diameter strain gauged rods positioned centrally in the cross-section and extending right through the specimen. Both plain mild steel and ribbed high yield steel (Torbar) reinforcement was used. The chosen cross-sections (70 mm x 70 mm, 100 mm x 100 mm 140 mm x 140 mm and 200 mm x 200 mm) gave a doubling of the cross-sectional area for each step-up in size, and the ratio of the rod areas was 3.0:1 (after deduction of the duct area). One early specimen had a 150 mm x 150 mm cross-section. This choice of specimen sizes gave a wide range of covers and reinforcement percentages.

In addition to the main test programme two further tests were undertaken. The first of these involved a specimen made with lightweight aggregate concrete (using Pellite aggregate) while the other used dense concrete but had a 300 mm x 100 mm rectangular cross-section. These two tests were largely viewed as a pilot studies for possible future developments of the work.

Details of the specimens are given in Fig. 9.2. A coding system has been adopted to identify each specimen consisting of cross-sectional dimension, followed by the

reinforcment type (R for mild steel, T for Torbar) followed by the bar diameter.

It will be noted that only fourteen specimens appear in Fig. 9.2. In the case of the first 100T12 specimen there were strain gauge stability problems and failure of the load measuring instrumentation during the test. This test was therefore repeated and only the repeat specimen is included in the Figure. The 70R12 specimen was also repeated because the expected gross yield of the reinforcement was not observed first time. However, both these specimens are included in Fig. 9.2 because they both yielded useful data. Subsequent hardness measurements revealed that the rod in the first test was unusually hard and thus had an untypically high yield strength.

9.2 Rod Gauging Layouts

The first rod gauged (for Specimen 100R12) had 40 gauges, 3 mm gauge length, overall size 9 mm by 3.5 mm, at 25mm centres along the central 1 m of one half to provide an overall picture of the strain distribution, whilst the other half had 30 similar gauges at 10 mm centres together with two strain concentration gauges. These latter, which contained 5 elements each of 1 mm gauge length at 2 mm centres, proved particularly difficult to install because of their side lead attachments. The second rod (for Specimen 150R12) had a similar arrangement, but with the position of the strain concentration gauges moved to the centre of the rod.

Experience with these two installations led to the abandonment of the strain concentration gauges on the grounds that there was no evidence of the very severe strain gradients initially anticipated and which had prompted the trials with these gauges in the first place. Instead it was thought more desirable to provide more uniform gauging along the central region of the rods.

The third rod (for the discarded Specimen 100T12) was gauged so that there were gauges every 8 mm over the central 500 mm and every 25 mm over the 250 mm each side of this central region. All subsequent rods (except that for Specimen 100T12P which is considered later) went to a standard layout with 80 gauges spaced at 12.5 mm intervals along alternate halves of the central 1 m of the rods. (Fig. 9.3). In addition two additional gauges were installed at each end of the rods, outside the zone of the concrete, to measure rod strains and so provide a correlation with the load measuring instrumentation. Thus each rod contained a total of 84 strain gauges.

Before concreting the rods were mounted in the test rig and load cycled in order to check the installation and minimise any hysteresis. The results from this procedure were also used to calculate an average value of cross-sectional area for each rod, as described later.

9.3 Other Gauging

All specimens carried sets of Demec gauge points (200 mm gauge length) to allow measurement of average surface strains (Fig. 9.4). Some specimens also contained embedment strain gauges in the concrete (12 mm gauge length, overall size 30 mm x 9 mm x 2.5 mm). These were always restricted to one half of the specimens as it was considered that they might act as crack inducers. Depending on the specimen cross-section one, two, three or five rows of embedment gauges were used to investigate the strain gradients from the reinforcing rod to the surface of the concrete. The layouts of the embedment gauges are shown in Fig. 9.5.

The gauges were positioned in the mould using a grillage of fine wires (Fig. 9.6). The number of wires was kept to a minimum but even so they were inevitably a potential source of disturbance in the concrete.

9.4 Mix Design Details

Concrete for the specimens had a maximum aggregate size of 10 mm (determined by the spacing of the embedment gauges), a water:cement ratio of 0.6 and an aggregate:cement ratio of 5.5. Three test cubes and three cylinders were cast along with each specimen for the determination of compressive strength and indirect tensile strength respectively. Specimens were cured for 7 days under damp hessian and were normally tested at or about 28 days after casting.

10. EQUIPMENT AND TEST PROCEDURE

10.1 The Data Collection System

10.1.1 Hardware

A data collection system was commissioned to handle the large quantity of data that the test programme would generate. The system consisted of an Intercole Spectra-ms logger linked to a Cifer 2684 microcomputer. It is illustrated in Fig. 10.1.

The logger handled 208 channels of input data and was constructed in modular form with individual modules for the microprocessor unit, analogue to digital converter, instrumentation amplifier and power units. In addition there were thirteen wiring modules each accommodating sixteen channels of input data. Switched, twin constant current energising was provided which was suitable for all resistive transducers.

The logger had a sensitivity of ±1 microstrain and readings from the strain gauge installation as a whole were accurate to better than ±5 microstrain. This was achieved at the expense of measurement speed which, at 8 channels/second, was low, but entirely satisfactory for the quasi-static conditions which prevailed.

The Cifer 2684 microcomputer featured 64K of memory and a built-in $5^1/_4$" floppy disk drive. An additional external $5^1/_4$" floppy disk drive was also acquired. Each disk gave approximately 384K of storage. The system ran

under a CP/M monitor control program which left around 56K of memory available for user-written programs.

At the time of purchase (April 1982) this data collection system offered a far more flexible and powerful data logging package than could be obtained at a similar price from an individual manufacturer. However, a side effect of this purchasing policy was that the interfacing of the logger with the microcomputer had to be done in-house. This major programming exercise was undertaken by the author and brief details of the software that was developed now follow.

10.1.2 Interfacing the Logger with the Microcomputer

The logger's own microprocessor had an 8K ROM and a 2K RAM. Together the ROM and the RAM interpreted instructions from the operator, operated the measurement and control hardware and returned results to the operator. Data was returned along an RS232 serial line link in volts for strain gauges and load transducers.

The microprocessor was sufficiently powerful to allow the logger to be operated from a standard keyboard via the RS232 link. However, in this configuration both input and output were rather cryptic. Much more flexibility and sophistication was achieved by having a supervising computer, since interactive input, enhanced output (such as display of strain gauge readings in microstrain rather than volts) and data storage for subsequent transfer to a

mainframe computer could then be developed to exploit the full potential of the logger's own software.

The interfacing program was written in FORTRAN and had two basic functions. Firstly it enhanced communication with the logger by giving assistance with input instructions and making output displays more comprehensive. Secondly a sophisticated file handling capability was introduced for the storage of data. The basic structure of the interfacing program is illustrated in Figure 10.2.

Commands entered from the keyboard started with either ; or *. The logger responded to ; but ignored * commands. These latter, used for cummunication with the computer only, initiated operations such as the listing of command data and the creation of disk files.

When a command was entered, the computer tested to see if it started with ; or *. If it was a ; command, it was then decoded and the appropriate subroutine called to deal with it. This occured during the time the logger took to decode the command, so that by the time the logger replied the subroutine had already been called and was ready to process the response. Often this processing would involve calling additional subroutines. There were a total of 26 subroutines which are listed in Fig. 10.3. Their inter-relationship is illustrated in Figure 10.4. Once execution was complete, the program re-cycled ready to receive the next command. Treatment of * commands was similar except that there were no logger repsonses to consider.

The FORTRAN software permitted up to nine disk files to be opened which enabled the hardware to log several experiments simultaneously, yet store the data on separate disk files. Storage of scan data was followed by a record of the time at which the scan occured (found by software interrogation of the logger's own clock). Messages could be recorded on the files so that a chronological record of events was maintained along with the data.

Other features were incorporated into the program to assist with the logging of long-term experiments. Details of these (which are not relevant to the experimental work in this thesis) will be found in the published descriptions of this data logging system and its associated software (29,30, 31). These papers also give more detailed descriptions than space here permits of the features outlined above.

10.1.3 Interfacing the Microcomputer with the Main Departmental Computer Facilities

At the end of a logging session the data was transferred from the disk files into the Department's own computer system. This was a Perkin-Elmer 3230 which had 4 megabytes of memory and served terminals throughout the Department.

The microcomputer was connected from its normal working position in the laboratory to the Perkin Elmer via an RS232 serial line link. File transfer was achieved using software already available in the University and written mainly in PASCAL. This enabled the power of the larger

machine to be used for a comprehensive data analysis operation, which will be described later.

10.2 Test Procedure

The short-term tests were conducted in a purpose-built test rig (Fig. 10.5) and were each completed within one day. A manual hydraulic loading system was employed with the jack being located at the bottom of the specimen. Load was measured by a flat load cell at the top of the specimen and displayed on a meter giving a direct digital read-out. The voltage output from the load cell was also connected directly into the data logger via an output from the meter.

The specimens were loaded incrementally with the increment sizes adjusted as the tests proceeded to reflect the rates at which changes were occurring within the specimen. In particular very detailed information was sought immediately before and after the formation of cracks and this often demanded load increments as fine as 0.5 kN.

The applied load and a full set of strain gauge readings were taken and stored at every load stage. Time constraints precluded Demec readings being taken at all load stages, so a selective procedure was adopted with emphasis being given to the period during which the cracks formed. Crack widths were measured, when appropriate, where the cracks crossed a set of three fine pencil lines drawn on each face (Fig. 9.4). This was done at the same time as the Demec readings, using an Ultra-Lomara 250 b microscope.

Loading of the specimens was halted when the reinforcement had fully yielded. With mild steel rods this often resulted in very high strain readings.

11. ANALYSIS AND DISCUSSION OF RESULTS

11.1 Determination of Rod Cross-Sectional Areas

A program was written by the author for the Department's Perkin Elmer computer to analyse the several thousand strain gauge readings generated by each test. The first function of the program was to present this data in a compact and readily comprehensible form.

With the early rods, which had the non-standard gauging patterns, the numbering sequence used by the data logger did not coincide with the order in which the gauges were mounted in the rod. In addition, some of the data recorded was later found to be surplus to requirements. Thus the program first reorganised all the data into a logical sequence, with the surplus readings omitted, and output this either on the screen or in hardcopy form. Perusal of the data was also assisted by an inter-active graphics routine written into the software. The readings were now in a form suitable for further computations, the first of these being the determination of an effective cross-sectional area for each rod.

It will be appreciated that although the 12 mm diameter rods had, in theory, a cross-sectional area of 88 mm^2, and the 20 mm diameter rods an area of 265 mm^2 (both allowing for the internal duct) these were only nominal values and variations were likely to occur both between rods and along individual rods due to machining inaccuracy.

After some trials with measuring rod diameters, this problem of rod area was resolved by the development of an analytical procedure which used the results of the load cycling procedure performed to eliminate strain gauge hystersis and referred to earlier.

As the final part of the load cycling procedure, each rod was incrementally loaded until a strain level of about 500 microstrain was recorded (safely within the elastic range of the stress-strain behaviour) and then unloaded using the same load steps. A linear regression (least squares) analysis was performed for both the loading and unloading curves using the average of all the strain gauge readings for each load stage. In all cases there was very little difference between the regression lines for the loading and unloading cases. The average of the two slopes was then taken which was proportional to the Young's modulus of the steel being used. This had already been determined as 207 kN/mm^2 for both the mild steel and Torbar reinforcement by tests on solid specimens of each (Figs. 11.1.1 & 11.1.2). Calculation of an average rod cross-sectional area thus followed directly. These are tabulated in Fig. 9.2.

As a check on variations along a rod, this procedure could be repeated for any individual strain gauge to yield a more localised value for cross-sectional area. Some variations in area were apparent but they were not large enough to cause concern.

11.2 Cracking - General Observations

The strain distributions for all fourteen specimens are shown in Figs. 11.2.1 to 11.2.14. Generally the load stages before and after the formation of each crack have been plotted, although sometimes more than one crack occured at a particular load stage. Each plot also shows typical strain distributions for the higher load levels.

The strain measuring technique recorded the strain distributions well and the way in which the strains peaked at the cracks and declined away from the cracks is shown most clearly.

All specimens exhibited some bending which was characterised by strain readings on one side of the rod being higher than those on the other. The amount of bending changed as each crack formed with the specimens tending to become more curved or to straighten depending on the faces in which the cracks formed. Cracks had a tendancy to form on the cast face of the specimens first, perhaps because the concrete here would be less well compacted than elsewhere in the specimen and so have a lower Young's modulus value. Some bending was also inevitably caused by endemic curvature of the reinforcement and an accumulation of minor tolerances in the rig and test specimens. However crack propogation was considered to be the dominant influence on bending.

Bending has been smoothed out from the plots of Figs. 11.2.1-11.2.14 by the use of a simple averaging technique. Each "raw" strain value (e) was recalculated by the computer

according to the following expression:-

$$e_1 = \frac{e_x + 2e + e_y}{4} \qquad (11.1)$$

where e_x = the raw strain value to the left of e

e_y = the raw strain value to the right of e

e_1 = the smoothed value of e

It is the e_1 strains which have been plotted and which are used in all subsequent calculations, except for specimens 100R12, 150R12 and 100T12P where the non-standard gauging layouts were not amenable to this procedure.

The data from the tests is summarized in Fig. 11.3. Results for the concrete control specimens are given, together with the number of cracks in each specimen and the strains and loads at which the first and last of these cracks formed. Specimens 300/100T20 and 100T12P are both included in this and subsequent Figures, but the discussion will now deal with the square, dense concrete specimens only. Specimens 300/100T20 and 100T12P are considered separately in Section 11.7. For the main batch of specimens a number of general observations can be made.

The number of cracks in a specimen decreased as the section size increased, from eight in the 70T12 to one only in the 200T20. Cracks generally went round three faces only of the specimens initially, with the back face going into compression, as indicated by the Demec readings. Sometimes a crack would propogate all round the specimen at a later

load stage but could do so straight away if it was formed at a high load level. Cracks were not continuous but consisted of a number of overlapping segments. Rod strains across a crack were typically 10% above the rod strains outside the specimen, due to crack-induced bending.

For a given cross-section and rod diameter there were more cracks in the specimens having the Torbar than in those having the mild steel reinforcement. For a given cross-section and rod type, there were more cracks with the 20 mm diameter than with the 12 mm diameter rods. Crack spacings were generally fairly equal in any given specimen and increased as the number of cracks decreased. The upper limit on specimen cross-section for a particular rod type and diameter was dependent on avoiding gross yield occurring outside the concrete before a crack formed. With the larger cross-sections the debonding which occurred at the end of the specimens would extend into the strain-gauged zone (e.g. Specimens 140R20, 150R12).

The strain distributions each side of a crack were remarkably linear which indicated that the bond stresses were essentially constant. This will be dealt with in greater detail later. Cracks always developed between the debonding zones and generally from a plateau strain level of about 100 microstrain. However some cracks formed quite late (crack 4 in 100R20, crack 7 in 100T20, and crack 4 in 140T20) and it will be shown that these should be classified separately.

The strain distributions caused by early cracks would often be influenced by the formation of later cracks nearby, the tendency being for the strain gradients to be reduced. A similar effect would occur when a crack formed adjacent to a debonding zone. There was more debonding each side of a crack with the mild steel rods than with the Torbar due, presumably, to more slip occurring between the rod and the concrete in the former case. The strain distributions for the 20 mm diameter rods had flatter peaks than those for the 12 mm diameter rods.

Creep would occur during the taking of Demec readings and could be quite marked (Fig. 11.4).

The crack width readings were a disappointment due to the difficulty of obtaining readings which were consistent from one load stage to another. Variations in crack width over the width of even a very fine pencil line could be very considerable, and the sensitivity of the microscope used (a standard model) was an order of magnitude worse than that of a Demec gauge. No further reference to these readings will be made.

11.3 Cracking - Detailed Analysis

11.3.1 Pre-Cracking Strains

The rate at which cracks propogate across a reinforced concrete tension specimen is very high. For all practical purposes crack formation can be considered to be

instantaneous with a sudden jump in reinforcement strain from its pre-cracking level to its post-cracking peak at the crack position.

Interestingly, a number of specimens exhibited localised peaks in the reinforcement strains at the crack positions, before the cracks actually propogated to the surface. Particularly marked examples were for the first crack in specimens 70R12/1 and 70T12 and for the second crack in specimen 70T12. The results for specimen 70R12/1 are shown in Fig. 11.5

Fig. 11.5 clearly indicates a ridge forming in the generally flat strain distribution as the load is increased, and by the time the cracking load of 12.0 kN is reached it has become quite extensive. It is not possible to be specific as to the cause of this, but two explanations suggest themselves. Either the rod cross-section was small at this point, thus raising the strains, or, perhaps more likely, debonding occured between the reinforcement and the surrounding concrete before the crack propogated rapidly to the surface. In practice a combination of the two would also be possible with a rod imperfection initiating localised cracking and hence debonding. This would be an interesting phenomenon to investigate further.

11.3.2 Reinforcement Strains

Detailed information regarding the loads and reinforcement strains pertaining to each crack is given in Fig. 11.6. The first crack in the four specimens which

contained embedment gauges always occured within the gauged zone and at reinforcement strains which were untypically low. It would seem that the embedment gauges influenced the cracking behaviour by acting to a certain extent as crack inducers. However, with three of these specimens (100T12, 100T20, 140T20) the second crack occured away from the embedment gauge zone and at load and strain levels more consistent with those for the first cracks in the other specimens (Specimen 200T20, the fourth embedment gauge specimen had one crack only). Thus when comparing the reinforcement strains at which the first cracks formed, it seemed more appropriate to use the crack 2 results for the embedment gauge specimens, (i.e. to treat crack 2 as the effective first crack). This comparison is shown in Fig. 11.7.

The reinforcement strains just before the effective first crack (e_f) appear to be independent of reinforcement type, diameter or specimen size. An average value of 99.1 microstrain was obtained with a standard deviation of 11.9 microstrain. (Specimen 200T20 was excluded as it contained embedment gauges and had one crack only). The corresponding values for the beams in Part I were 89.3 microstrain and 43.0 microstrain respectively (Section 7.4). This agreement was good. The reinforcement strains at which the last crack formed (e_ℓ) are also tabulated in Fig.11.7 and a plot of e_ℓ/e_f against reinforcement percentage is shown in Fig. 11.8. Fig. 11.8 indicates that the data falls into two

groups. The majority of the specimens have values of e_ℓ/e_f which lie in the range $1.0 \leqslant e_\ell/e_f \leqslant 1.75$ and which tend to increase with reinforcement percentage. Three specimens (100R20, 100T20, 140T20) however have values of e_ℓ/e_f of 4.34, 3.40 and 5.72 respectively which separate them from the majority. These high e_ℓ/e_f values are caused by the last crack forming at an untypically high strain level (360, 272 and 561 microstrain respectively). Inspection of the strain distributions for these specimens revealed that the last cracks did not form from the usual plateau strain level of around 100 microstrain, but instead were propogated from a rather higher datum later in the test. It thus seemed more appropriate to use the penultimate cracks for these specimens as these cracks formed from the general plateau level and would provide a consistent comparison. The values of e_{penult}/e_f for these cracks are also shown in Fig. 11.7 and the revised points they yield for specimens 100R20, 100T20 and 140T20 are indicated in Fig. 11.8.

A rather more consistent picture now emerges for all the specimens. The regression line for this revised set of points indicates a slight upward trend, but this is really somewhat conjectural. For this revised set of points, e_ℓ/e_f is largely independent of reinforcement percentage and has an average value of approximately 1.4.

To attempt a comparison with the beam results in Part I (Fig. 7.4) e_ℓ/e_f was plotted against $(EA)_u/(EA)_{cr}$, the uncracked and cracked stiffnesses for the specimen

respectively (Fig. 11.9). $(EA)_u$ was calculated using the expression

$$(EA)_u = \frac{P_f}{e_f} \qquad (11.2)$$

where P_f was the load to cause the effective first crack, a linear load/strain relationship being assumed up to this point. $(EA)_{cr}$ was based on the reinforcement area only.

Fig. 11.9 again shows how specimens 100R20, 100T20 and 140T20 are isolated from the main group when e_l/e_f is based on the last crack, but join the group when data for the penultimate crack is used. These points indicate a slight downward trend in contrast to the distinct upward trend of Fig. 7.4.

It is thus suggested that cracks in tension specimens can be categorized into two types.

(i) Plateau Cracks which form from a general strain level in the specimen of around 100 to 200 microstrain and all occur over a fairly narrow band of loading.

(ii) High Strain Cracks which form at higher strain levels in excess of 200 microstrain after the existing cracks have broken-up the pre-cracking strain plateau. They can occur at high load levels and in this test series

only one occured in any particular specimen. The final cracks in Specimens 100R20, 100T20 and 140T20 are in this category.

An essential difference between plateau cracks and high strain cracks is that plateau cracks form a crack pattern that is largely repeatable between similar specimens. High strain cracks, in contrast, seem to be determined by the conditions pertaining in a particular specimen and are thus specimen dependent. It is interesting to relate this to the work of Goto (32) who identified primary cracks and secondary cracks in tension specimens. The former provided the main crack pattern, whilst the latter were caused by some of the internal cracks around the reinforcement propogating sufficiently to reach the surface after the primary cracks had all formed. Thus Goto's secondary cracks could be analogous to the high strain cracks observed in this work.

11.3.3 Concrete Stresses

The average concrete stresses just before the formation of the effective first crack, the last crack and, where appropriate, the penultimate crack were calculated and are tabulated in Fig. 11.7. The stresses were calculated at the crack position in each case.

As with rod strains, these stresses appeared to be independent of the specimen parameters. Again excluding specimen 200T20, an average concrete stress of 0.67 f_t was

obtained for the effective first crack with a standard deviation of 0.08 f_t.

For the last crack there was again a dichotomy between specimens with plateau cracks only and those with a high strain crack. When the penultimate crack data was used for these latter specimens an average concrete stress of 0.82 f_t was obtained with a standard deviation of 0.14f_t. The high strain crack specimens (100R20, 100T20 and 140T20) gave values of 1.39 f_t, 1.43 f_t and 1.27 f_t respectively when using the data for the last (high strain) crack.

It is interesting to note that these concrete stresses appear to be independent of rod type, at least for plateau cracks. For so long as the bond between the reinforcement and the surrounding concrete remains unimpaired, the development of cracks in a specimen seems to be dependent on the attainment of limiting stresses and strains in the concrete. As will be discussed in the next secion, it is with the post-cracking behaviour and the development of bond stresses that the differences between plain and ribbed rods become marked.

The stress values of 0.67 f_t and 0.82 f_t may be compared with the values of 0.80 f_t and 1.06 f_t obtained for the beams in Part I (Section 7.4). Cracks in tension specimens would seem to occur at lower stress levels and over a narrower stress band than those in beams. Interestingly the ratio of the two extremes is similar in

both cases (1.22 for tension specimens, 1.33 for beams). Above a stress of $0.82f_t$ in tension specimens high strain cracks can occur. It is not known if similar cracks can form in beams and if they do, on which side of the $1.06\ f_t$ limit they will lie.

11.4 Bond Stresses

11.4.1 General

For equilibrium the change in the tensile force along a reinforcing rod must be balanced by the bond between the rod and the concrete. Thus for a small length δx over which the tensile force changes by δT, the bond stress f_b is given by

$$f_b = \frac{\delta T}{\delta x . u} \qquad (11.3)$$

where u is the rod perimeter.

If the reinforcement is behaving elastically then (11.3) can be re-written as

$$f_b = \frac{E_s \delta e A_s}{\delta x . u} \qquad (11.4)$$

where

E_s = Young's modulus of the reinforcement

A_s = Cross-sectional area of the reinforcement

δe = Change in reinforcement strain over the distance δx

In the limit

$$f_b = \frac{E_s A_s}{u} \frac{de}{dx} \qquad (11.5)$$

Thus for elastic behaviour, the bond stress is proportional to the slope of the longitudinal reinforcement strain distribution, and a constant slope means that the bond stress is constant. But it should be remembered that a linear strain distribution having values in the post-linear range of the reinforcement stress-strain relationship does not imply a constant bond stress. The change in tensile forces over succeeding lengths δx of the reinforcement will decrease as the strains increase meaning that the bond stress will be reducing. This will apply at strain levels above 1300 microstrain for the mild steel rods and above 1600 microstrain for the Torbar.

Bearing this in mind it is interesting to re-examine the strain plots of Figs. 11.2.1 to 11.2.12.

Immediately apparent is the linear nature of the elastic strain distributions implying that the bond stresses were essentially constant at any given load stage. Exceptions to this were short zones adjacent to the cracks themselves and at the ends of the bond stress zones where in both cases the rate of reduction of bond stress was quite marked. In the latter case this was due to the transition from a zone of bond breakdown to a zone where the bond was unimpaired. Adjacent to the cracks bond stresses were

decreased due to gross bond breakdown between the reinforcement and the surrounding concrete, exacerbated by slip, or by yield of the reinforcement itself. With mild steel rods, in particular, a combination of these effects is likely to occur, especially at high load levels.

Specimens 70R12/2 and 140T12 were exceptions to the norm of essentially constant bond stress distributions. The case of specimen 140T12 is straightforward as the reinforcement yielded as soon as the specimen cracked with strains of up to 6000 microstrain being recorded at the crack positions. For specimen 70R12/2 no specific cause can be suggested, but this specimen was an isolated exception amongst the group.

11.4.2 Bond Stresses at Crack Formation

For all specimens except 70R12/2 and 140T12, a comprehensive programme of bond stress calculations was undertaken, within the elastic range of the reinforcement, involving manual measurement of the strain gradients from large scale (A2 size) plots of the strain distributions. Bond stresses were evaluated before and after the formation of cracks and then at typical load levels once the full crack pattern was established.

The bond stresses developed each side of each crack immediately after its formation are tabulated in Fig. 11.10. The stresses are also shown normalized with respect to f_t, the indirect tensile strength of the concrete. f_t is recognized as being a dominant parameter in bond performance

(33). Specimen 70R12/2 and 140T12 are omitted for the reasons already indicated, and other blanks in the table are due to cracks occurring outside the strain gauged zone or due to local deviations from linear behaviour hindering sensible bond stress determinations. Tabulated also are the corresponding stresses in the reinforcement across each crack. Some interesting points emerge.

When a crack formed in isolation the bond stresses on each side of the crack were similar, as would be expected. When a crack formed near to a debonding zone or adjacent to existing cracks, the bond stresses on each side of the crack could be markedly different (e.g. crack 2 in specimen 100T20, crack 1 in specimen 140R20, crack 2 in specimen 140T20). Usually the bond stresses were reduced, but specimen 200T20 indicates that the reverse was also possible.

Fig. 11.10 shows that there is no unique value of bond stress developed in a particular specimen, but that bond stresses are dependent on the reinforcement stresses across the cracks. With Torbar specimens, bond stresses tend to increase with reinforcement stress, whilst with mild steel specimens they tend to decrease. This will be demonstrated in greater detail shortly, but here it means that care has to be exercised when using Fig. 11.10 to compare bond stresses between specimens as is it more correct to make the comparison at a common level of reinforcement stress rather than compare crack with crack.

On this basis, bond stresses in specimens reinforced with Torbar rods are higher than their mild steel companions by up to 70%. There are exceptions but they are isolated and caused by the strong influences of existing adjacent cracks. An example can be seen when comparing specimens 100R20 and 100T20.

11.4.3 Bond Stress - Rod Stress and Bond Stress - Slip Relationships

Bond stress - rod stress relationships were plotted for each specimen in order to investigate further the rising and falling trends suggested by Fig. 11.10 for the Torbar and mild steel rods respectively. Bond stresses were evaluated for each crack at typical load stages, from its inception through to the onset of yield in the reinforcement.

The plots all confirmed the rising and falling trends, as appropriate, but data for specimens with only a few cracks was sparse. Consequently the results for specimens 70R12/1, 70T12, 100R20, 100T20 are presented as typical of the group (Figs. 11.11.1 to 11.11.4). There is some scatter due to the influence of later cracks on those already formed.

These results are consistent with previous work such as the comprehensive bond investigation by Snowdon (34) which was the basis for the CP110 recommendations. They show than on crack propogation the bond stresses start quite some way up the bond stress-rod stress curve (shown dotted).

With Torbar, further increases in rod stress will raise the bond stresses, but with mild steel rods bond stresses are already in or near to the plastic range of the bond stress-rod stress relationship, and may reduce with rod stress increase.

This significant difference in the performance of the two rod types is due to the different nature of their individual bond stress-slip relationships. No specific slip measurements were made in this work but nevertheless an approximate estimation can be obtained by integrating along the reinforcement from a point of zero slip to obtain rod displacements and using the embedment gauge or Demec results to obtain concrete displacements.

Points of zero slip were assumed to occur at the troughs in the longitudinal strain distributions (Figs. 11.2.1 to 11.2.12). In practice the embedment gauge results proved to be unsuitable due their location relative to the cracks and so the Demec data was used.

Typical post-cracking results for R20 and T20 rods are shown in Fig. 11.12. They were obtained from specimens 140R20 and 200T20 and were calculated at the typical locations shown in Figs. 11.2.9 and 11.2.12 respectively, both being 200 mm away from the adjacent trough.

Fig. 11.12 shows that the points obtained lie on curves which are typical for the respective reinforcement types (34). The bond stress-slip relationship is widely recognised as the fundamental relationship in bond work and

the two curves demonstrate the markedly different performance of the two rod types. Again post-cracking bond stresses are seen to lie some way along these curves.

With specimens 140R20, 150R12 and 200T20, the end debonding zones extended far enough into the gauged zone to permit the calculation of the resulting bond stresses. At pre-cracking load levels these stresses were low, as would be predicted by the bond stress-rod stress and bond stress-slip relationships. However, even when cracks had formed these stresses were still lower than the bond stresses adjacent to the cracks themselves. This may have been due to additional slip and hence higher bond stresses being induced by the sudden pulling action of rapid crack propogation, but this is conjectural.

The bond stress-rod stress and bond stress-slip relationships provide the explanation for the low crack 1 bond stresses in the specimens having embedment gauges. Since these first cracks occured at low loads and hence low rod stresses, due to the crack inducing tendencies of these gauges, then a reduction in bond stress was in fact both inevitable and consistent with established theory.

11.4.4 Design Considerations

In design terms, this work has been concerned with bond behaviour under essentially working load conditions, or at what CP110(13) refers to as the Serviceability Limit State. CP110 classifies bond into two categories, local bond and anchorage bond, the former

applying where there are high shear forces caused by a rapidly changing bending moment distribution, and the latter being concerned with the progressive transfer of load from a rod into the surrounding concrete. This work belongs to the anchorage bond category, but as with local bond, CP110 limits its recommendations to the Ultimate Limit State only. Design considerations for anchorage bond at the Serviceability Limit State would thus appear to be useful.

Dealing first with initial bond stress values after the propogation of the first crack, it will be appreciated that these differ between specimens because they occur at different points on the various bond stress-slip relationships. However, by using the data for the first effective crack (Fig. 11.10) and eliminating bond stresses that were obviously influenced by adjacent debonding zones, a reasonable basis for comparison is achieved to give initial bond stresses of around 1.1 f_t, 1.4 f_t, 0.9 f_t and 1.0 f_t for the R12, T12, R20 and T20 rods respectively, where f_t is the indirect tensile strength of the concrete. These values are approximate as rod stresses between specimens reinforced with the same rod type sometimes varied quite widely.

Looking now at the variation of bond stress with rod stress, this was less straightforward to quantify in view of the sparse data for specimens with one or two cracks only (Section 11.4.3). So a procedure was developed which widened the database by allowing the results for specimens

reinforced with the same rod type to be combined. Each bond stress value (f_b) was divided by its initial value (f_{bi}) immediately after crack propogation and similarly each associated rod stress (f_{st}) was also normalised with respect to its starting value (f_{sti}) immediately after crack propogation. Graphs of (f_b/f_{bi}) against (f_{st}/f_{sti}) were then plotted for the four rod types with each graph now being an amalgam of the results for several specimens (Figs. 11.13.1 to 11.13.4).

Results for the R12, T12 and R20 rods were all distinctly banded with downward, upward and level trends respectively. Results for the T20 rods were rather more scattered with two bands appearing. One band contained the bulk of the data and rose quite steeply while the other, which contained data from one specimen only, rose rather more slowly. Apart from this last case there was good intermingling of the data between specimens and the small amount of debonding data available also appeared to fit into the general pattern.

A regression line analysis was performed for each of the main data bands to yield the following relationships:-

$$\text{R12:} \quad \frac{f_b}{f_{bi}} = -0.2 \frac{f_{st}}{f_{sti}} + 1.2 \qquad (11.6)$$

$$\text{T12:} \quad \frac{f_b}{f_{bi}} = 0.4 \frac{f_{st}}{f_{sti}} + 0.6 \qquad (11.7)$$

R20: $$\frac{f_b}{f_{bi}} = 1.0 \qquad (11.8)$$

T20: $$\frac{f_b}{f_{bi}} = 0.5 \frac{f_{st}}{f_{sti}} + 0.5 \qquad (11.9)$$

These results have been plotted on Figs. 11.13.1 to 11.13.4. A small degree of selectivity was applied to the T12 data to avoid the unrepresentative skewing of the regression line that would have resulted had all the early data points been included.

Equations (11.6) to (11.9) are only applicable for $f_{st}/f_{sti} > 1.0$ and should not be used when f_{st}/f_{sti} exceeds about 2.0. Effectively they represent a linearization of the bond-slip relationship over the range $1.0 \leq f_{st}/f_{sti} \leq 2.0$. They enable the variation of bond stress with rod stress to be estimated, but should be applied with care since, as the T20 results indicate, the changes may sometimes not be as marked as the equations indicate.

In general terms, bond stresses for mild steel rods will at best remain unchanged as the rod stresses increase, but are more likely to decrease, while with Torbar bond stresses will probably increase but at worse remain unchanged. The assumption of an unchanging bond stress would be conservative for Torbar, but distinctly not so for mild steel reinforcement.

11.5 Bond Influence Lengths

The lengths over which the bond stresses were effectively constant on each side of a crack were measured for each specimen immediately after the crack formed. To aid uniformity between specimens, only those cracks which formed in isolation were used i.e. zones which were influenced by adjacent debonding were ignored. Variations within specimens were small.

Fig. 11.14 relates the bond influence lengths (B) to the concrete covers (C), both being expressed in terms of rod diameter (θ).

Both the mild steel and Torbar specimens yielded a linear relationship irrespective of the rod diameter. Linear regression analyses yielded the following relationships:-

For mild steel

$$\frac{B}{\theta} = 5.59 \frac{C}{\theta} - 4.73 \qquad (11.10)$$

For Torbar

$$\frac{B}{\theta} = 4.45 \frac{C}{\theta} - 4.14 \qquad (11.11)$$

where

B = bond influence length

C = cover to the outside of the reinforcement

θ = rod diameter

The linearity with the Torbar was very good. There was some scatter with the mild steel points due to the flatter peaks of the strain distributions making identification of the boundaries of the linear zone less certain.

Equations (11.10) and (11.11) have only been shown to be valid for $16 \geqslant C/\theta \geqslant 2$. None of the tests yielded data for $C/\theta < 2$ and it is regretted that neither a 70R20 or a 70T20 specimen was tested as these would have had C/θ values of 1.25.

The line representing a 45^0 spread of stress from the reinforcement to the surface of the concrete is also shown on Fig. 11.14. It would seem reasonable to assume that this is a lower bound curve and it highlights the effect that debonding has on the transfer of stress. Intriguingly the experimental curves both intersect this line near the point where the cover equals the rod diameter. In practice a smooth transition in the region of the intersection points would be anticipated, and testing of the two extra specimens listed above would have helped to establish this. However the experimental curves are valid over a wide range of realistic C/θ values permitting the corresponding B/θ value to be determined.

Fig. 11.14 can also be used to yield a lower limit on crack spacings for a given specimen cross-section and rod diameter.

11.6 Embedment Gauges

Embedment gauges were cast into four specimens (Fig. 9.2) at the positions shown in Fig. 9.5. (Specimen 300/100T20 also had embedment gauges). Bond between the gauges and the surrounding concrete was good, even at quite high strain levels, and the gauges performed well, albeit with the crack inducing tendencies reported earlier.

Specimen 200T20 with its three rows of embedment gauges in each face (giving 48 gauges in all) yielded data which was typical for the group and will now be discussed.

Figs. 11.15.1 and 11.15.2 show strain distributions across the specimen at distances of 450 mm and 250 mm from the centre as indicated on Fig. 11.2.12 (Positions 1 and 2 respectively). The plots are typical for both directions across the section. Surface strain measurements were taken from the Demec data and were thus average values over a 200 mm gauge length, whereas the embedment gauges had a gauge length of 12 mm.

At Position 1 (Fig. 11.15.1) the early loss of strain compatibility at the steel/concrete interface due to debonding became steadily more pronounced as the load increased. Position 1 was sufficiently remote from the crack position (approx. 300 mm) for there to be a modest increase only in reinforcement strain when the crack formed. Pre-cracking strains in the concrete were uniform across the section and showed only a small increase with load. With

post-cracking strains a slight strain gradient was established from the reinforcement to the faces of the section, and there was evidence of strain relaxation occuring at the surface. When the crack first formed at 65.2 kN the peak concrete strain was 67 microstrain and the rod strain was 626 microstrain . At the end of the test (100.3 kN) these values had risen to 83 microstrain and 1122 microstrain respectively. Thus an increase in rod strain of 496 microstrain had produced only a 16 microstrain increase in the peak concrete strain. This indicates a marked degree of debonding.

At Position 2 (Fig. 11.15.2) which was about 100 mm from the crack position, there was less debonding prior to cracking and strain compatibility was maintained up to about 40 kN. Consequently there was a big increase in the reinforcement strain when the crack formed, from 195 microstrain up to 741 microstrain. A more marked strain profile was established in the concrete after cracking with a peak strain of 193 microstrain at the end of the test, a rise of 45 microstrain since the crack formed. Over the same load range the reinforcement strain rose by 674 microstrain to 1415 microstrain but one embedment gauge remote from the reinforcement showed a rise of only 8 microstrain.

At Position 3, 150 mm from the centre of the specimen and right on the crack itself, a rather different picture emerged. The crack formed on face A (Fig. 9.1) of the

specimen and initially extended around the two adjacent faces, B and D, but did not appear on C, the back face. Before the crack formed, compatibility at the steel/concrete interface was good, but after cracking there were marked differences between the strain distribution through the concrete from A to C and that from B to D

From face A to the reinforcement the measured strains were very much lower than would be expected across a major crack. A peak value of 712 microstrain at 100.3 kN was recorded compared with the corresponding average surface strain reading of about 4200 microstrain. Debonding between the gauges and the concrete at what must have been very high local strain levels seemed likely.

Between the reinforcement and face C, the strains peaked midway at up to around 11000 microstrain and then declined quite sharply towards the outside face. This was consistent with the Demec data which indicated compressive strains on this face. Near the end of the test the crack was propogated right round the specimen and face C then went into tension (causing relaxation on face A). Strains in excess of 30000 microstrain were developed which, even with those gauges which did not fail, were outside the selected measurement range of the data logger.

In the B-D direction strains rose rapidly from the reinforcement towards both sides of the specimen. A peak of 18000 microstrain was recorded but undoubtedly strains considerably above this were actually attained. (Fig.

11.15.3).

Although the reinforcement strains and the concrete strains are apparently consistent in Fig. 11.15.3, this does not indicate an absence of debonding since strain compatibility is obviously lost where a reinforcing rod crosses a crack. At Position 3, in the B-D direction, the embedment gauges were effectively measuring crack widths as they were located where the crack formed. Fig. 11.15.3 indicates qualitatively how the crack widths varied with increasing load. The restraining effect of the reinforcement is particularly apparent.

11.7 Specimens 100T12P and 300/100T20

Specimens 100T12P and 300/100T20 were both isolated examples of their type tested primarily as pilot studies for possible future developments. Results for these specimens have been included in the tables and graphs for the main batch of square, dense concrete specimens to aid comparison. Since they were one-off tests, only general observations can be made about them.

Specimen 100T12P used lightweight aggregate (Pellite) and an early gauged rod which had a non-standard gauging pattern and performed disappointingly. There were six cracks (Fig. 11.2.14), two more than in its dense concrete companion. Both the load and strain at which the first crack formed were low (Figs. 11.3 and 11.6) but the concrete stress was comparable with the other specimens at 0.6 f_t. (Fig. 11.7). The cracks were all plateau cracks. Bond

stresses were difficult to measure accurately but appeared to be comparable to the other specimens in absolute terms (Fig. 11.10) but much higher when normalised with respect to the concrete's indirect tensile strength (the lowest of any specimen at 1.89 N/mm^2). Bond stresses rose with rod stress. The high bond stresses and low cracking loads meant that the bond influence lengths were shorter than in the equivalent dense concrete specimen.

Specimen 300/100T20, the only rectangular specimen tested, had one plateau crack and one high strain crack (Figs. 11.2.13, 11.3, 11.7 & 11.8). It was the only specimen to exhibit longitudinal cracking along the line of the reinforcement, both at the ends and adjacent to crack 1, the plateau crack. In addition a short transverse crack appeared approximately midway between the two main cracks. This had very little effect on the rod strains although there was a small ridge at about the crack position (Fig. 11.2.13). This secondary cracking behaviour is consistent with previous work (26).

The crack 1 bond stresses appeared to be on the high side (Fig. 11.10) but very little data was obtainable. The bond influence lengths did not fit the curves of Fig. 11.14 irrespective of whether the cover was based on the long or short side.

This was an interesting test as it demonstrated clearly that rectangular sections behave quite differently from square sections so far as crack pattern and spacing are

concerned. This test, which is really a simple model for slab behaviour, posed rather more questions than it answered and it would be a fruitful area for further research.

11.8 Further Work

A number of interesting possilities arise from the work described in this thesis.

Firstly it is desirable that the work on tension specimens described in Part II should be correlated with the beam work described in Part I. This would involve calculating the curvatures and deflections of typical beams using the bond stress results of Part II to estimate the tension stiffening effects. Calculated curvatures and deflections would be compared with existing test results, but a programme of beam tests using strain gauged reinforcing rods would be required to assess the validity of the bond stress assumptions. It is hoped that this work will begin shortly.

Next there is the problem of time-dependent effects which have not been considered in this thesis, but are obviously important when calculating long-term deflections. Here a start has been made as a series of long-term tests on tension specimens is currently nearing completion. These are funded by the same Science and Engineering Research Council research grant as the short-term tension tests of Part II. Again the results will need to be applied to beams.

Looking further ahead, the strain measurement technique which has been described in this thesis has proved itself to be extremely effective and reliable and its potential for further applications is very wide indeed. An investigation of the strains in lapped reinforcement is already in hand and a start will be made shortly on an investigation of the performance of beam/column connections, which will involve the internal strain gauging of links and other bent reinforcement. Both these programmes are receiving SERC support. In the longer term, a move from the laboratory into the field is currently under consideration, although this is potentially a complex and expensive undertaking. However, the prospect of monitoring a full-size structure has the promise of being a uniquely demanding and rewarding challenge.

11.9 Publications

Preliminary reports of the work described in Part II of this thesis have been given at conferences in Lancaster and Vancouver (35, 36). Other publications associated with this thesis have been referenced at the appropriate points in the text, and more are in preparation. A listing of all the publications to date is given in the Appendix.

12. CONCLUSIONS

12.1 Part I

12.1.1 The results of the regression line analysis of the beam Demec data support the common assumption of a linear strain distribution across a beam section when considering large gauge lengths.

12.1.2 For design purposes, the first major crack in a reinforced concrete beam forms at a concrete stress of $0.8f_t$ and a strain of 100 microstrain at the bottom (tensile) face. The last major crack forms at a concrete stress of $1.1f_t$ and a strain of $100\ (EI)_u/(EI)_{cr}$ microstrain. This latter strain value increases as the percentage of tensile reinforcement decreases. For strains in excess of $100*(EI)_u/(EI_{)cr}$ the concrete stress falls and approaches zero when the tensile reinforcement has yielded.

12.1.3 The behaviour of the tensile conrete in a reinforced concrete beam can be modelled using the concept of a stress-strain envelope with the boundary of the envelope describing the stress-strain behaviour at the bottom (tensile) face of

the section. The stress distribution across the section can be assumed to be linear with a value at the neutral axis of zero, and a value at the bottom face determined by the appropriate point on the boundary curve of the envelope.

12.1.4 A tri-linear form can be given to the stress-strain envelope with the origin, the points of the first and last major cracks and the yield of the tension reinforcement being the descriptive parameters (Fig. 7.5).

12.2 Part II - Square Section, Dense Concrete Specimens

12.2.1 The technique of installing strain gauges in a duct milled longitudinally through the centre of the reinforcement is a very effective way of measuring reinforcement strains.

12.2.2 For a given cross-section and rod diameter there are more cracks in specimens having Torbar reinforcement than in those having mild steel.

12.2.3 For a given cross-section and rod type there are more cracks when 20 mm diameter reinforcement is used than when 12 mm diameter is used.

12.2.4 Strain distributions each side of a crack are essentially linear which indicates zones of constant bond stress when the reinforcement is within its elastic range.

12.2.5 Cracks always develop between the end debonding zones and the strain distributions adjacent to early cracks are influenced by cracks occurring later.

12.2.6 There is evidence to suggest that bond breakdown may occur locally at a crack position before the crack propogates to the surface.

12.2.7 Reinforcement strains just before the effective first crack appear to be independent of reinforcement type, diameter and specimen size. An average value of 99.1 microstrain (standard deviation 11.9 microstrain) was obtained.

12.2.8 Cracks in tension specimens may be categorized into two types: Plateau Cracks which form from a general strain level of 100 to 200 microstrain, and High Strain Cracks which occur at strain levels in excess of 200 microstrain.

12.2.9 The crack pattern formed by Plateau Cracks is repeatable between similar specimens, whilst High Strain Cracks are specimen dependent.

12.2.10 The concrete stress at which the effective first crack forms is $0.67f_t$ (standard deviation $0.08f_t$). The stress for the last crack is $0.82f_t$ (standard deviation $0.14f_t$) except when the last crack is a High Strain Crack. The stress is then higher.

12.2.11 When a crack forms in isolation, the bond stresses on each side are essentially similar. However, bond stresses are decreased by the presence of an adjacent crack or debonding zone.

12.2.12 After crack propogation, the bond stresses start some way up the bond stress-rod stress and bond stress-slip relationships. With Torbar, further load increase leads to increased bond stresses, with mild steel rods bond stresses decrease.

12.2.13 For design purposes, initial post-cracking bond stresses are approximately $1.1f_t$, $1.4f_t$, $0.9f_t$ and $1.0f_t$ for R12, T12, R20 and T20 rods respectively.

12.2.14 For design purposes, bond stresses and rod stresses are related thus:

$$\text{R12:}\quad \frac{f_b}{f_{bi}} = -0.2\frac{f_{st}}{f_{sti}} + 1.2$$

$$\text{T12:}\quad \frac{f_b}{f_{bi}} = 0.4\frac{f_{st}}{f_{sti}} + 0.6$$

$$\text{R20:}\quad \frac{f_b}{f_{bi}} = 1.0$$

$$\text{T20:}\quad \frac{f_b}{f_{bi}} = 0.5\frac{f_{st}}{f_{sti}} + 0.5$$

$$\text{Valid range: } 1.0 \leqslant \frac{f_{st}}{f_{sti}} \leqslant 2.0$$

For Torbar rods these equations represent an upper limit on behaviour, for mild steel rods they are a lower limit.

12.2.15 Bond influence lengths and cover are related thus:-

$$\text{For mild steel } \frac{B}{\theta} = 5.59\frac{c}{\theta} - 4.73$$

$$\text{For Torbar } \frac{B}{\theta} = 4.45\frac{c}{\theta} - 4.14$$

Valid range: $2 \leqslant \frac{c}{\theta} \leqslant 16$

12.3 Part II - Specimens 300/100T and 100T12P

12.3.1 Specimen 100T12P exhibited higher bond stresses relative to its indirect tensile strength than its dense concrete companion. The rod strain at which crack 1 formed was low at 60 microstrain.

12.3.2 Specimen 300/100T20 was the only specimen to exhibit longitudinal cracking and a short transverse crack midway between the two main cracks. Its behaviour was generally different from that of the main batch.

12.4 Developments

12.4.1 The strain gauging technique described in Part II of this thesis has proved itself to be extremely effective and reliable. To date it has been applied only to simple tension specimens but its potential for further applications to much more complex situations is almost unlimited. It is the hope of the author that this potential can be fully realised and so advance our understanding of that

most fascinating, challenging and complex structural material which is called reinforced concrete.

APPENDIX

The following is the list of publications which have resulted, to date, from the work described in this thesis. The listing is in chronological order.

1. Scott, R.H. & Gill, Gill, P.A.T. "Developments in the Measurement of Reinforcement Strain Distributions in Reinforced Concrete Members". Strain, May 1982, p. 61, 63, 79.

2. Scott, R.H. "The Short-Term Moment-Curvature Relationship for Reinforced Concrete Beams". Proc. ICE, Part 2, Vol. 75, Dec 1983, p. 725-734.

3. Scott, R.H., Gill, P.A.T. & Munro, M. "A Modern Data Collection System and Its Interfacing Requirements". Proc. Symposium on Civil and Structural Engineering Software and Applications, London, Nov. 1983, p. 297-307.

4. Scott, R.H. & Gill, P.A.T. "A Modern Data Collection System" Strain, May 1984, p. 63 - 68.

5. Scott, R.H. & Gill, P.A.T. "Long-Term Testing of Reinforced Concrete Tension Members" Proc. RILEM/ACI Symposium on Long-Term Observation of Concrete Structures, Budapest, Sept. 1984, p. 298-307.

6. Scott,R.H. & Gill, P.A.T. "Reinforcement Strains in Reinforced Concrete Tension Members" Proc. 12th Congress IABSE, Vancouver, Sept. 1984, p. 919 - 925.

7. Scott, R.H. & Gill, P.A.T. "Measurement of Reinforcement Strains in Concrete" Proc. BSSM Conf on Structural Integrity, Lancaster, Sept. 1984.

8. Scott, R.H., Stevens, A.T. & Black, S. "The Analysis of Reinforced Concrete Beam and Column Sections" To be published in Proc. Symposium on Civil and Structural Engineering Computing, London, Dec. 1985.

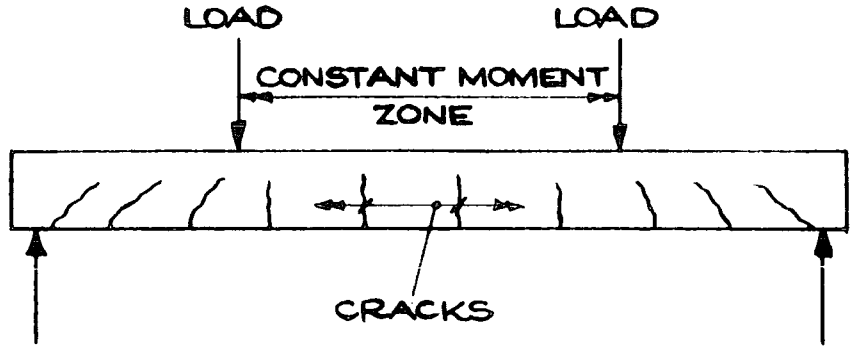

Fig 2.1 : TYPICAL CRACK PATTERN FOR A REINFORCED CONCRETE BEAM

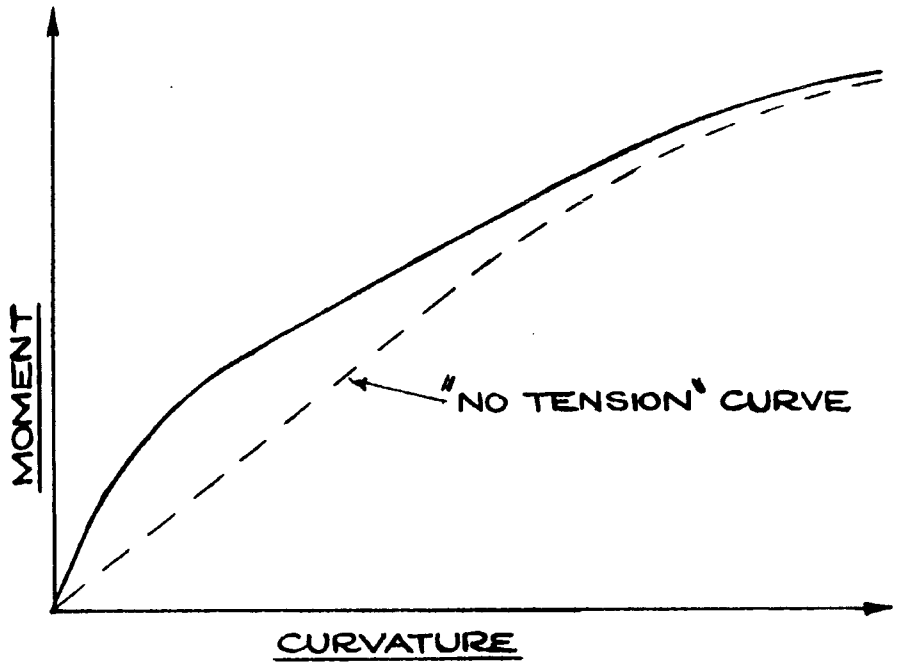

Fig 2.2: TYPICAL MOMENT-CURVATURE RELATIONSHIP FOR A REINFORCED CONCRETE BEAM

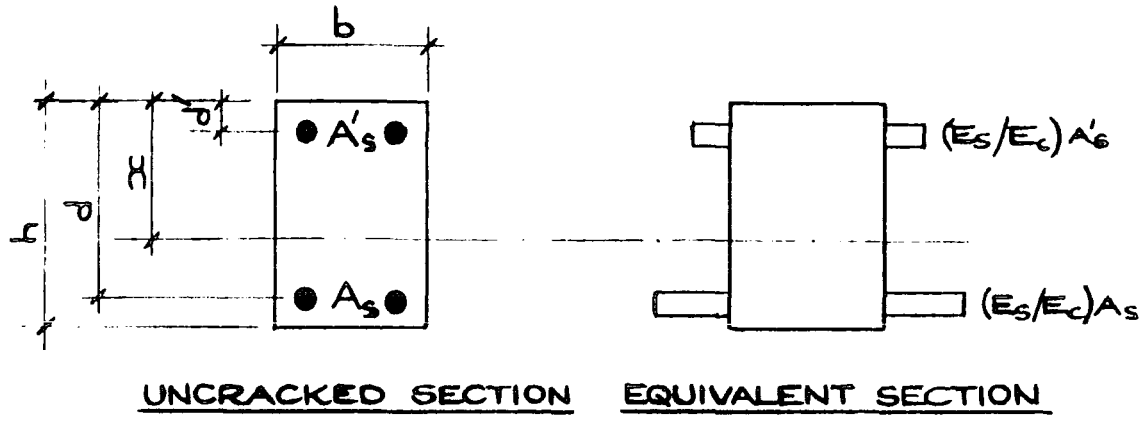

Fig 3.1: THE UNCRACKED SECTION

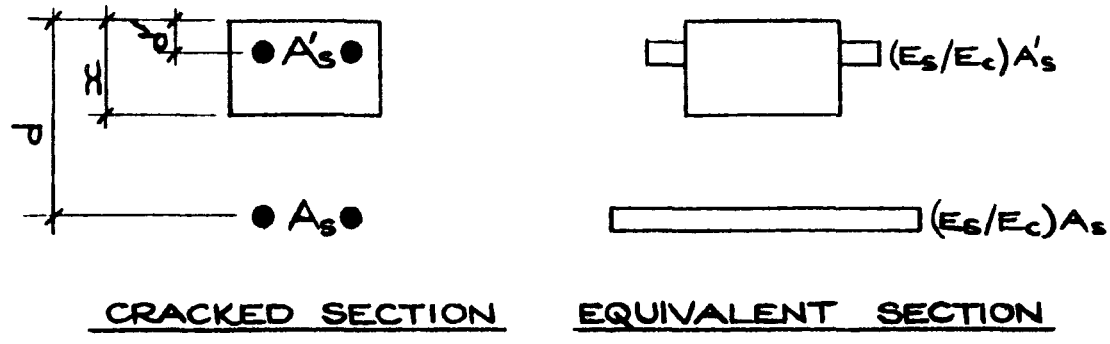

Fig3.2: THE CRACKED SECTION

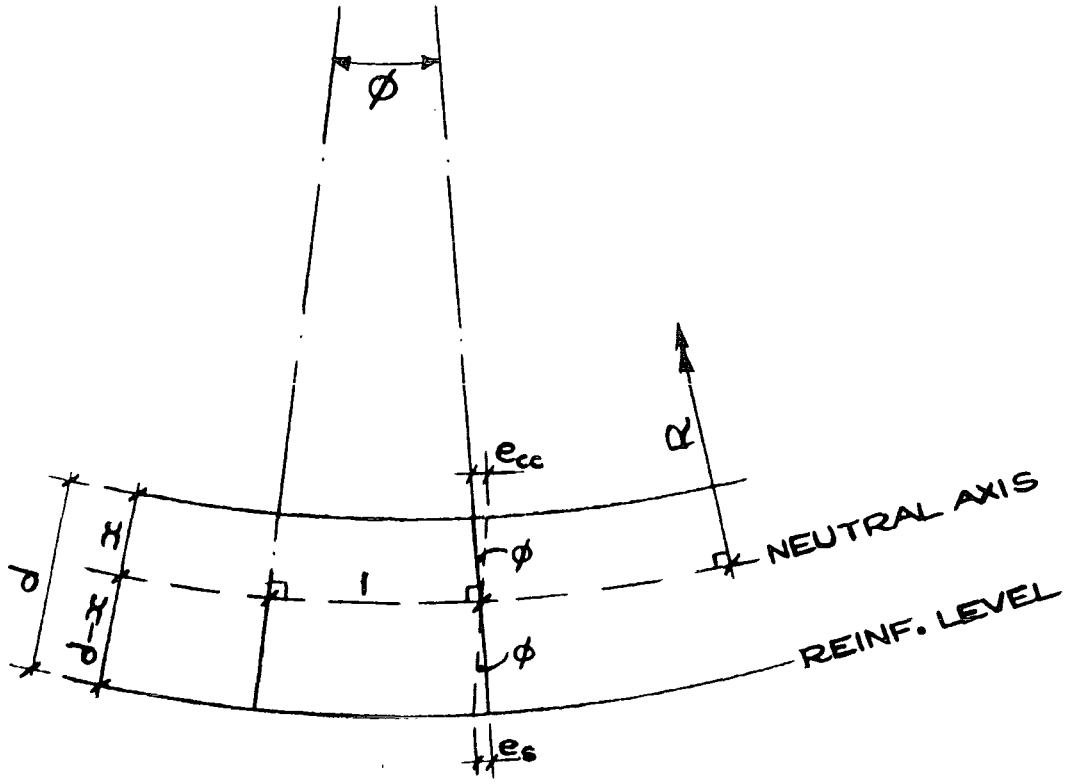

Fig 3.3: CURVATURE & STRAIN DISTRIBUTIONS

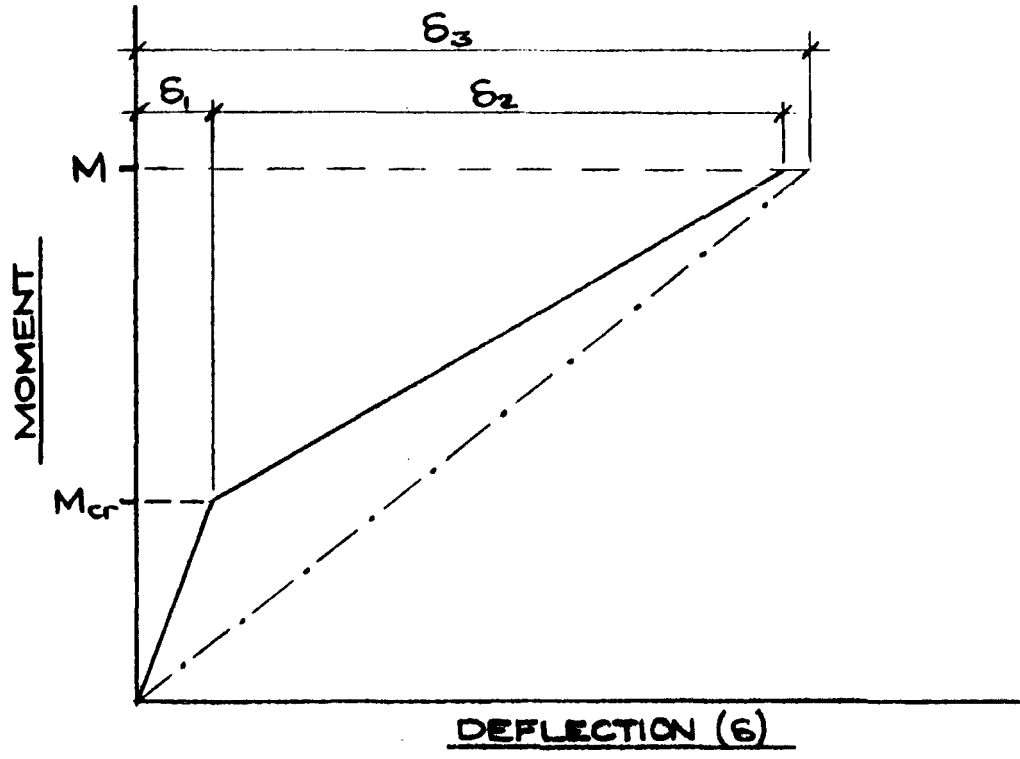

Fig 3.4: CEB DEFLECTION RECOMMENDATIONS

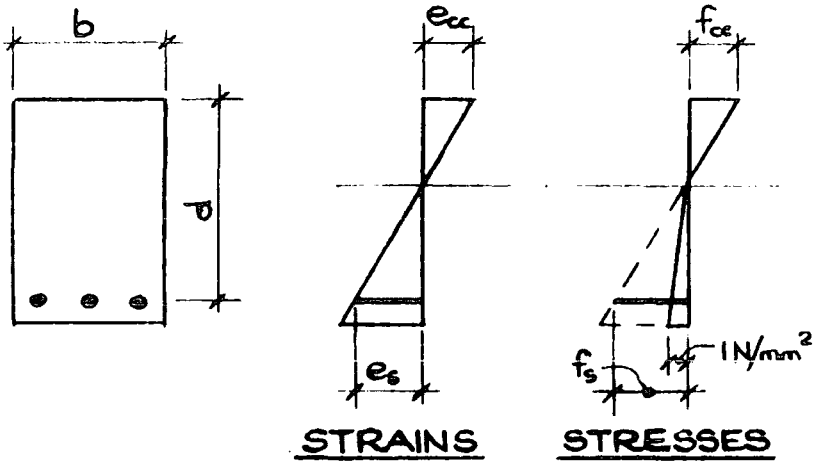

Fig 3.5 : CP110 STRAIN & STRESS DISTRIBUTIONS

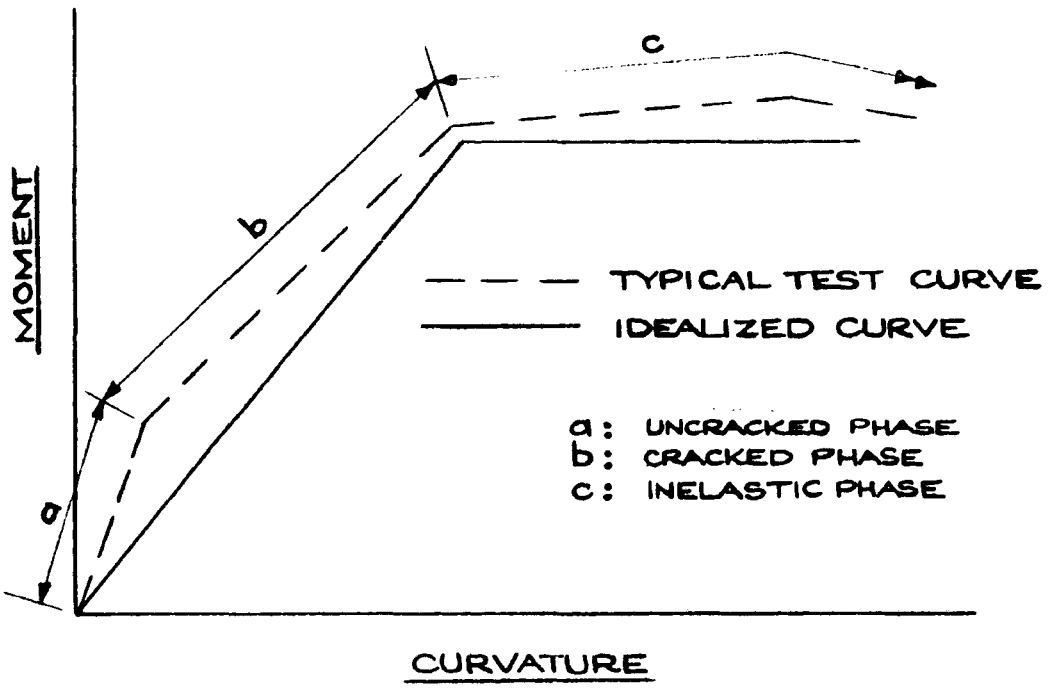

Fig 3.6 : I.C.E. MOMENT-CURVATURE RELATIONSHIPS

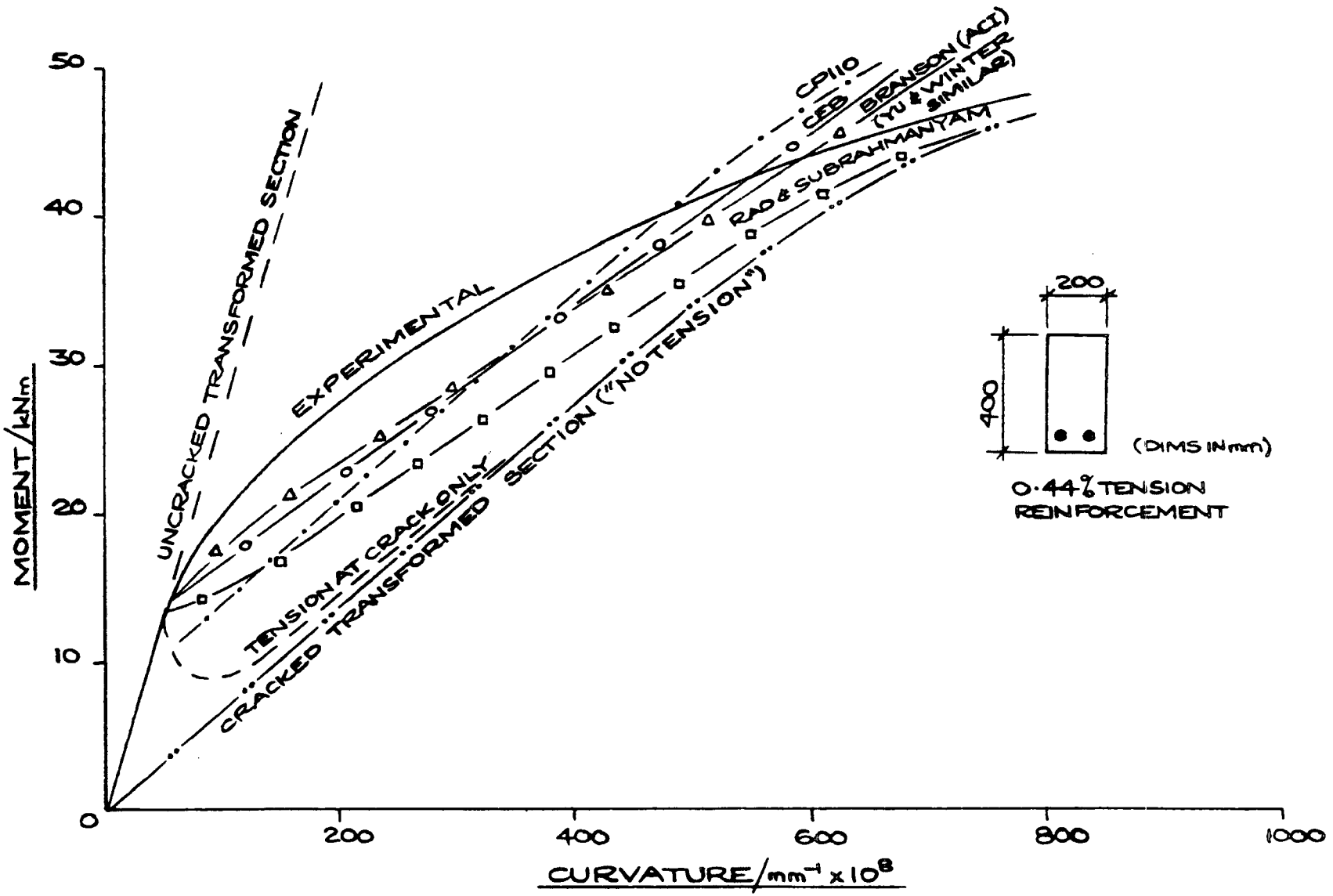

Fig 3.7: COMPARISON OF MOMENT–CURVATURE RELATIONSHIPS

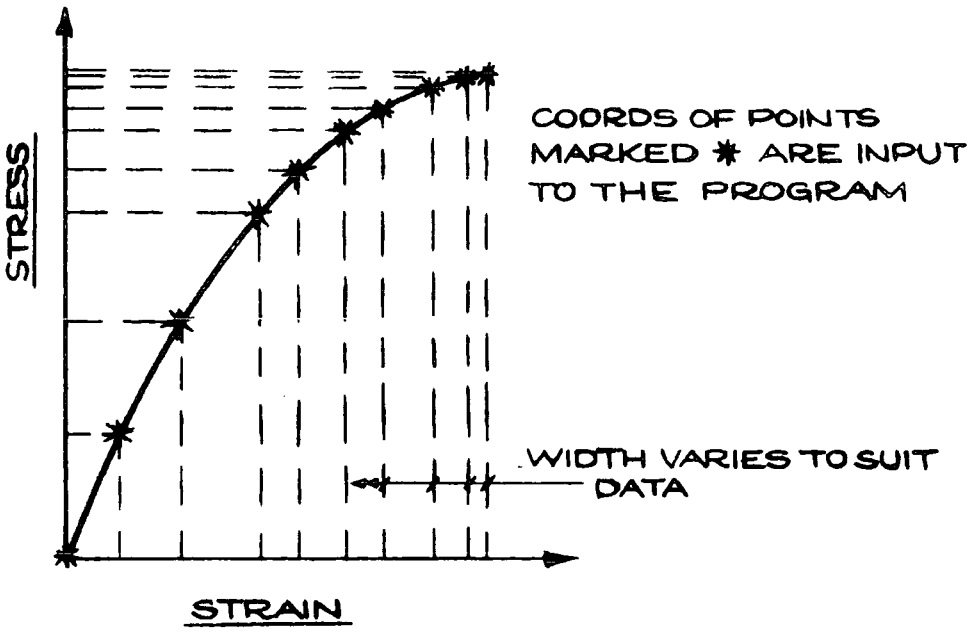

Fig 4.1 : LINEARIZATION OF STRESS – STRAIN CURVES

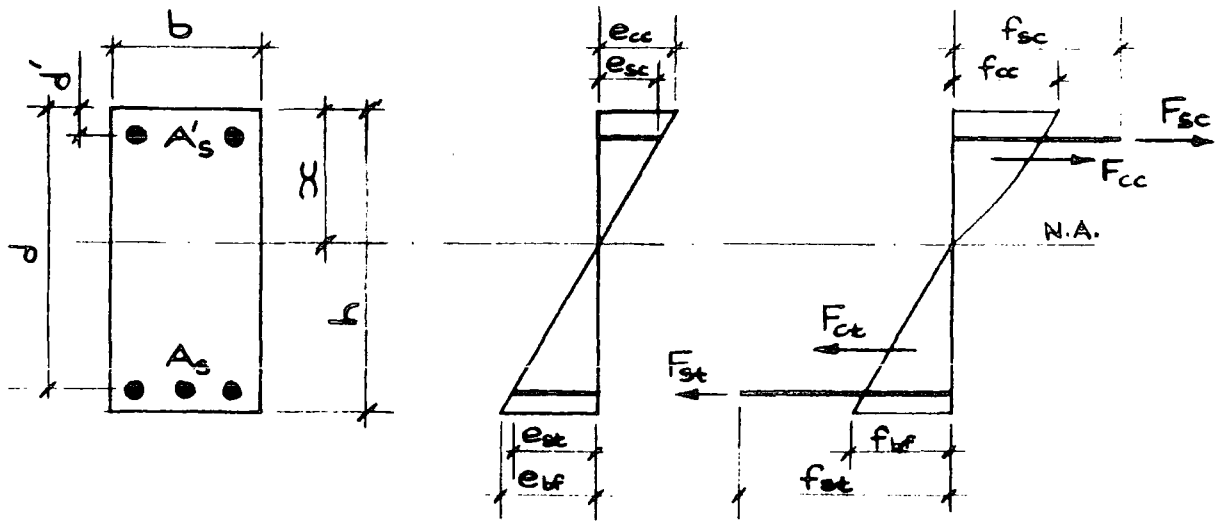

TENSILE CONCRETE CAN BE IGNORED COMPLETELY (AT THE USER'S DISCRETION)

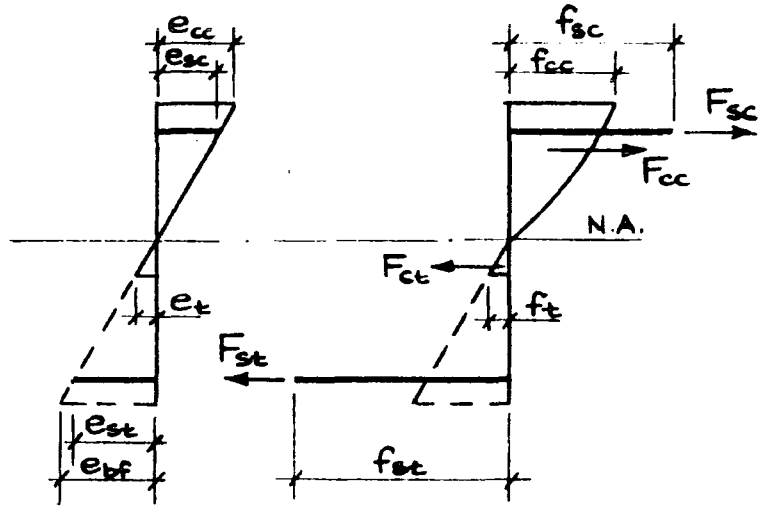

Fig 4.2 : PROGRAM NOMENCLATURE

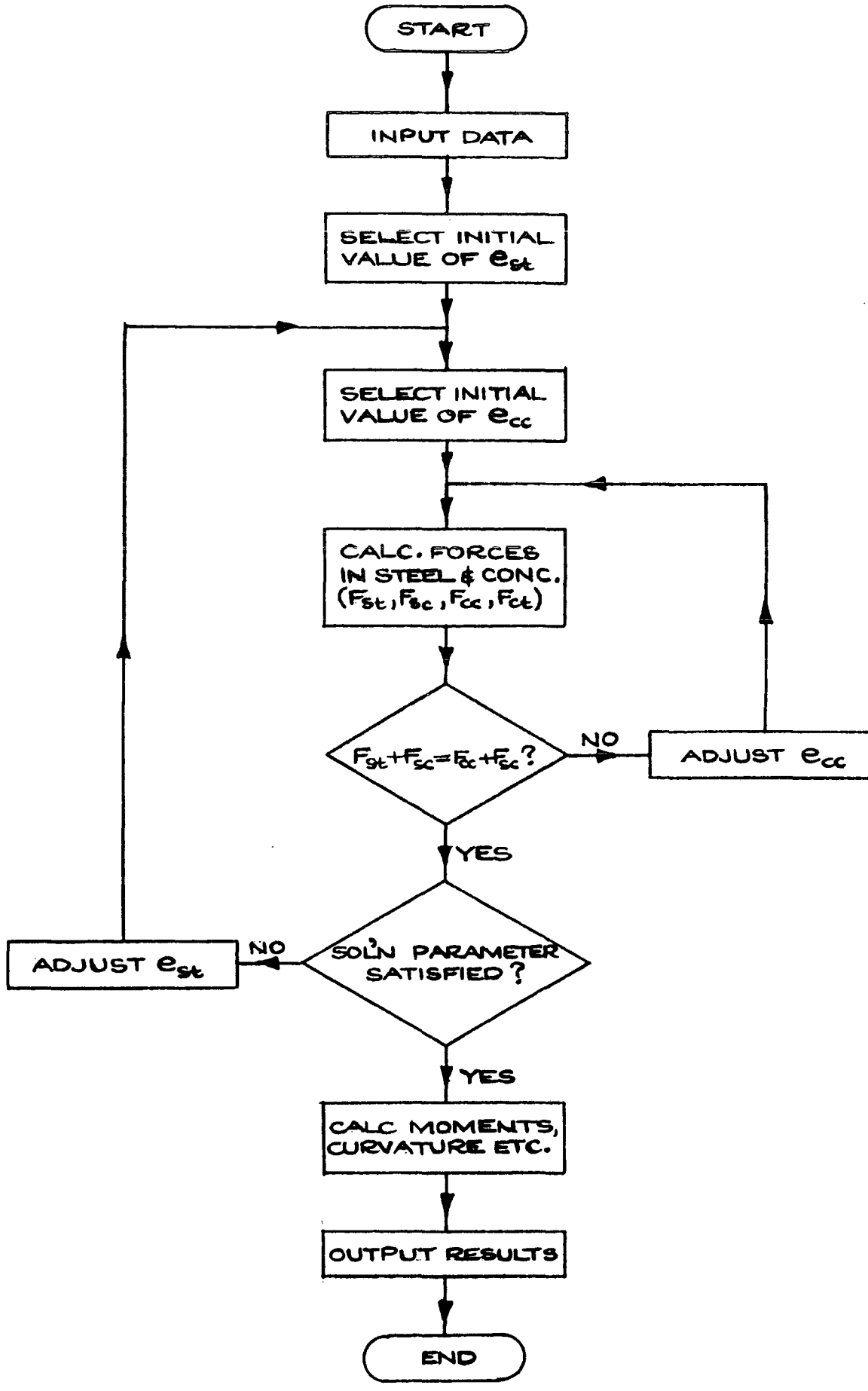

Fig 4.3: FLOWCHART FOR SECTION ANALYSIS

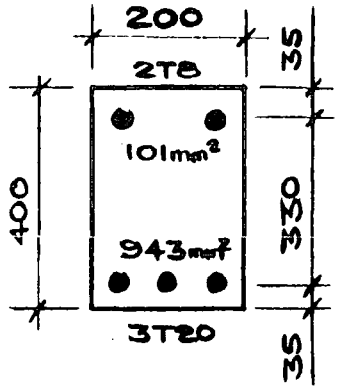

SECTION

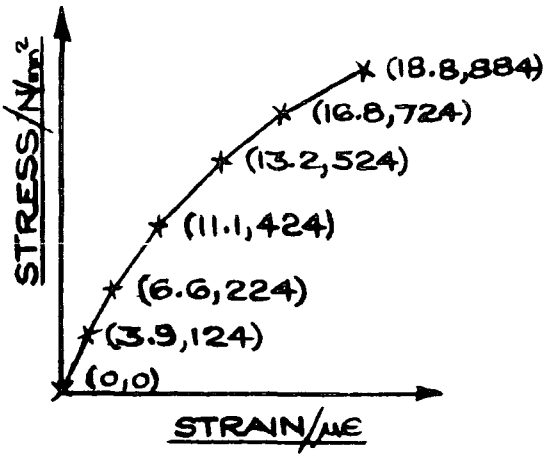

CONC. COMPRESSION

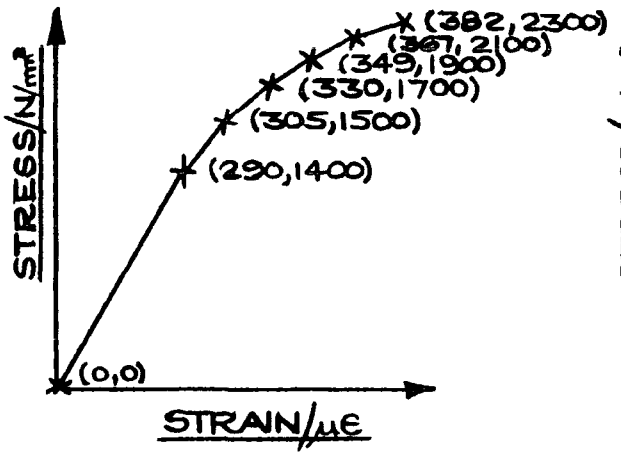

REINF. TENSION

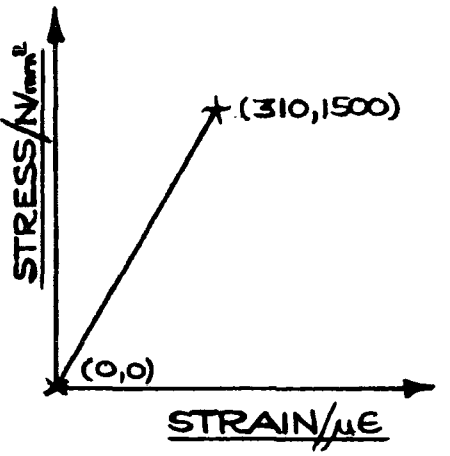

REINF. COMPRESSION

ALL DIMENSIONS IN mm
ALL DIAGRAMS N.T.S.
CONCRETE IN TENSION TO BE IGNORED
COORDS ARE (STRESS, STRAIN)

Fig 4.4 : PROGRAM INPUT DATA

DEMONSTRATION BEAM : 400*200 3T20 TENS (1.3%) 2T8 COMP
UNITS : N & MM
STRAINS ARE IN MICROSTRAIN

Fig 4.5: PROGRAM OUTPUT

SECTION PROPERTIES

OVERALL DEPTH	=	400.000
BREADTH	=	200.000
AREA OF TENSION REINF	=	943.000
COVER TO CENTRE OF TENSION REINF	=	35.000
AREA OF COMP REINF	=	101.000
COVER TO CENTRE OF COMP REINF	=	35.000

CONCRETE STRESS-STRAIN DATA (COMPRESSION)

STRESS	STRAIN
0.00	0.0
3.90	124.0
6.60	224.0
11.10	424.0
13.20	524.0
16.80	724.0
18.80	884.0

REINFORCEMENT STRESS-STRAIN DATA (TENSION)

STRESS	STRAIN
0.00	0.0
290.00	1400.0
305.00	1500.0
330.00	1700.0
349.00	1900.0
367.00	2100.0
382.00	2300.0

REINFORCEMENT STRESS-STRAIN DATA (COMPRESSION)

STRESS	STRAIN
0.00	0.0
310.00	1500.0
0.00	0.0
0.00	0.0
0.00	0.0
0.00	0.0
0.00	0.0

SHEET 1 OF 4

DEMONSTRATION BEAM : 400*200 3T20 TENS (1.3%) 2T8 COMP
UNITS : N & MM
STRAINS ARE IN MICROSTRAIN

STRAINS

	REINFORCEMENT TENSION	BOTTOM FACE	CONCRETE COMPRESSION	REINFORCEMENT COMPRESSION
1	315.51	360.84	157.23	111.89
2	1000.00	1147.71	540.43	392.72
3	1418.85	1631.61	800.00	587.23

LINE 1 : OUTPUT FOR MOMENT = 20.0 kNm
LINE 2 : OUTPUT FOR $\varepsilon_{st} = 1000\mu\varepsilon$
LINE 3 : OUTPUT FOR $\varepsilon_{sc} = 800\mu\varepsilon$

DEMONSTRATION BEAM : 400*200 3T20 TENS (1.3%) 2T8 COMP
UNITS : N & MM
STRAINS ARE IN MICROSTRAIN

STRESSES

	REINFORCEMENT TENSION	BOTTOM FACE	CONCRETE COMPRESSION	REINFORCEMENT COMPRESSION
1	65.36	0.00	4.80	23.12
2	207.14	0.00	13.50	81.18
3	292.83	0.00	17.75	121.36

DEMONSTRATION BEAM : 400*200 3T20 TENS (1.3%) 2T8 COMP
UNITS : N & MM
STRAINS ARE IN MICROSTRAIN

	NEUTRAL AXIS DEPTH	DEPTH IN TENSION BELOW NA	LEVER ARM	MOMENT	CURVATURE	EI
1	121.39	0.00	324.51	0.1999986000E+08	0.1295162000E-05	0.1544197000E+14
2	128.05	0.00	320.63	0.6262968000E+08	0.4220357000E-05	0.1483990000E+14
3	131.60	0.00	318.80	0.8803343000E+08	0.6079035000E-05	0.1448148000E+14

DEMONSTRATION BEAM : 400*200 3T20 TENS (1.3%) 2T8 COMP
UNITS : N & MM
STRAINS ARE IN MICROSTRAIN

MOMENTS ABOUT NA

	REINF TENSION	CONCRETE COMP	CG FROM NA	CONCRETE TENSION	CG FROM NA	REINF COMP
1	0.1501348000E+08	0.4784600000E+07	0.8067E+02	0.0000000000E+00	0.0000E+00	0.2017828000E+06
2	0.4628418000E+08	0.1558271000E+08	0.8327E+02	0.0000000000E+00	0.0000E+00	0.7627862000E+06
3	0.8445019000E+08	0.2239915000E+08	0.8488E+02	0.0000000000E+00	0.0000E+00	0.1184075000E+07

SHEET 3 OF 4

DEMONSTRATION BEAM : 400*200 3T20 TENS (1.3%) 2T8 COMP
UNITS : N & MM
STRAINS ARE IN MICROSTRAIN

FORCES

	REINF TENSION	CONCRETE COMP	CONCRETE TENSION	REINF COMP	SUM
1	0.61630190000E+05	0.59294280000E+05	0.00000000000E+00	0.23356080000E+04	-.30078130000E-01
2	0.19533570000E+06	0.18713800000E+06	0.00000000000E+00	0.81973200000E+04	-.37500000000E+00
3	0.27613600000E+06	0.26388010000E+06	0.00000000000E+00	0.12257520000E+05	0.15625000000E+01

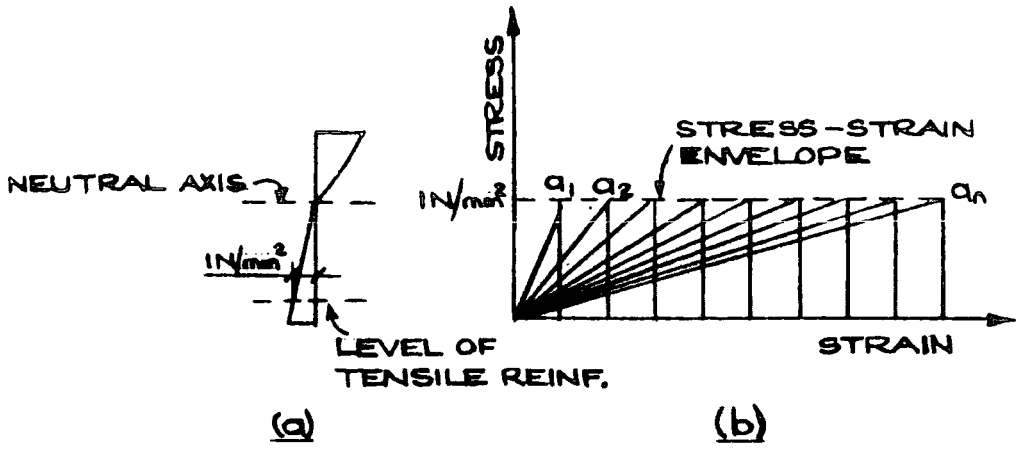

Fig 5.1 : CP110 STRESS DISTRIBUTIONS
(a) IN CONCRETE OVER FULL DEPTH OF SECTION
(b) IN CONCRETE IN TENSION

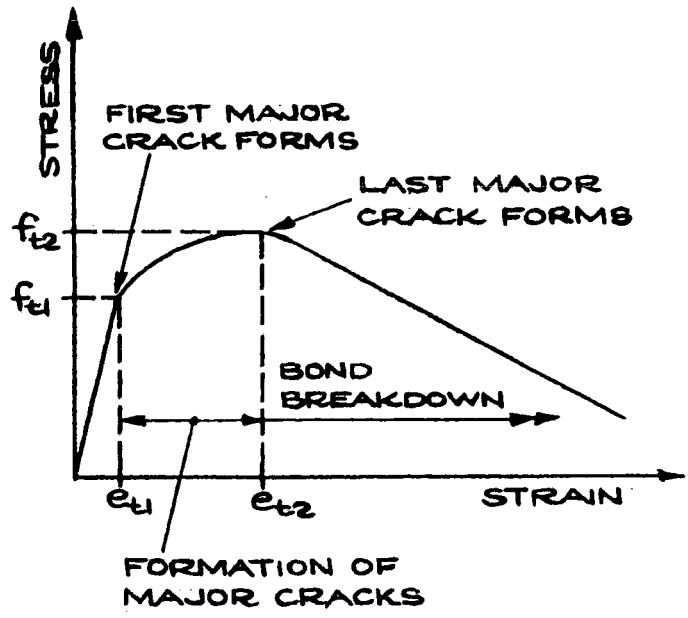

Fig 5.2 : THEORETICAL CONCRETE STRESS-STRAIN RELATIONSHIP ON BOTTOM FACE OF SECTION

			Bottom steel					Top steel			
Beam No.	Width (mm)	Depth (mm)	No. of bars	Diameter (mm)	Area (mm^2)	Depth (mm)	Amount (%)	No. of bars	Diameter (mm)	Area (mm^2)	Depth (mm)
1	203	410	3	25	1472	380	1.91	2	16	402	37
2	202	412		25	1472	368	1.99		16	402	35
3	203	408		20	943	363	1.28		8	101	20
4	204	408		20	943	367	1.26		8	101	24
5	204	407		16	603	373	0.79		8	101	33
6	204	409		16	603	376	0.79		8	101	34
7	204	409		12	339	379	0.44		8	101	35
8	204	406		12	339	370	0.45		8	101	38
9	203	204		16	603	167	1.78		12	226	26
10	202	202		16	603	169	1.77		12	226	28
11	203	306		16	603	268	1.11		8	101	30
12	203	308		16	603	273	1.09		8	101	30
13	203	513		16	603	480	0.62		8	101	37
14	204	511		16	603	473	0.63		8	101	32

Fig. 6.1 : Details of Test Beams
(After Clark & Speirs : Ref 20)

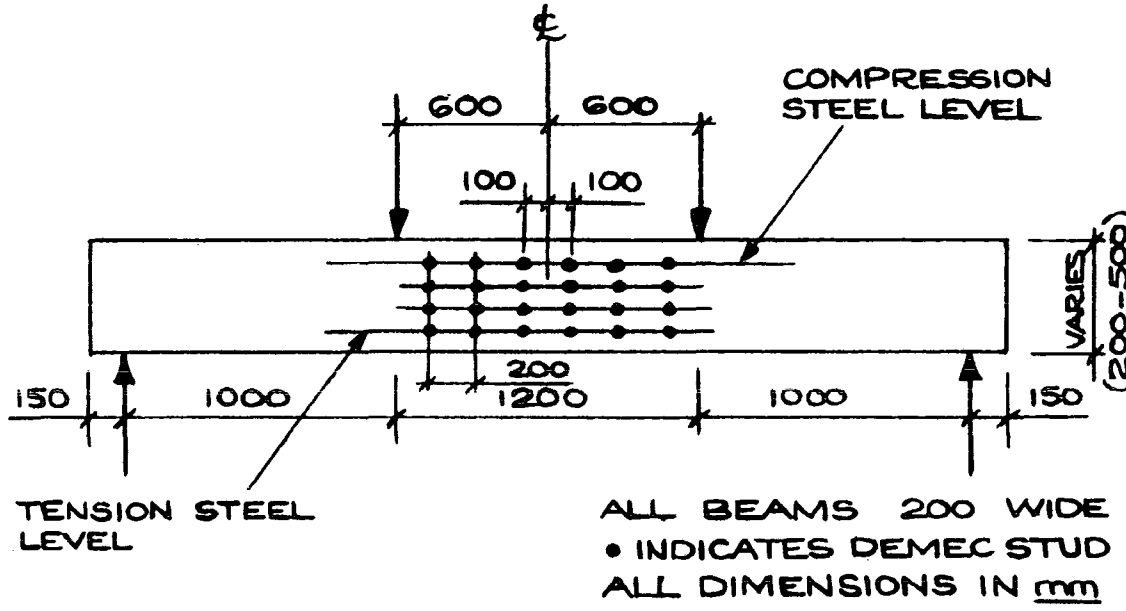

Fig 6.2: LAYOUT OF TEST BEAMS
(After Clark & Speirs : Ref 20)

Beam No.	Age at Test (Days)	Cube Strength (N/mm^2)	Indirect Tensile Strength (N/mm^2)
1	24	33.8	2.08
2	28	34.7	2.78
3	21	33.3	2.12
4	23	39.6	2.74
5	21	38.1	3.05
6	22	36.5	2.51
7	33	28.9	2.17
8	22	31.1	2.31
9	41	29.3	2.18
10	27	35.3	3.19
11	28	26.3	2.64
12	29	34.1	2.88
13	28	23.0	2.05
14	24	29.3	2.18

Fig 6.3 : Test Results for Control Specimens

C&CA BEAM 1 3Y25 TENS 2Y16 COMP 1.91% TENS REINF 416 X 283 N&MM
LOAD STAGE 13 44.33 KN A

DEMEC READINGS

COL 1	COL 2	COL 3	COL 4	COL 5
768.18	833.28	845.00	812.00	821.50
843.50	916.20	834.80	846.10	846.00
829.60	899.10	846.90	864.30	870.00
948.00	885.20	851.80	895.20	891.20

Fig 6.4: TYPICAL PAGE OF DEMEC OUTPUT

UNITS : N & mm
STRAINS IN MICROSTRAIN

STRAINS

COL 1	COL 2	COL 3	COL 4	COL 5	COLS 234	COLS 12345
-228.31	-199.87	-218.04	-210.93	-209.35	-209.61	-213.30
-15.50	-45.82	-21.33	-34.76	-23.70	-33.97	-28.28
261.40	170.64	169.06	168.27	177.75	169.32	189.44
513.50	349.18	334.17	392.53	364.90	358.66	390.89

REGRESSION LINE PARAMETERS

M	-2.28	-1.63	-1.62	-1.77	-1.69	-1.67	-1.79
C	576.18	398.75	393.24	435.62	416.42	409.20	444.44

RESULTS CALCULATED FROM REGRESSION LINES

	COL 1	COL 2	COL 3	COL 4	COL 5	COLS 234	COLS 12345	AV 234	AV 12345
NA DEPTH	147.55	166.08	167.29	163.39	162.14	165.52	160.45	145.58	161.29
E TOP	-323.91	-271.49	-271.04	-288.61	-273.71	-277.05	-285.75	-277.05	-285.75
E LINE 1	-242.60	-211.01	-211.09	-223.25	-211.25	-215.12	-219.86	-215.12	-219.86
E LINE 2	7.58	-24.65	-26.39	-21.86	-18.83	-24.31	-16.83	-24.31	-16.83
E LINE 3	257.86	161.71	156.32	179.49	173.64	166.51	186.20	166.51	186.20
E LINE 4	508.13	348.07	343.02	380.86	346.08	357.32	389.23	357.32	389.23
E REINF	518.32	349.71	344.64	382.62	367.77	356.99	391.01	358.99	391.01
E BOTTOM	576.18	398.75	393.24	435.62	416.42	409.20	444.44	409.20	444.44

CURVATURE 0.163474E-05 0.176641E-05 0.167378E-05 0.167378E-05
0.219536E-05 0.162819E-05 0.168810E-05 0.178096E-05 0.178096E-05

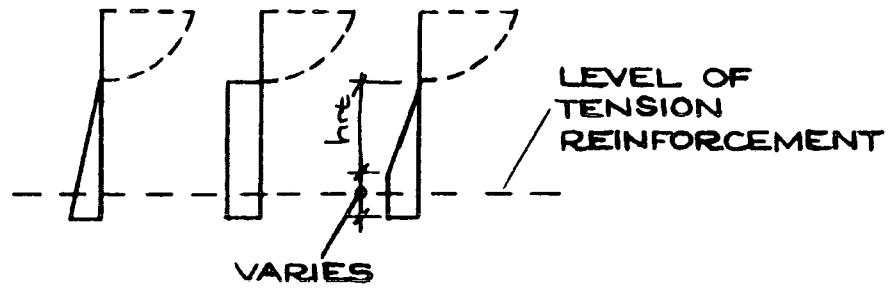

Fig 7.1: TRIAL STRESS BLOCK SHAPES
(a) TRIANGULAR
(b) RECTANGULAR
(c) RECTANGULAR - TRIANGULAR

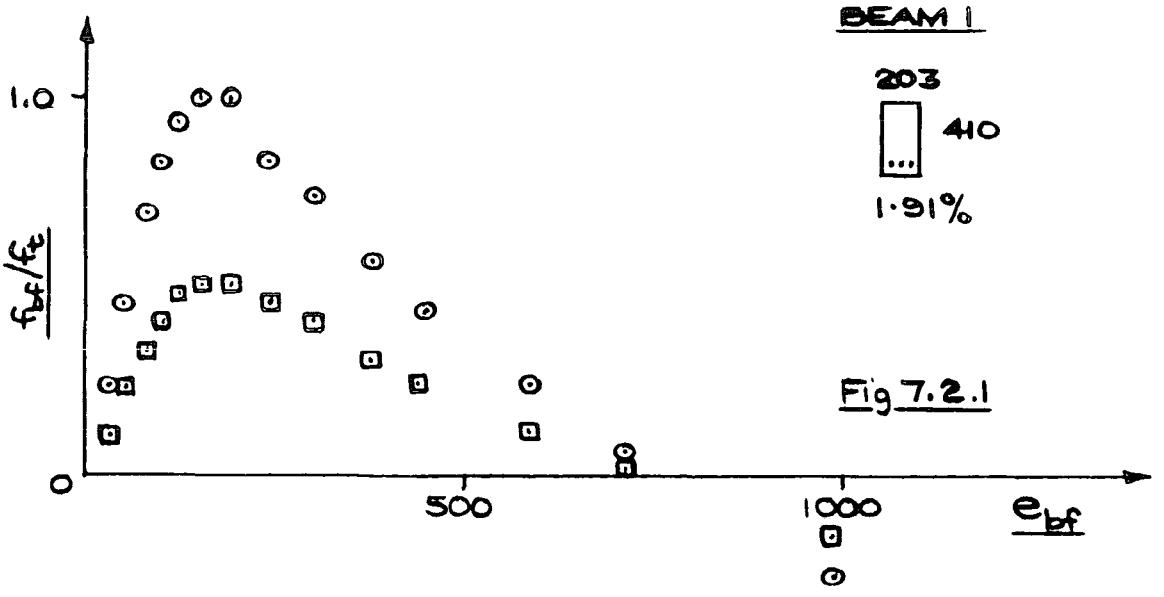

Fig 7.2.1

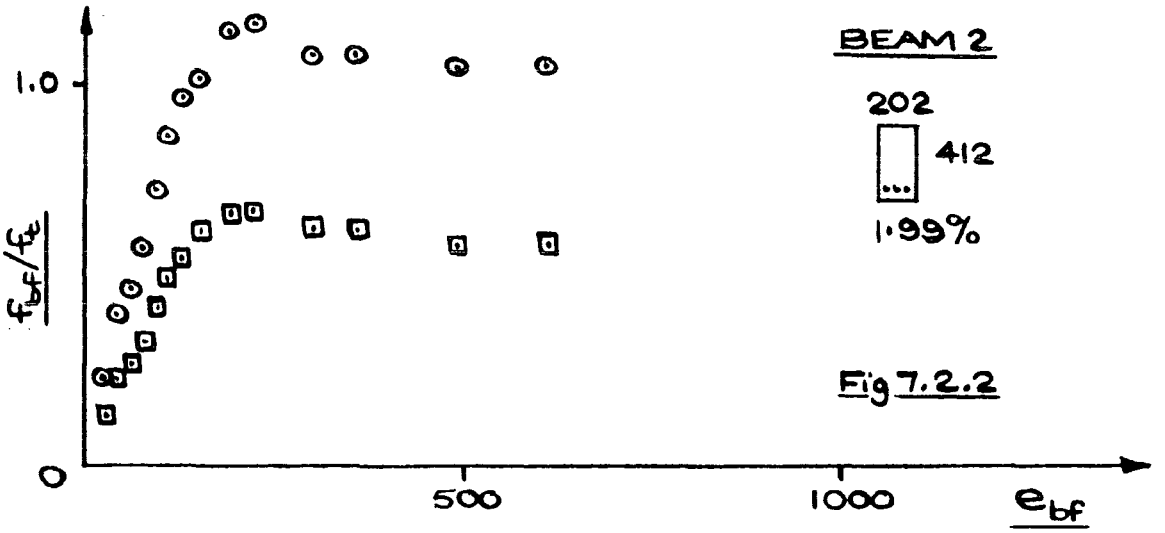

Fig 7.2.2

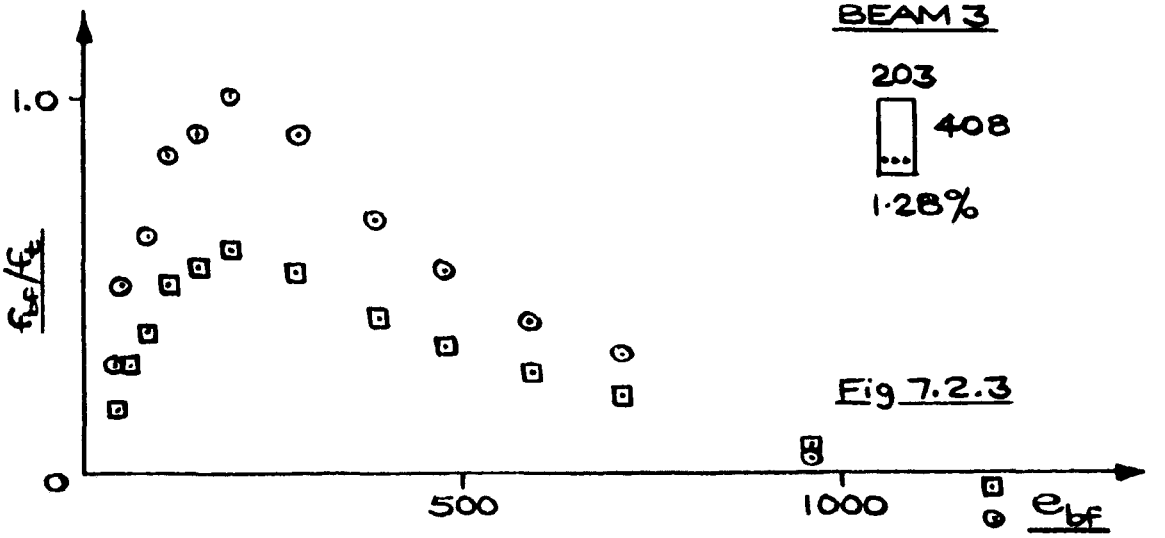

Fig 7.2.3

e_{bf} – MICROSTRAIN ⊙-TRIANGULAR ⊡-RECTANGULAR STRESS BLOCK

RELATIONSHIPS BETWEEN f_{bf}/f_t & e_{bf}

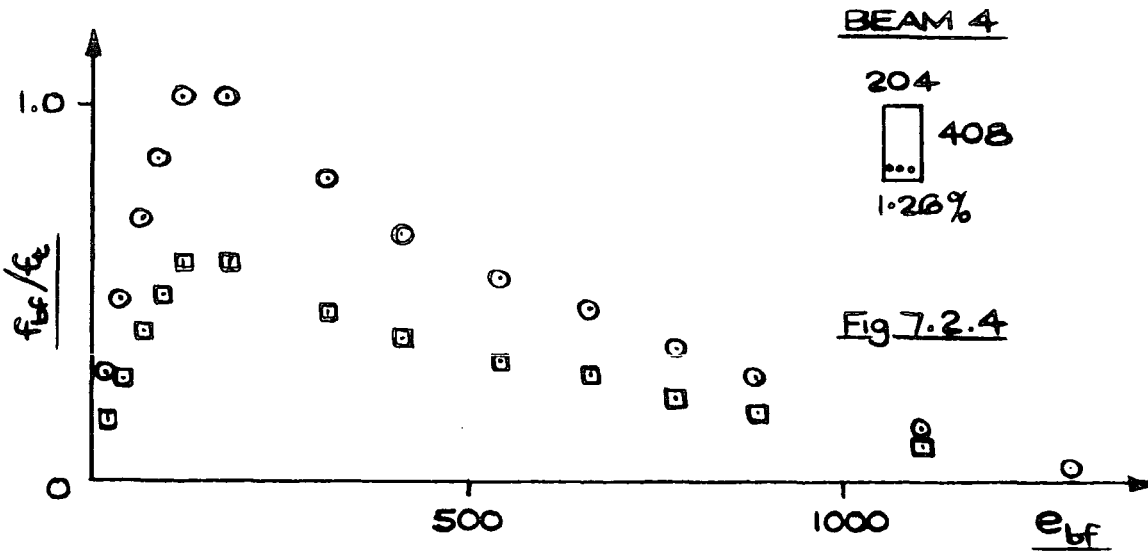

Fig 7.2.4

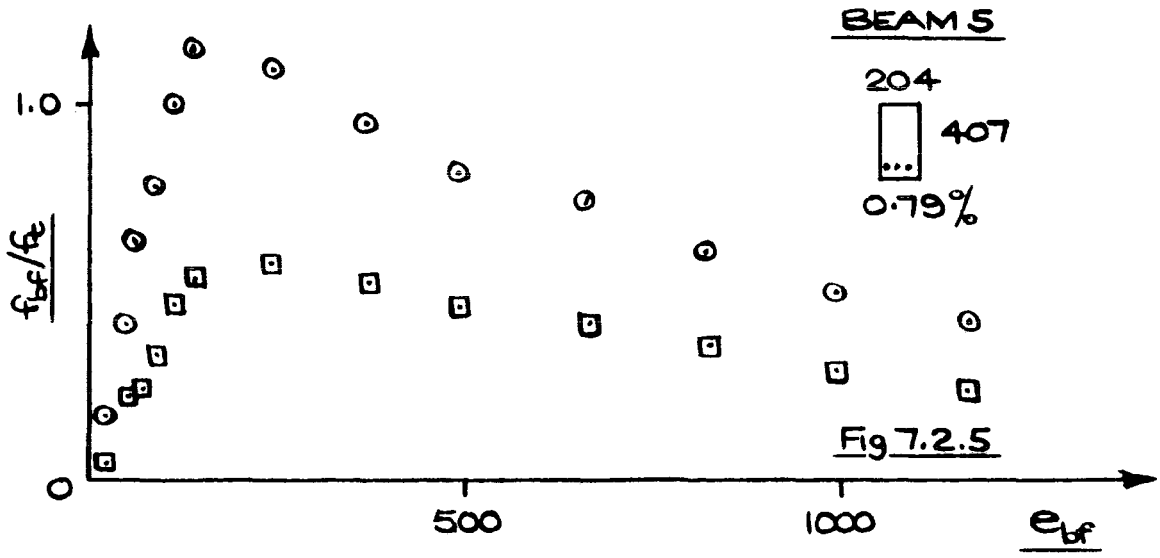

Fig 7.2.5

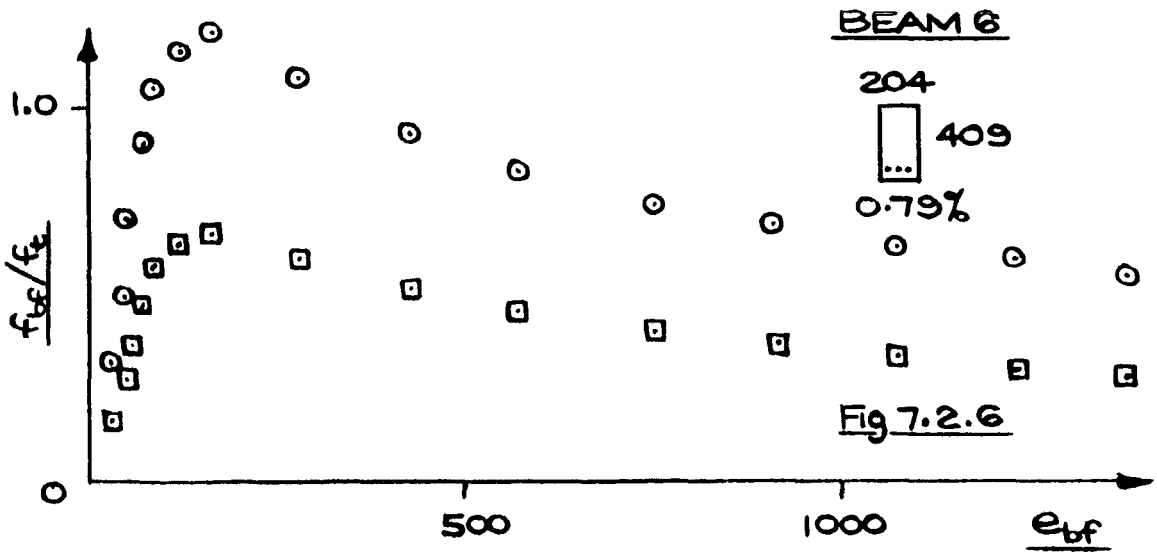

Fig 7.2.6

e_{bf} - MICROSTRAIN ⊙ - TRIANGULAR ⊡ - RECTANGULAR STRESS BLOCK

RELATIONSHIPS BETWEEN f_{bf}/f_t & e_{bf}

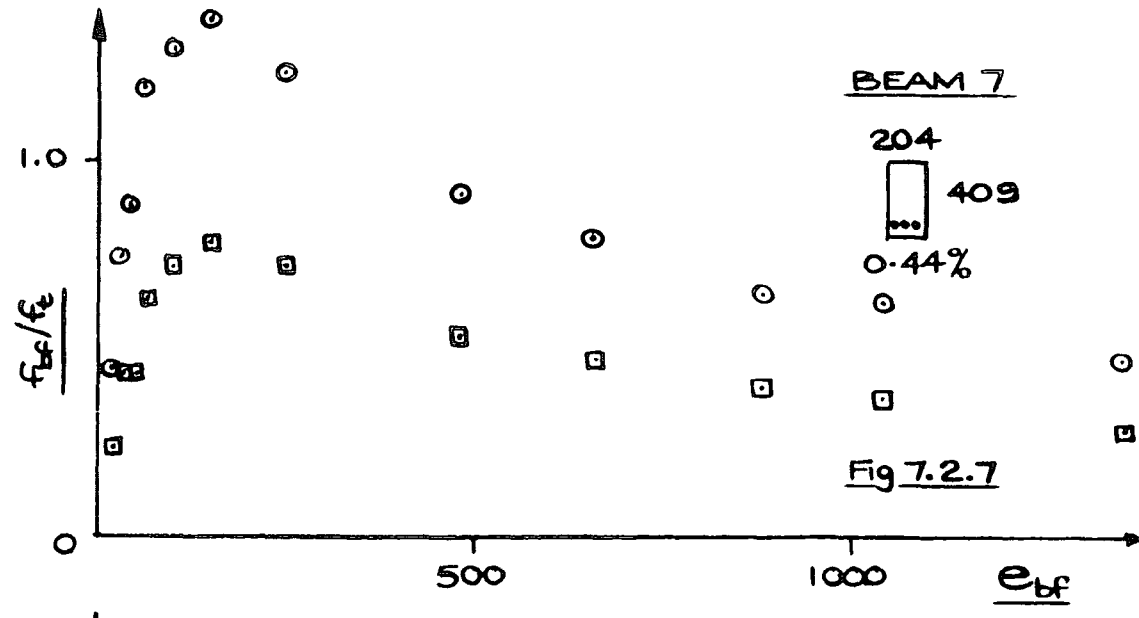

Fig 7.2.7

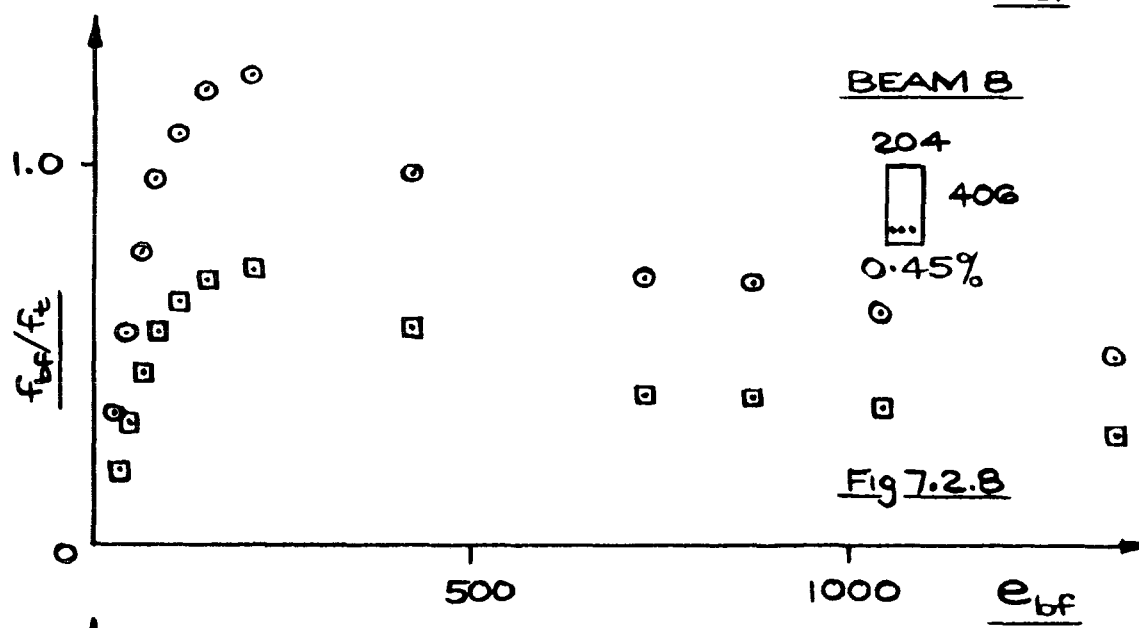

Fig 7.2.8

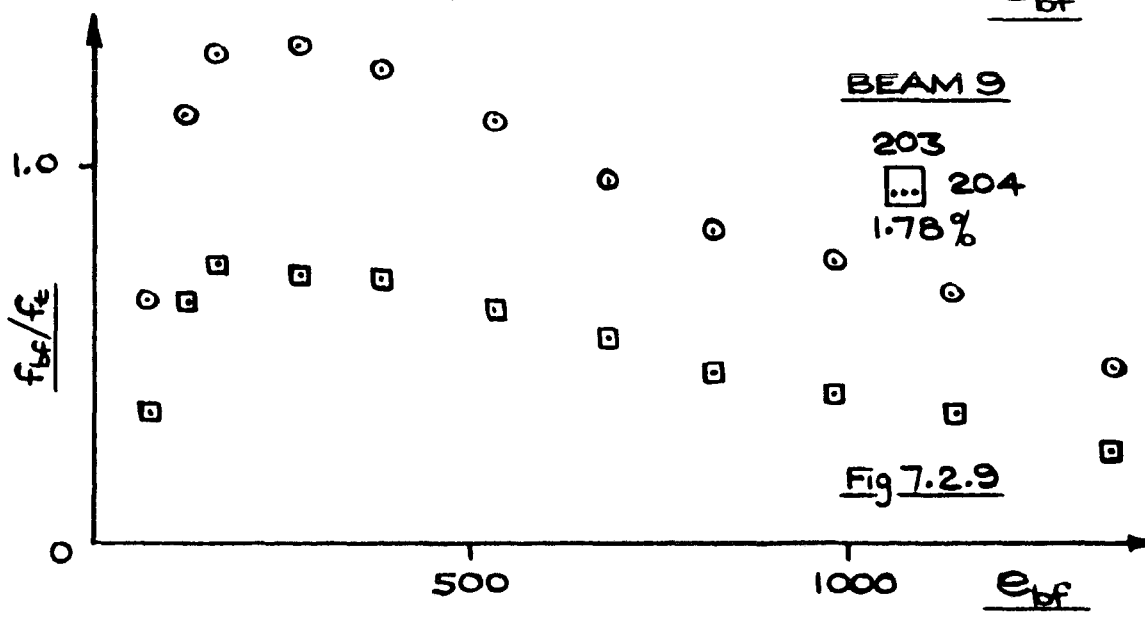

Fig 7.2.9

e_{bf} - MICROSTRAIN ⊙ - TRIANGULAR ⊡ - RECTANGULAR STRESS BLOCK

RELATIONSHIPS BETWEEN f_{bf}/f_t & e_{bf}

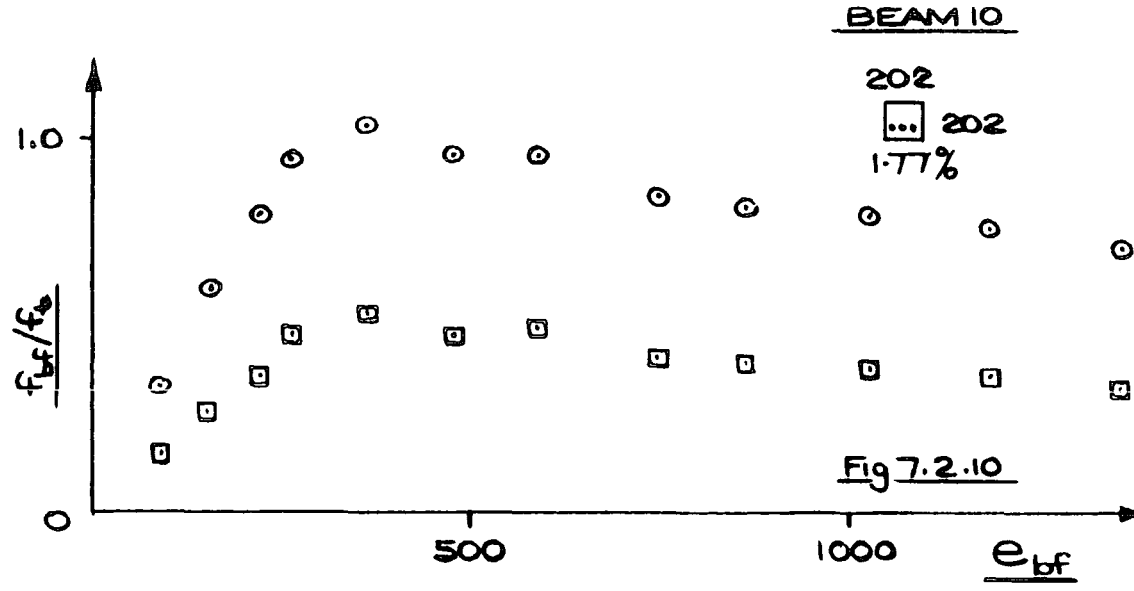

Fig 7.2.10

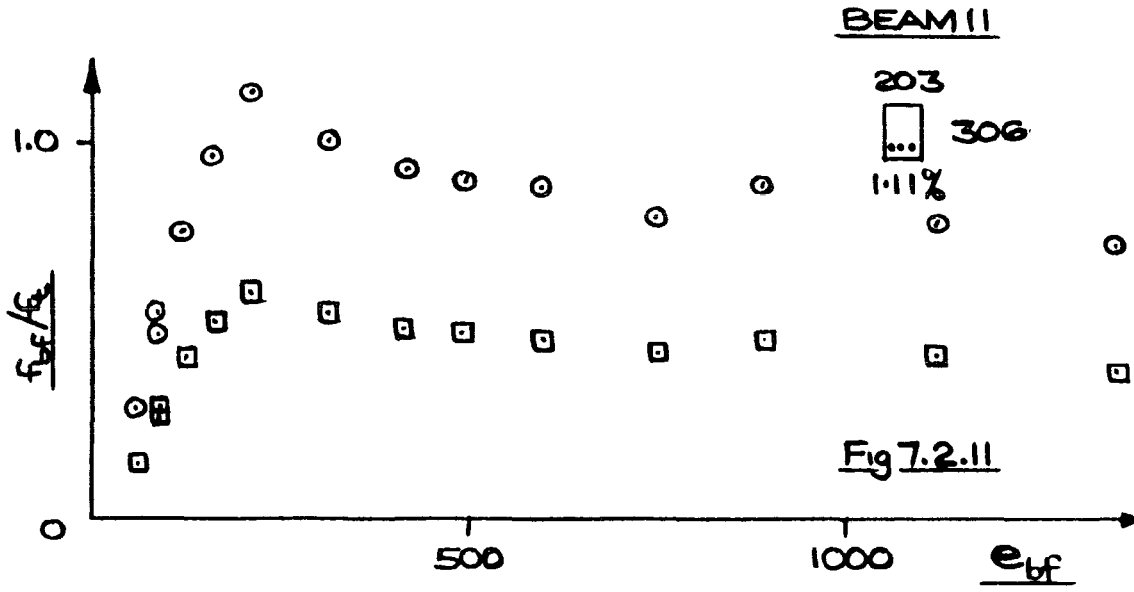

Fig 7.2.11

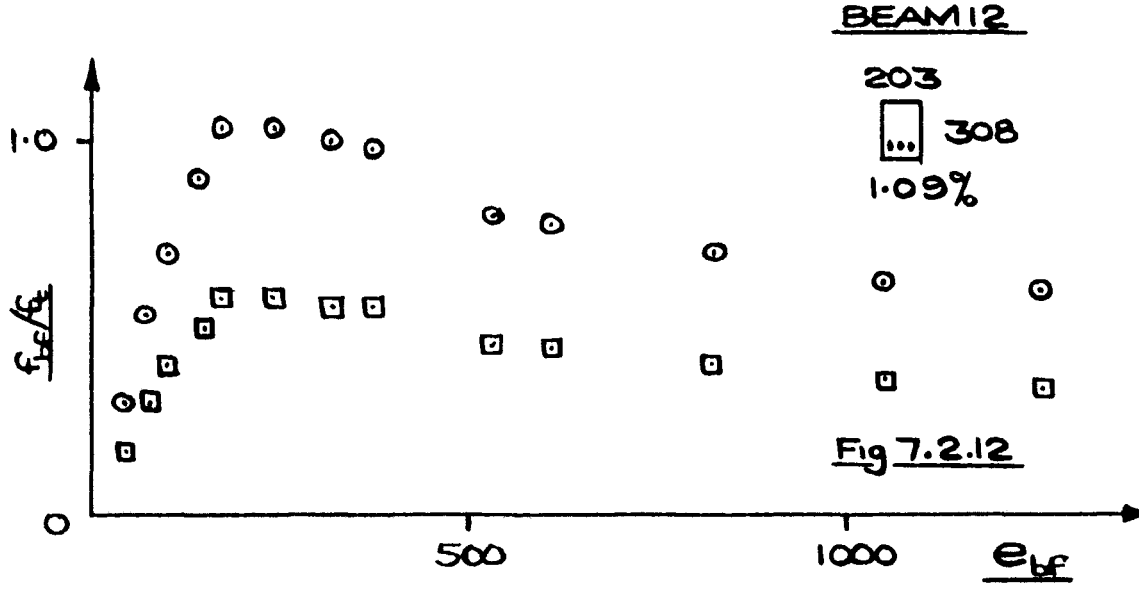

Fig 7.2.12

e_{bf} - MICROSTRAIN ⊙ - TRIANGULAR ⊡ - RECTANGULAR STRESS BLOCK

RELATIONSHIPS BETWEEN f_{bf}/f_t & e_{bf}

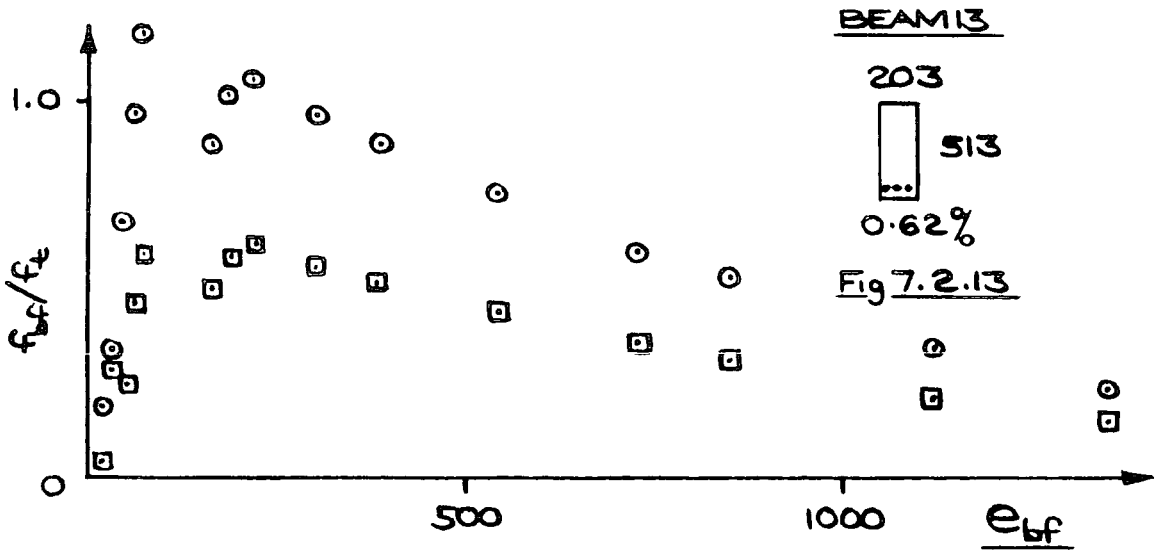

Fig 7.2.13

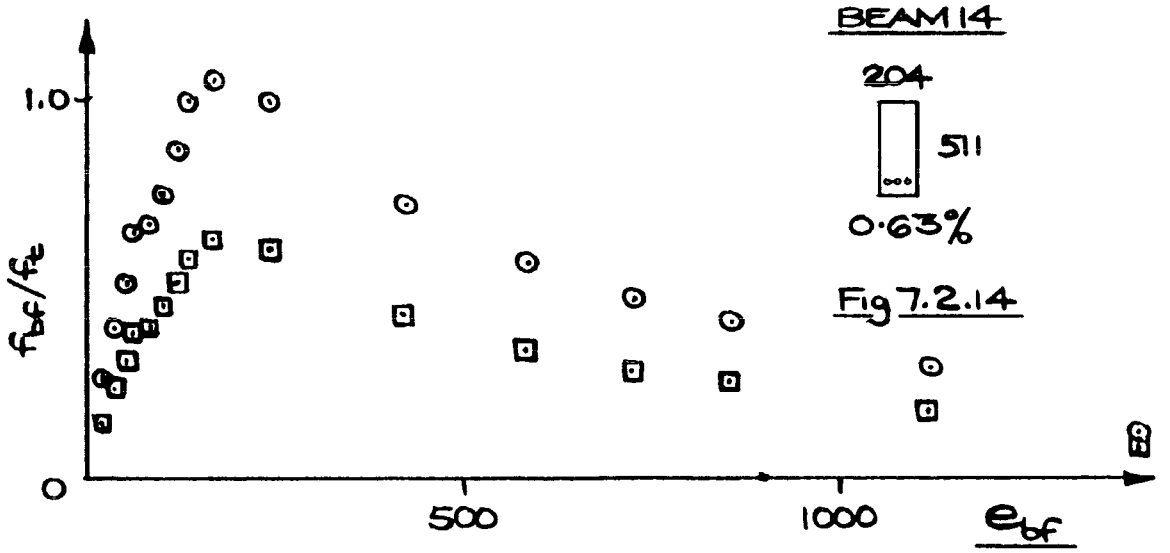

Fig 7.2.14

e_{bf} - MICROSTRAIN ⊙ - TRIANGULAR ⊡ - RECTANGULAR STRESS BLOCK

RELATIONSHIPS BETWEEN f_{bf}/f_t & e_{bf}

Beam No.	% Tension Reinf.	e_{t1} microstrain	e_{t2} microstrain	f_{t1}/f_t	f_{t2}/f_t
1	1.91	116	144	0.94	0.99
2	1.99	104	222	0.87	1.17
3	1.28	86	280	0.63	0.90
4	1.26	63	176	0.70	1.02
5	0.79	55	240	0.64	1.09
6	0.79	86	277	1.06	1.08
7	0.44	42	482	0.88	0.92
8	0.45	58	205	0.77	1.24
9	1.78	117	160	1.14	1.31
10	1.77	217	359	0.79	1.04
11	1.11	87	210	0.49	1.13
12	1.09	70	170	0.54	1.03
13	0.62	70	302	1.18	0.96
14	0.63	80	240	0.66	1.00

Fig. 7.3 : Stresses & Strains for First and Last Cracks

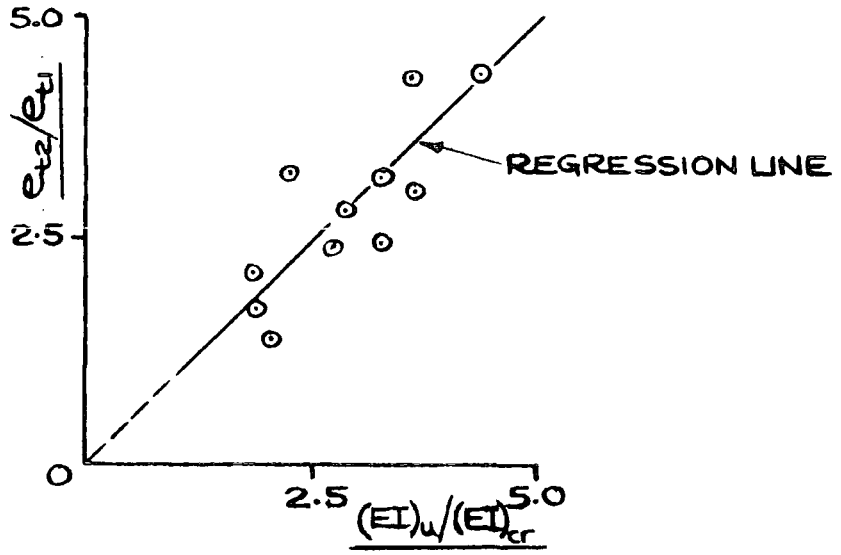

Fig 7.4: RELATIONSHIP BETWEEN e_{t2}/e_{t1} & $(EI)_u/(EI)_{cr}$

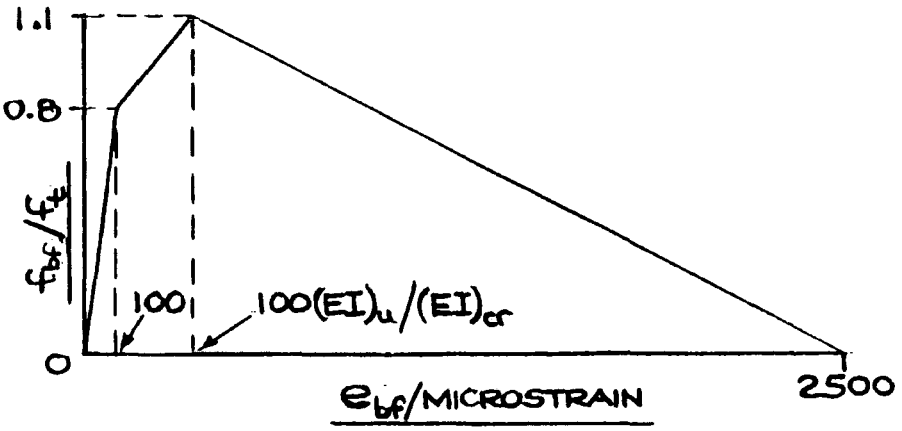

Fig 7.5: PROPOSED STRESS-STRAIN ENVELOPE FOR DESIGN

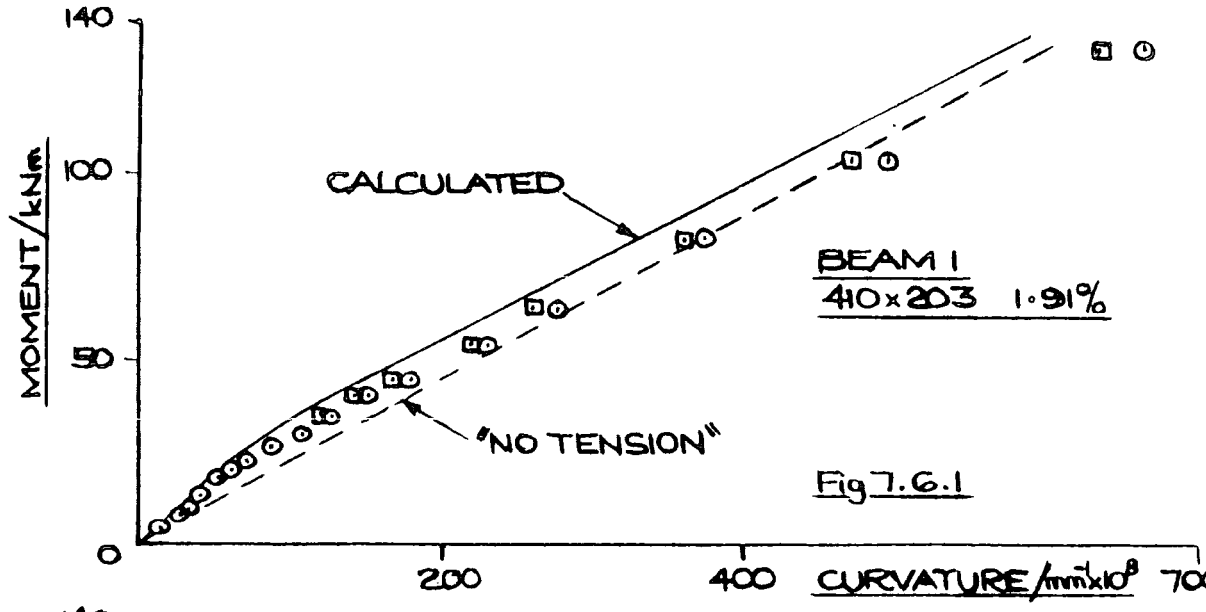

Fig 7.6.1

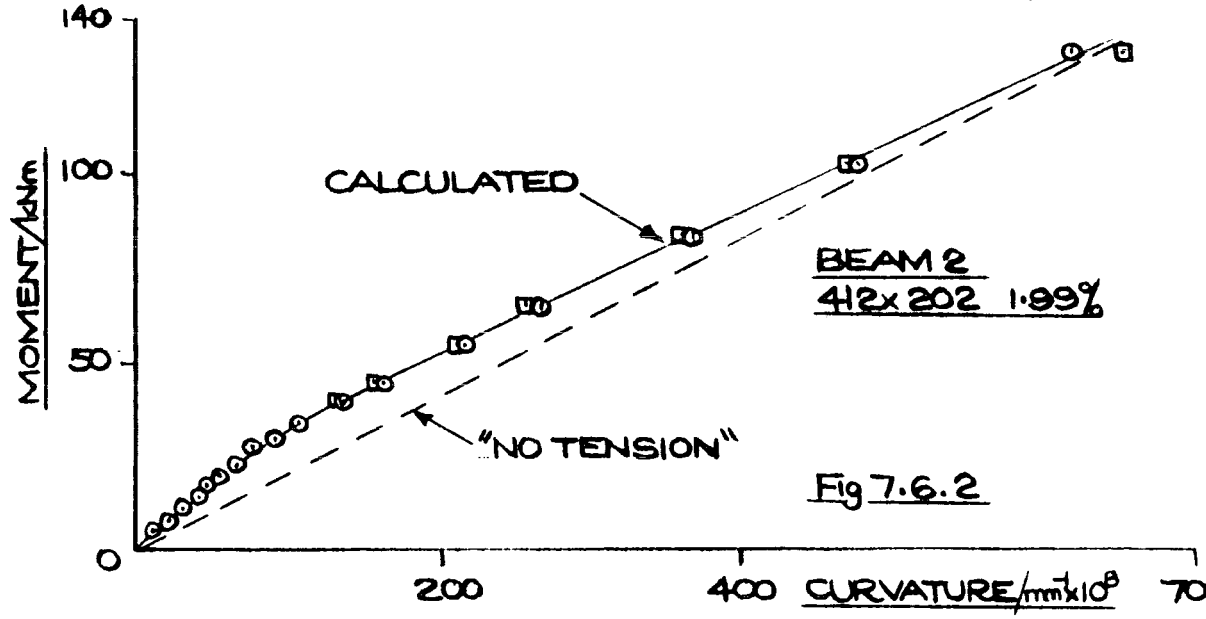

Fig 7.6.2

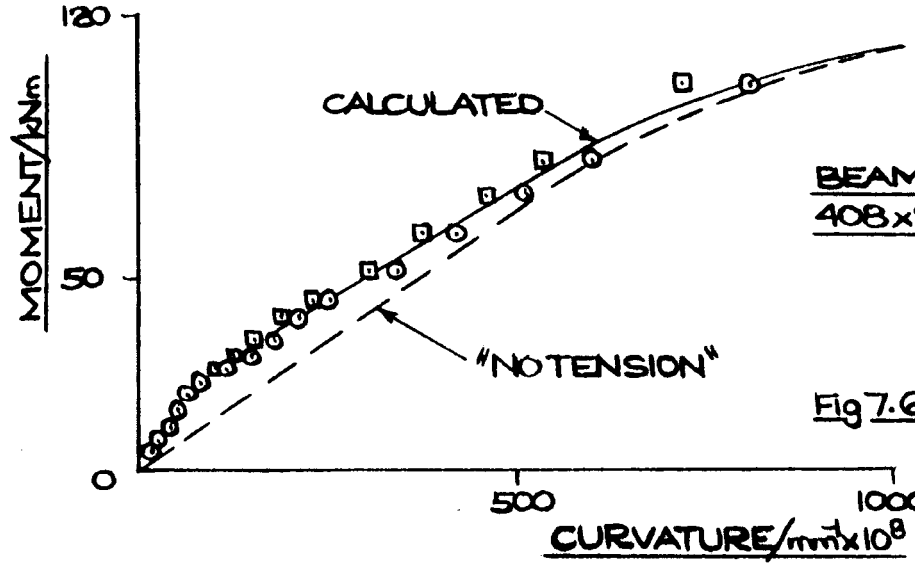

Fig 7.6.3

⊙ – 5 COLS DEMECS ⊡ – 3 COLS DEMECS

MOMENT–CURVATURE RELATIONSHIPS

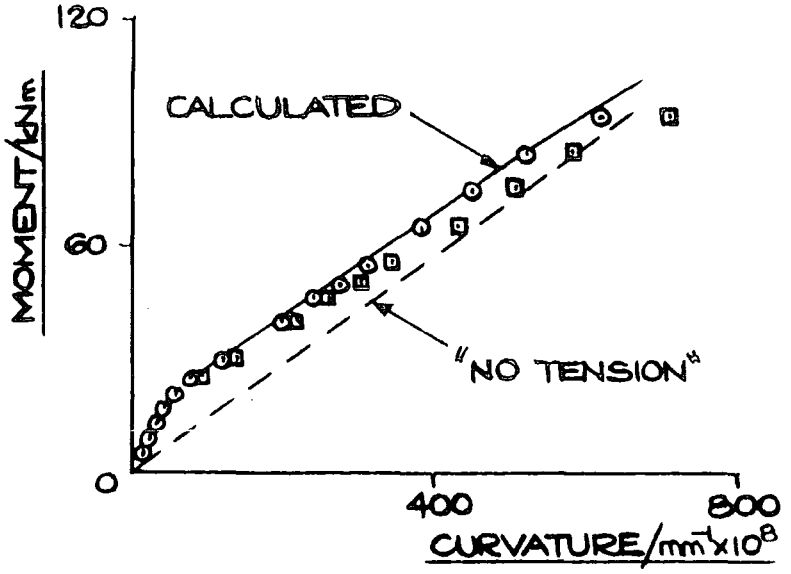

BEAM 4
408x204 1·26%

Fig 7.6.4

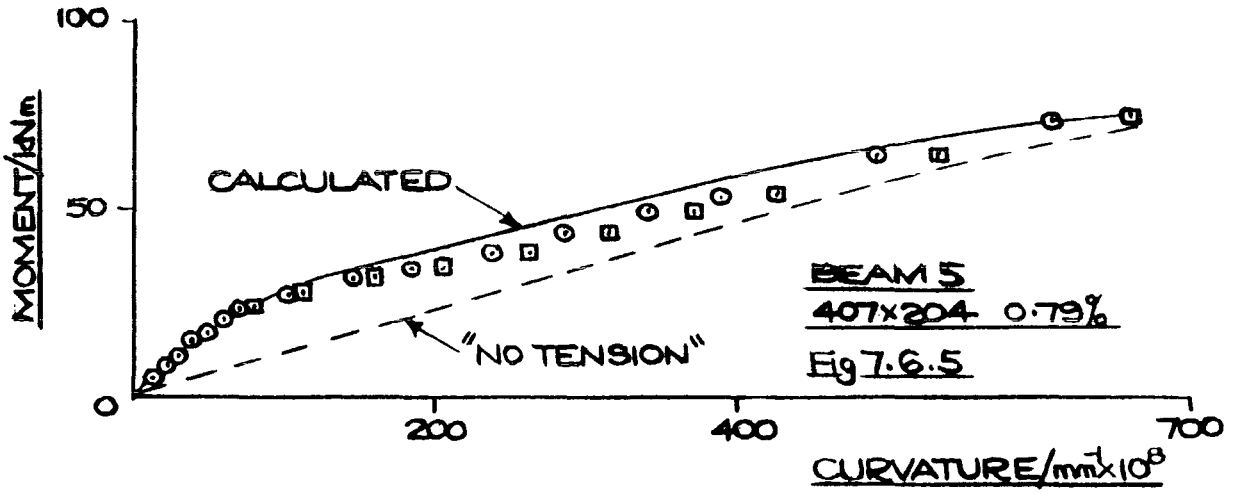

BEAM 5
407x204 0·79%

Fig 7.6.5

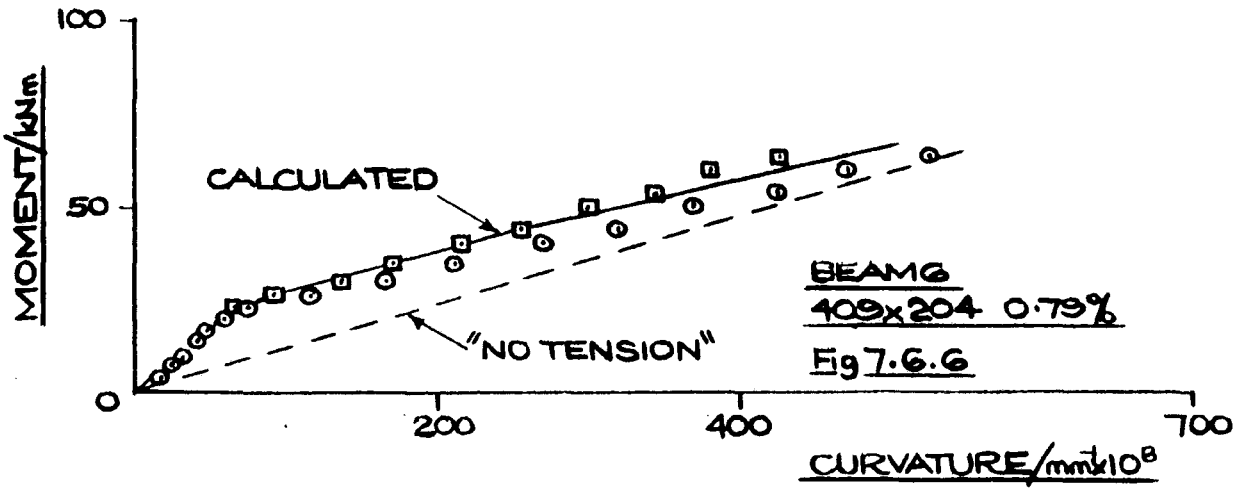

BEAM 6
409x204 0·79%

Fig 7.6.6

⊙ - 5 COLS DEMECS ⊡ - 3 COLS DEMECS

MOMENT - CURVATURE RELATIONSHIPS

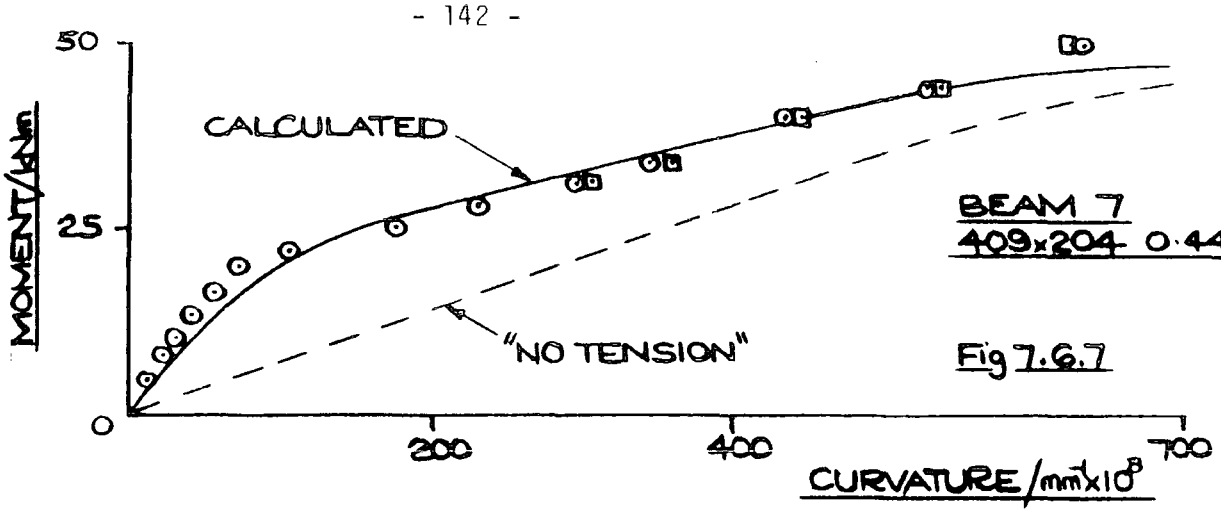

BEAM 7
409x204 0.44

Fig 7.6.7

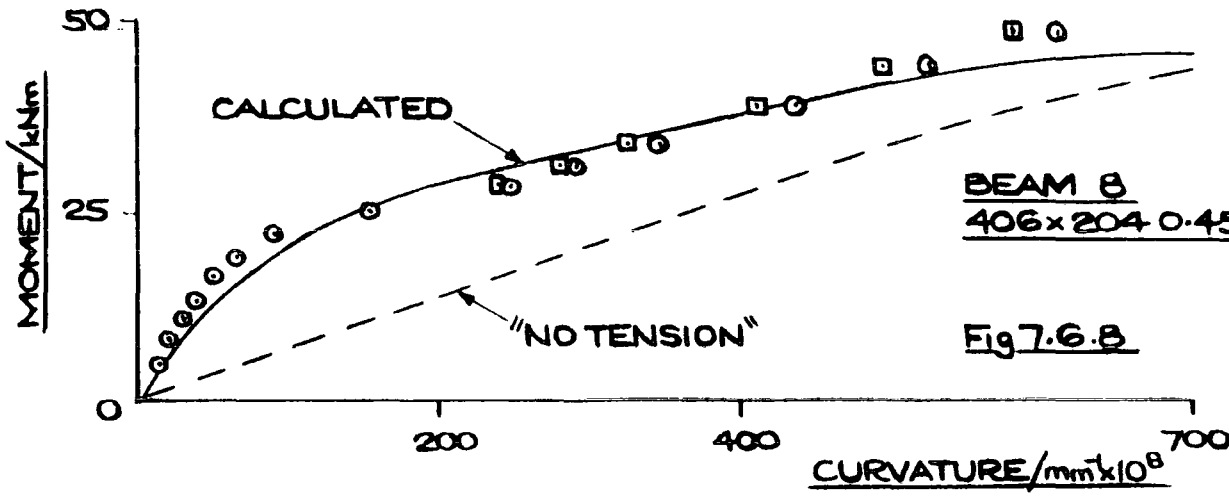

BEAM 8
406x204 0.45

Fig 7.6.8

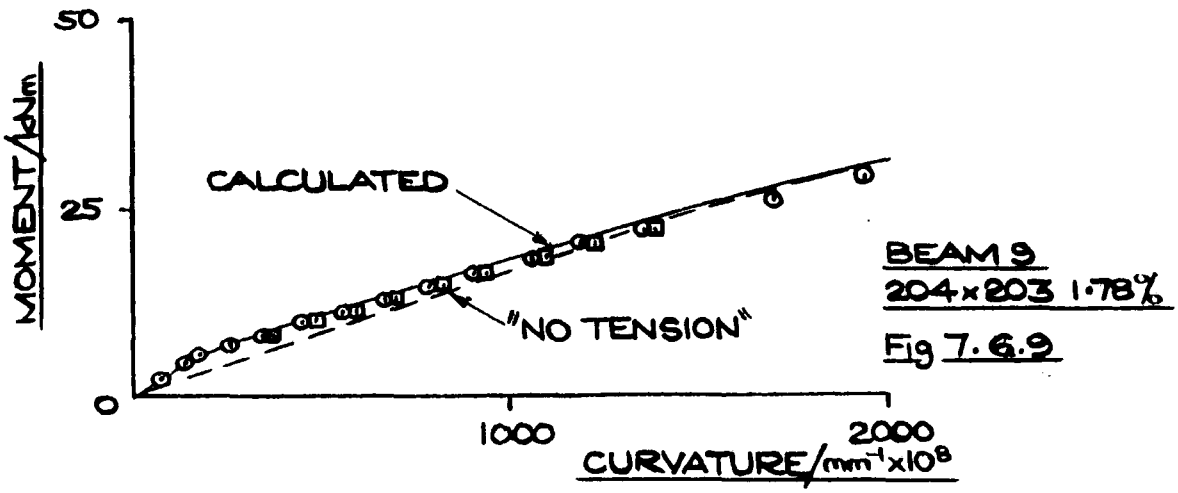

BEAM 9
204x203 1.78%

Fig 7.6.9

⊙ - 5 COLS DEMECS ⊡ - 3 COLS DEMECS

MOMENT-CURVATURE RELATIONSHIPS

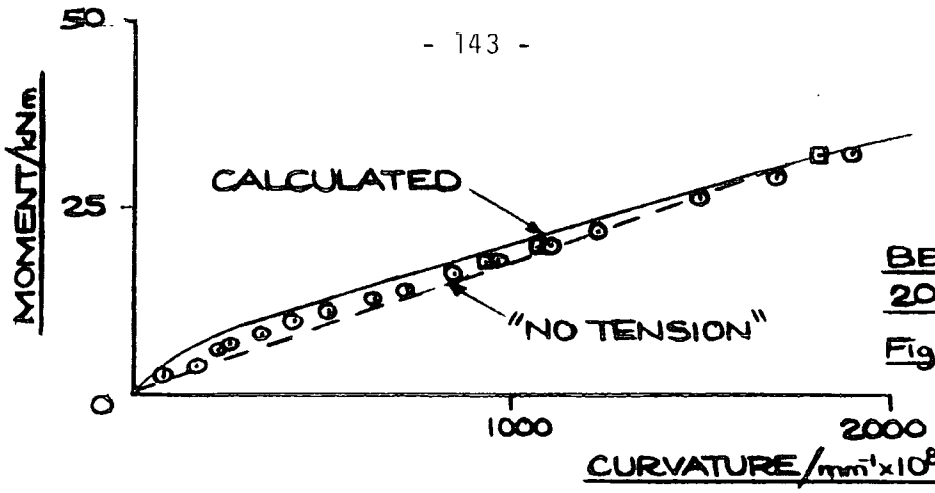

BEAM 10
202x202 1·77%

Fig 7.6.10

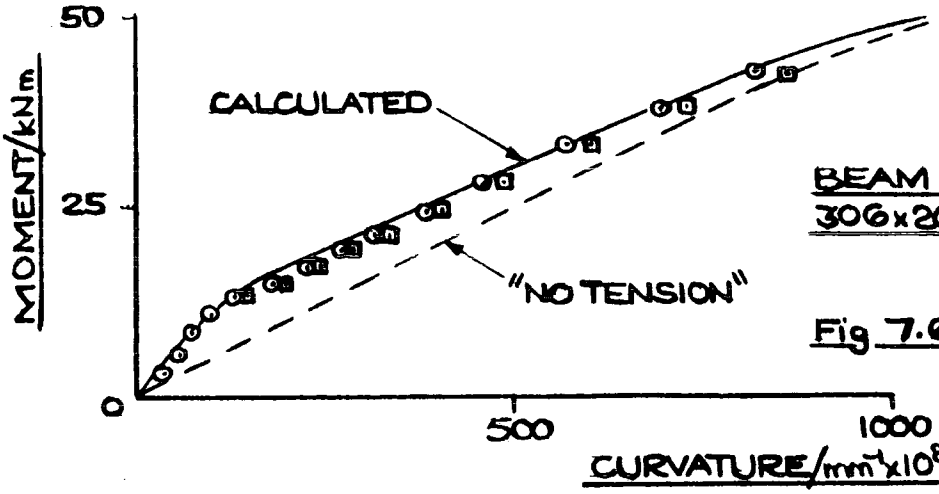

BEAM 11
306x203 1·11%

Fig 7.6.11

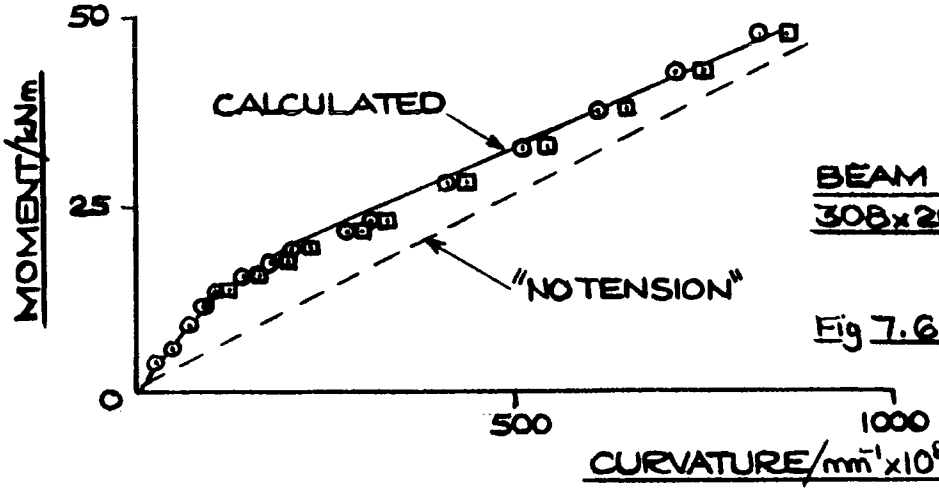

BEAM 12
308x203 1·09%

Fig 7.6.12

⊙ - 5 COLS DEMECS ⊡ - 3 COLS DEMECS

MOMENT-CURVATURE RELATIONSHIPS

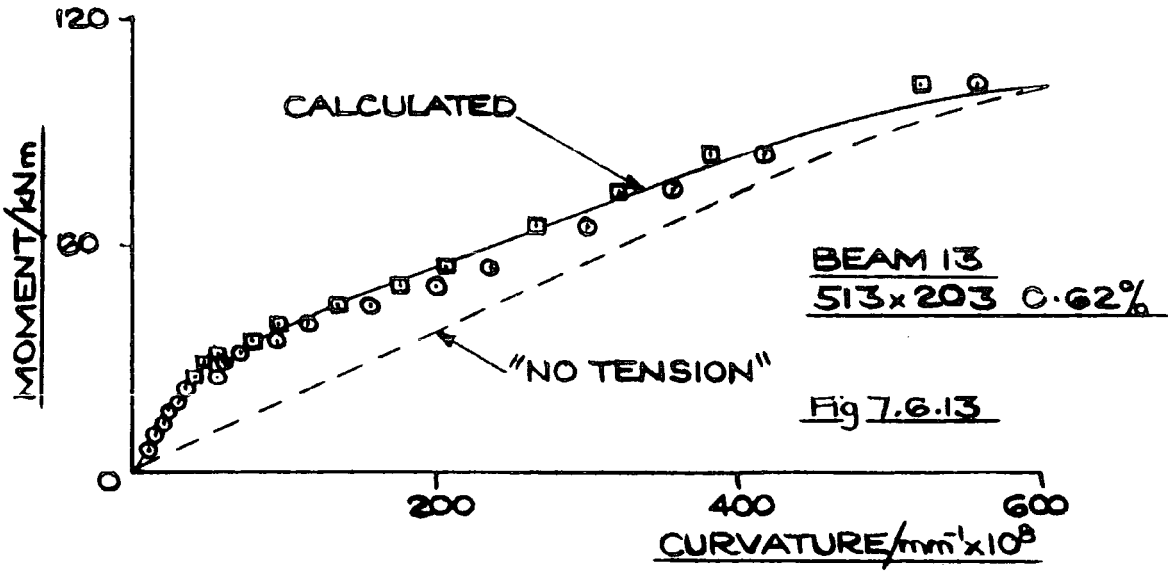

BEAM 13
513x203 0·62%

Fig 7.6.13

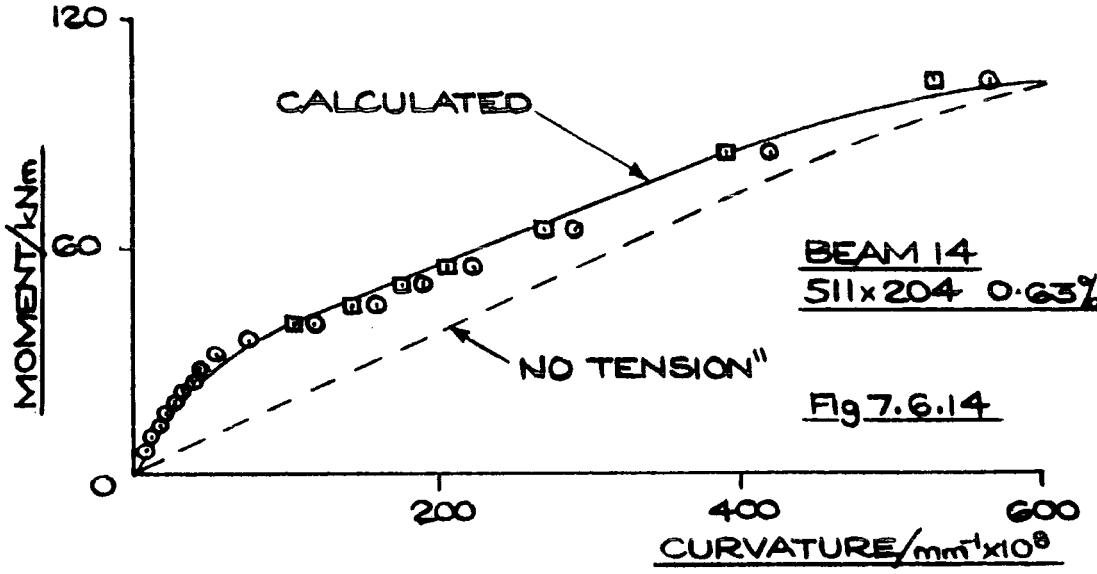

BEAM 14
511x204 0·63%

Fig 7.6.14

⊙- 5 COLS DEMECS ⊡-3 COLS DEMECS

MOMENT-CURVATURE RELATIONSHIPS

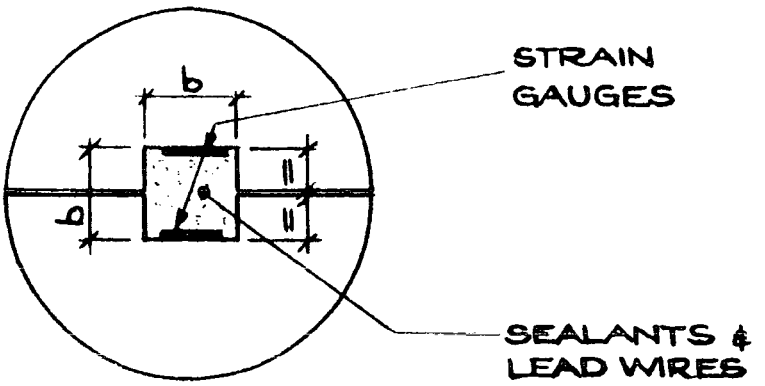

12mm DIA. RODS : b = 5mm
20mm DIA. RODS : b = 7mm

Fig 8.1 : SECTION THROUGH MILLED ROD

Figure 8.2: Strain Gauges & Wiring

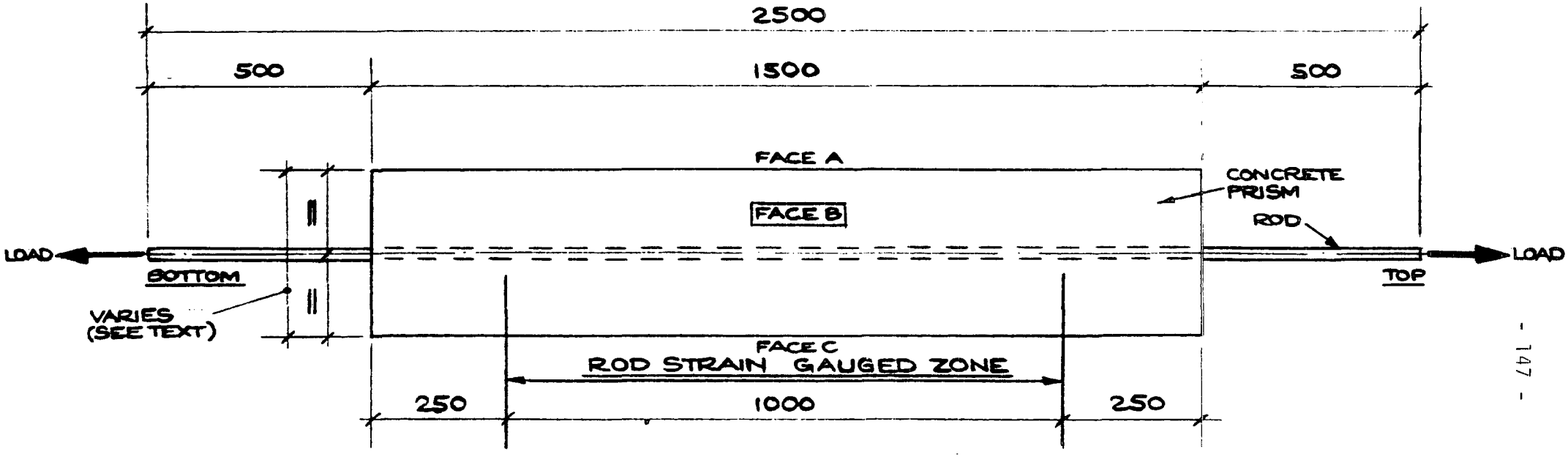

ELEVATION

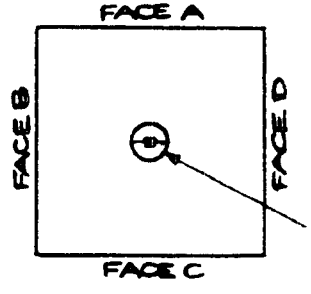

FACE A IS THE CAST FACE
ALL DIMENSIONS IN mm

R12, T12, R20 or T20
POSITIONED CENTRALLY

VIEW FROM TOP

Fig 9·1: LAYOUT OF TENSION SPECIMENS

SPECIMEN	CROSS-SECTION DIMS/(mm x mm)	ROD TYPE & DIA/(mm) [R-MILD T-TORBAR]	ROD AREA WITH DUCT/ (mm^2)	% REINF	ROD PERIMETER/ (mm)	EMBEDMENT GAUGES/ (YES/NO)	ORDER TESTED
70R12/1	71x70	R12	86	1·73	37·7	NO	3
70R12/2	72x70	R12	83	1·65	37·7	NO	11
70T12	71x71	T12	81	1·61	37·7	NO	4
100R12	103x101	R12	86	0·83	38·4	NO	1
100T12	103x101	T12	86	0·83	37·7	YES	9
100R20	104x101	R20	281	2·68	64·2	NO	5
100T20	104x101	T20	260	2·48	62·8	YES	7
140T12	141x141	T12	86	0·43	37·4	NO	10
140R20	140x142	R20	268	1·35	62·8	NO	6
140T20	141x142	T20	266	1·33	62·8	YES	8
150R12	150x150	R12	91	0·40	37·7	NO	2
200T20	200x200	T20	258	0·65	62·0	YES	12
300/100T20	300x100	T20	262	0·87	62·2	YES	14
100T12P	102x100	T12	86	0·84	37·7	NO	13

Fig 9.2: DETAILS OF TEST SPECIMENS

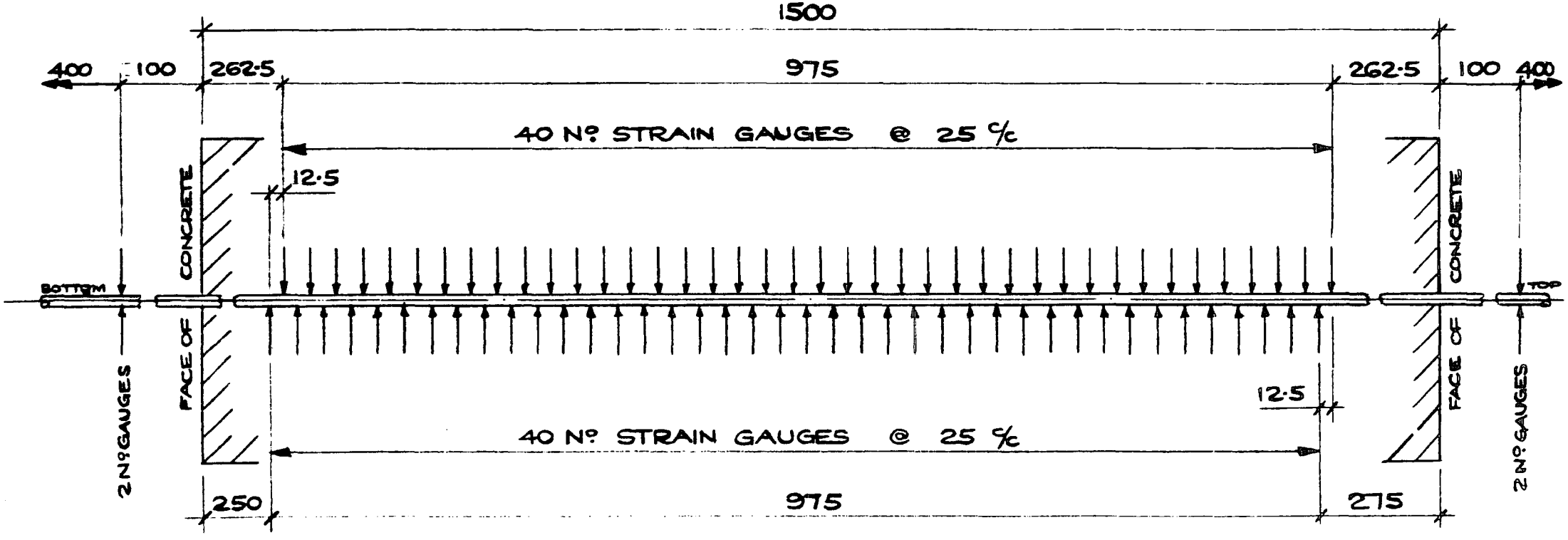

ROD LENGTH = 2500 c/c
84 Nº STRAIN GAUGES TOTAL

ALL DIMENSIONS IN mm
NOT TO SCALE

Fig 9.3: STANDARD ROD GAUGING LAYOUT

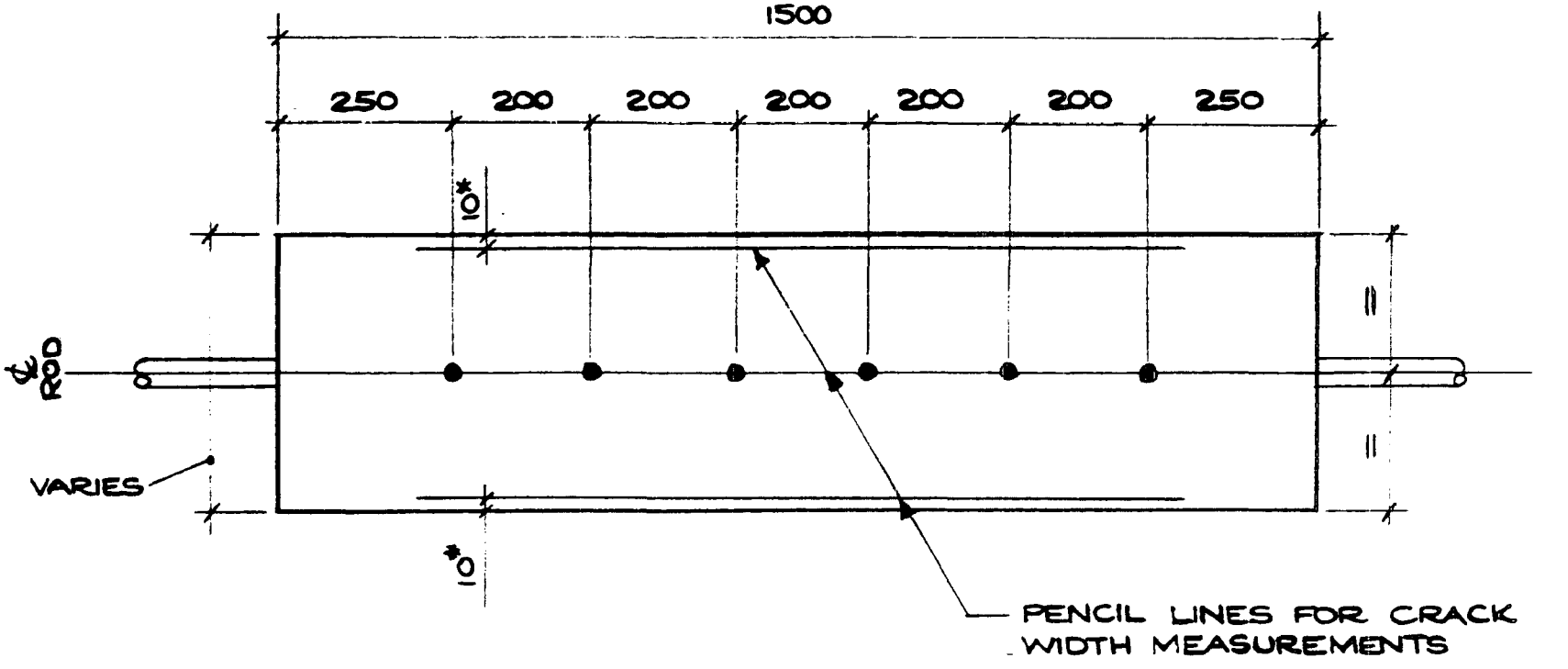

Fig 9.4: LAYOUT OF DEMEC STUDS & CRACK WIDTH LINES

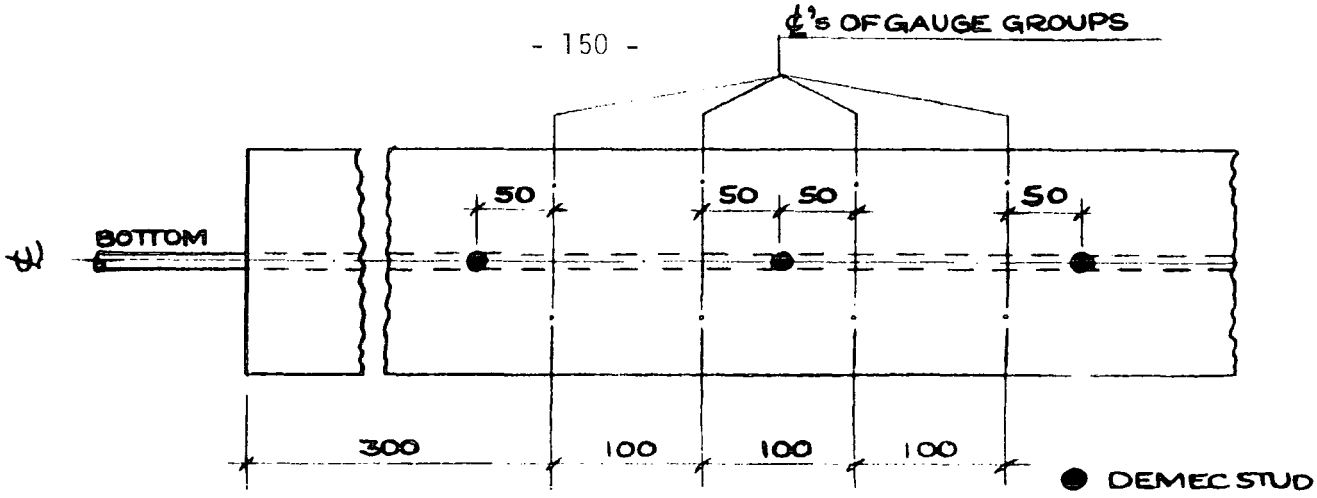

GAUGE GROUP LOCATIONS

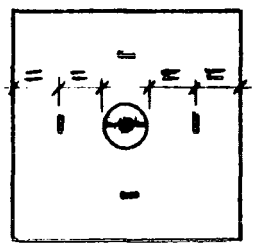

100T12 } 16Nº
100T20 }

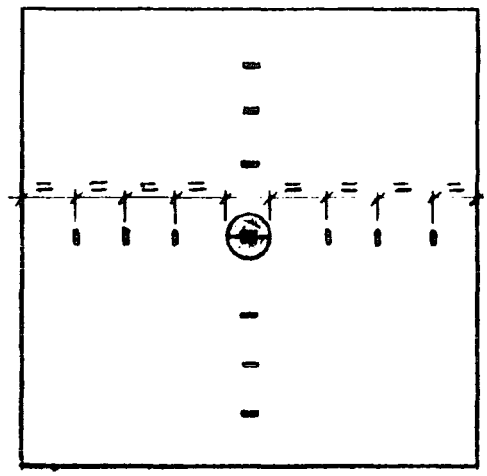

200T20 - 48Nº

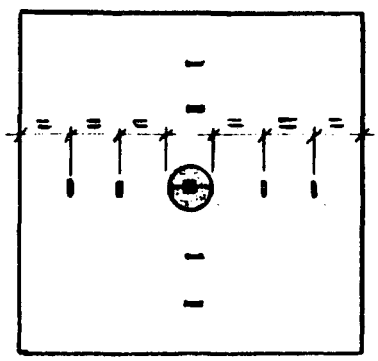

140T20 - 32Nº

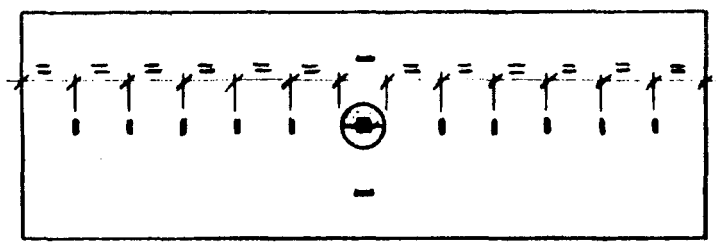

300/100T20 - 48Nº

CROSS-SECTIONS AT GAUGE GROUP LOCATIONS

Fig 9.5 : EMBEDMENT GAUGE LAYOUTS

Figure 9.6: Embedment Gauges (Specimen 200T20)

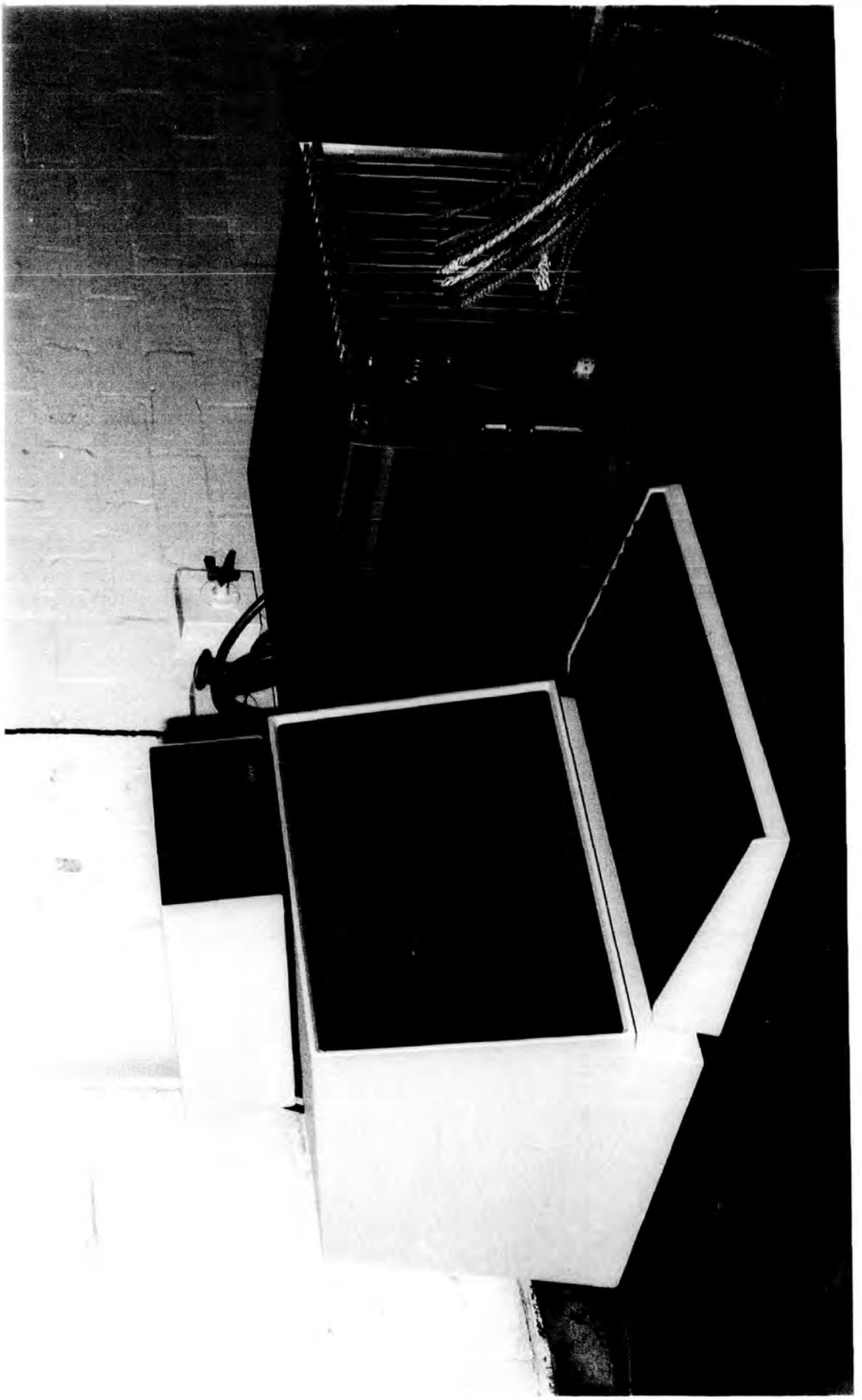

Figure 10.1: Data Logging Hardware

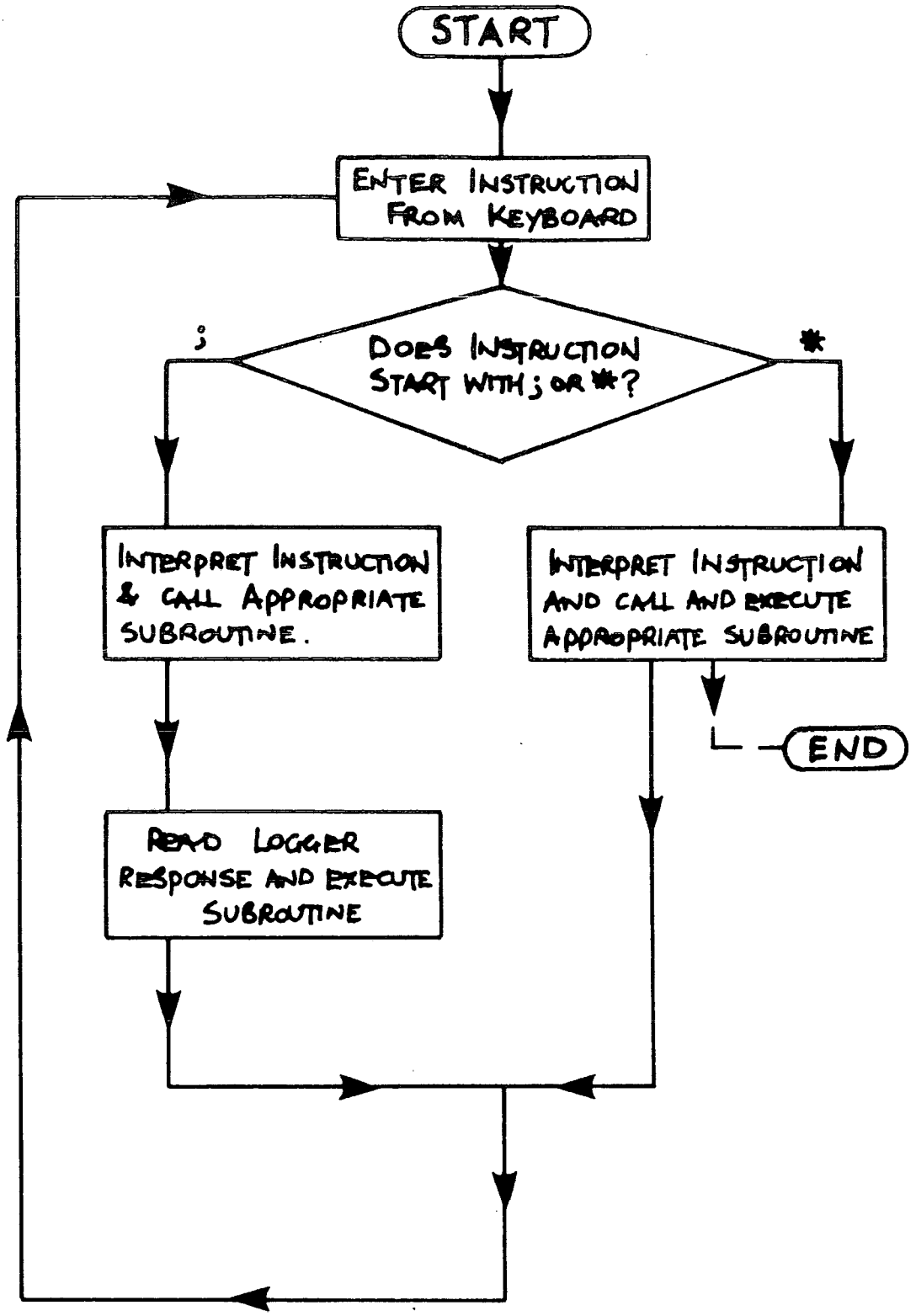

Fig 10.2: FLOWCHART FOR PROGRAM STRUCTURE.

NAME	COMMAND PROCESSED	DESCRIPTION
SEMIA	;A	Scans all groups
SEMIB	;B	Autobalances a designated group
SEMIG	;G	Scans a designated group
SEMIP	;P	Periodic scan of a designated group
SEMIQ	;Q	Checks logger is responding
SEMIR	;R	Cancels a designated group
SEMIS	;S	Sets up a group of channels
SEMIT	;T	Initialises the time
SEMIU	;U	Reads the time
SEMIY	;Y	Summarises setting-up data in brief
ASTA	*A	Inputs autobalance values
ASTB	*B	Reads autobalance values
ASTC	*C	Closes a data file & opens a replacement
ASTD	*D	Lists a data file
ASTF	*F	Ends program
ASTG	*G	Summarises setting-up data in detail
ASTL	*L	Lists titles of data files
ASTM	*M	Inputs messages to data files
ASTO	*O	Opens data file
ASTV	*V	Permits use of all ; commands not covered by above subroutines
SCAN	-	Data Analysis
TIME	-	Time calculation for periodic scans
LIST	-	Data Listing
ERROR	-	Analyses error codes from logger
NUMSUM	-	Number conversion
NOCHAN	-	Orders group data for SEMIA

Figure 10.3: List of Subroutines

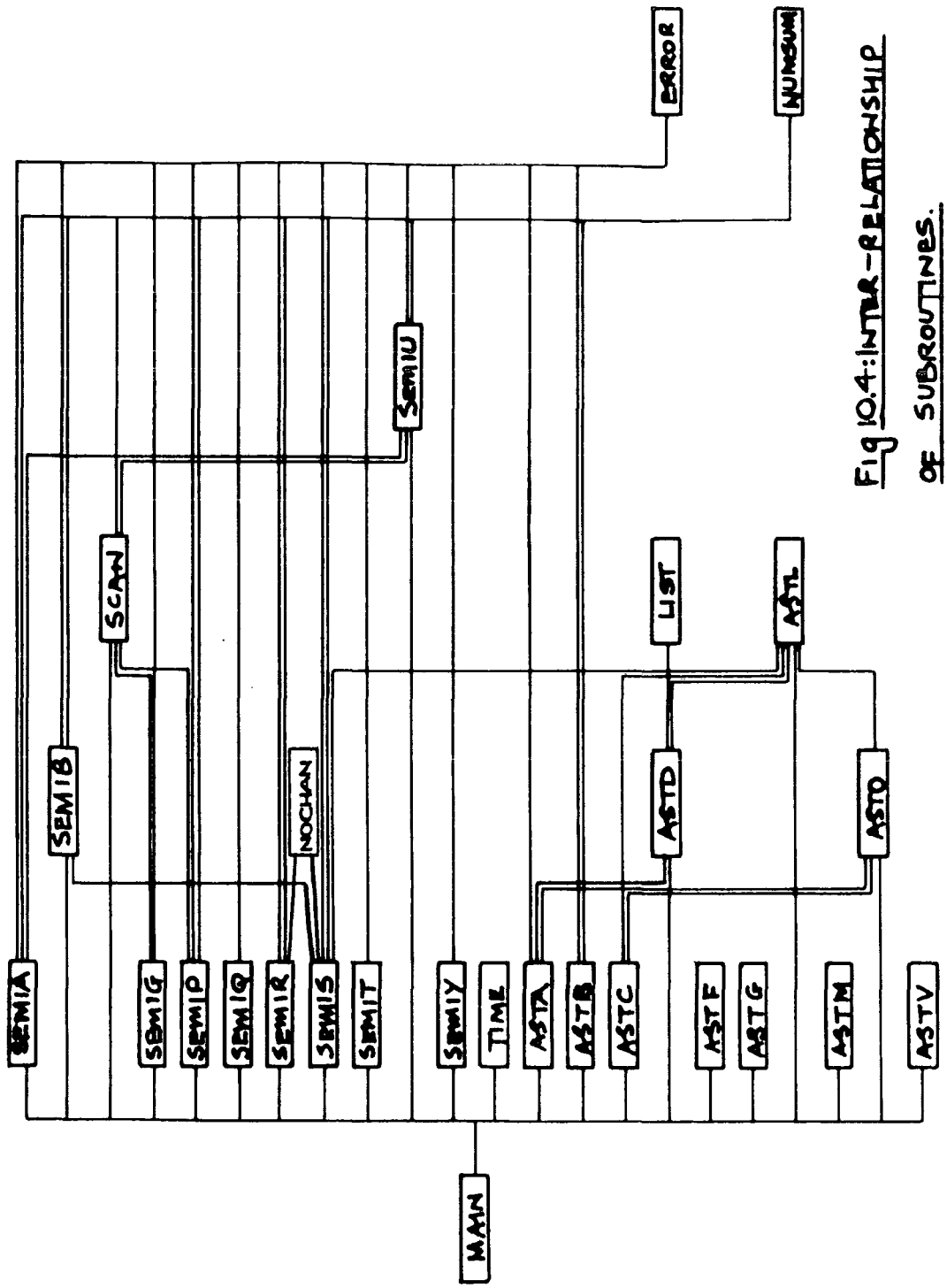

Fig 10.4: INTER-RELATIONSHIP OF SUBROUTINES.

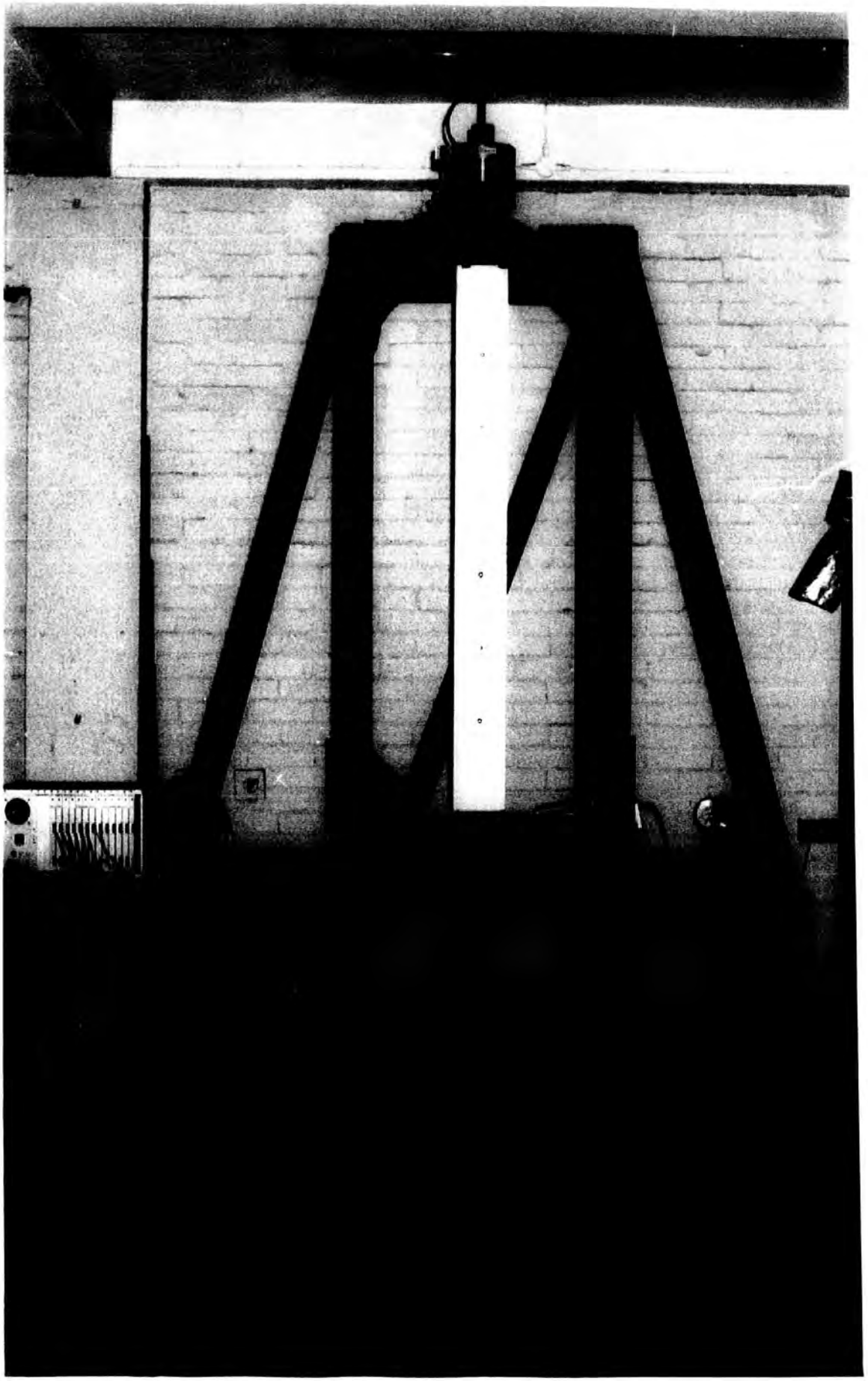

Figure 10.5: The Test Rig

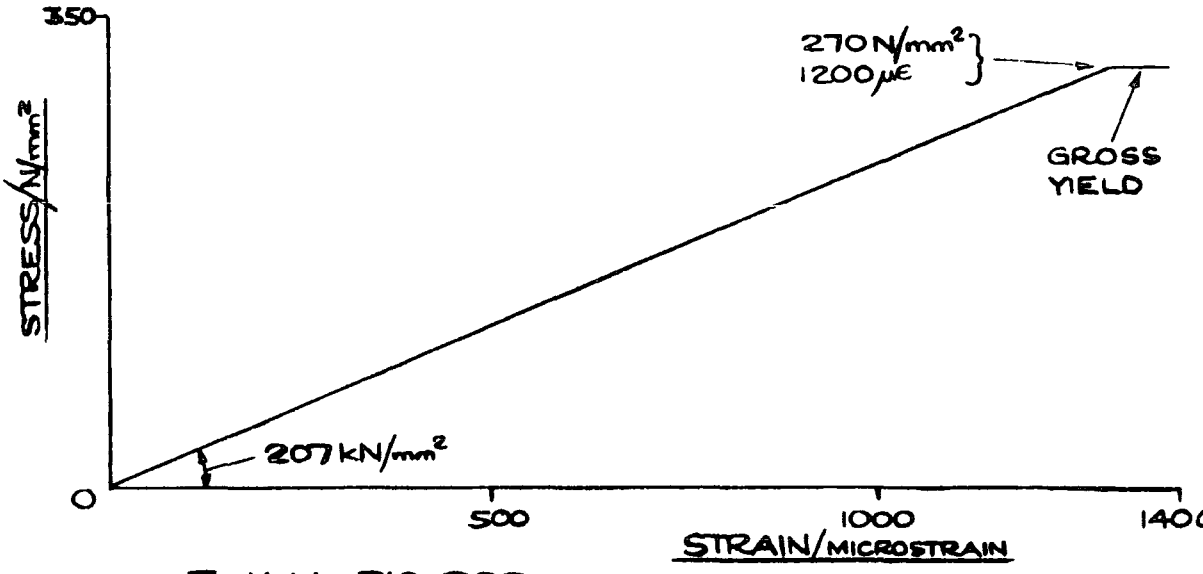

Fig 11.1.1 : R12 ROD

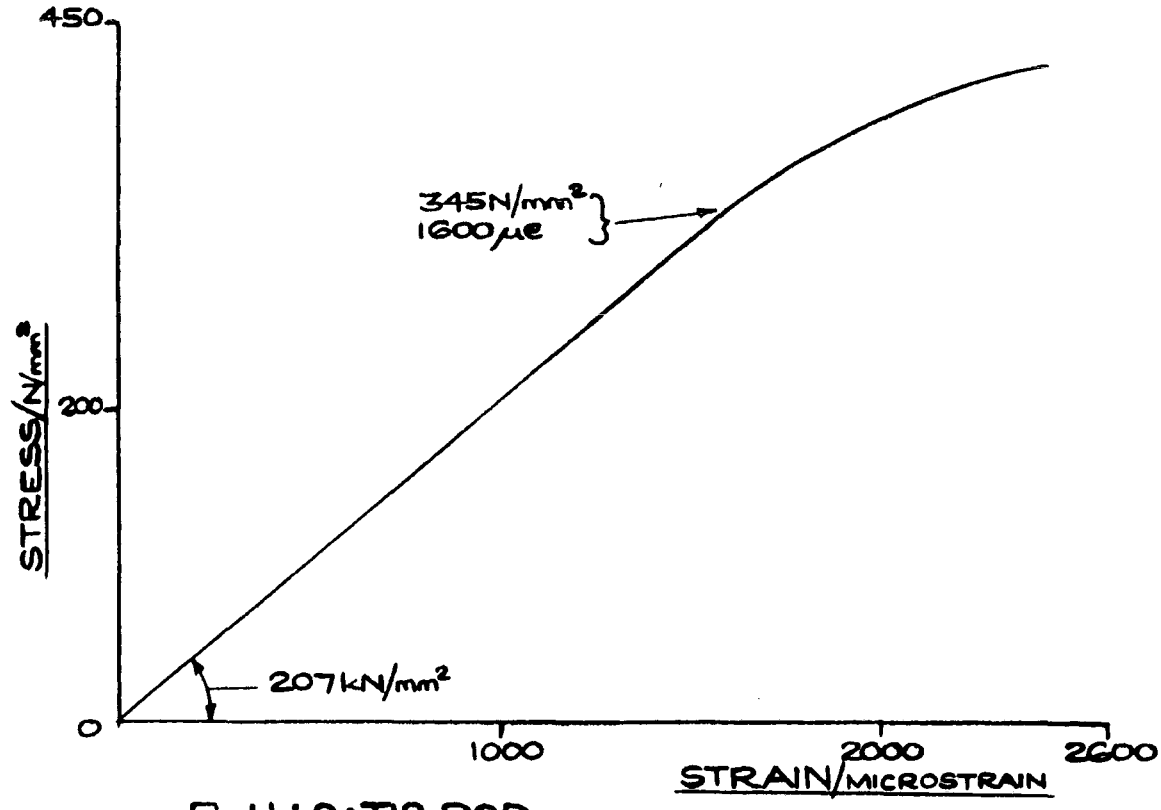

Fig 11.1.2 : T12 ROD

Fig 11.1 : TYPICAL STRESS-STRAIN RELATIONSHIPS

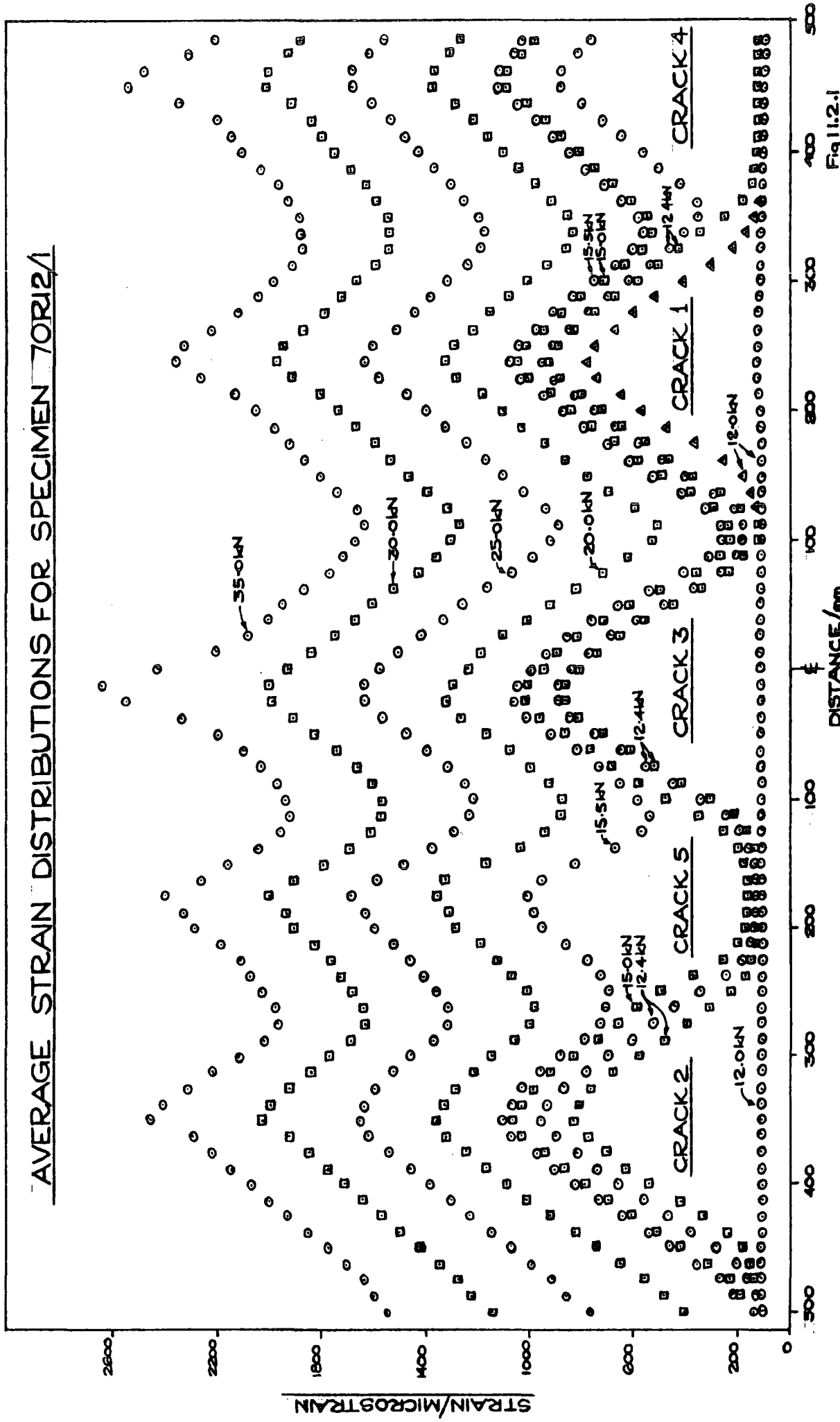
AVERAGE STRAIN DISTRIBUTIONS FOR SPECIMEN 70R12/1
STRAIN/MICROSTRAIN
DISTANCE/mm
CRACK 1
CRACK 2
CRACK 3
CRACK 4
CRACK 5
35·0kN
30·0kN
25·0kN
20·0kN
15·5kN
15·0kN
12·4kN
12·0kN

Fig 11.2.1

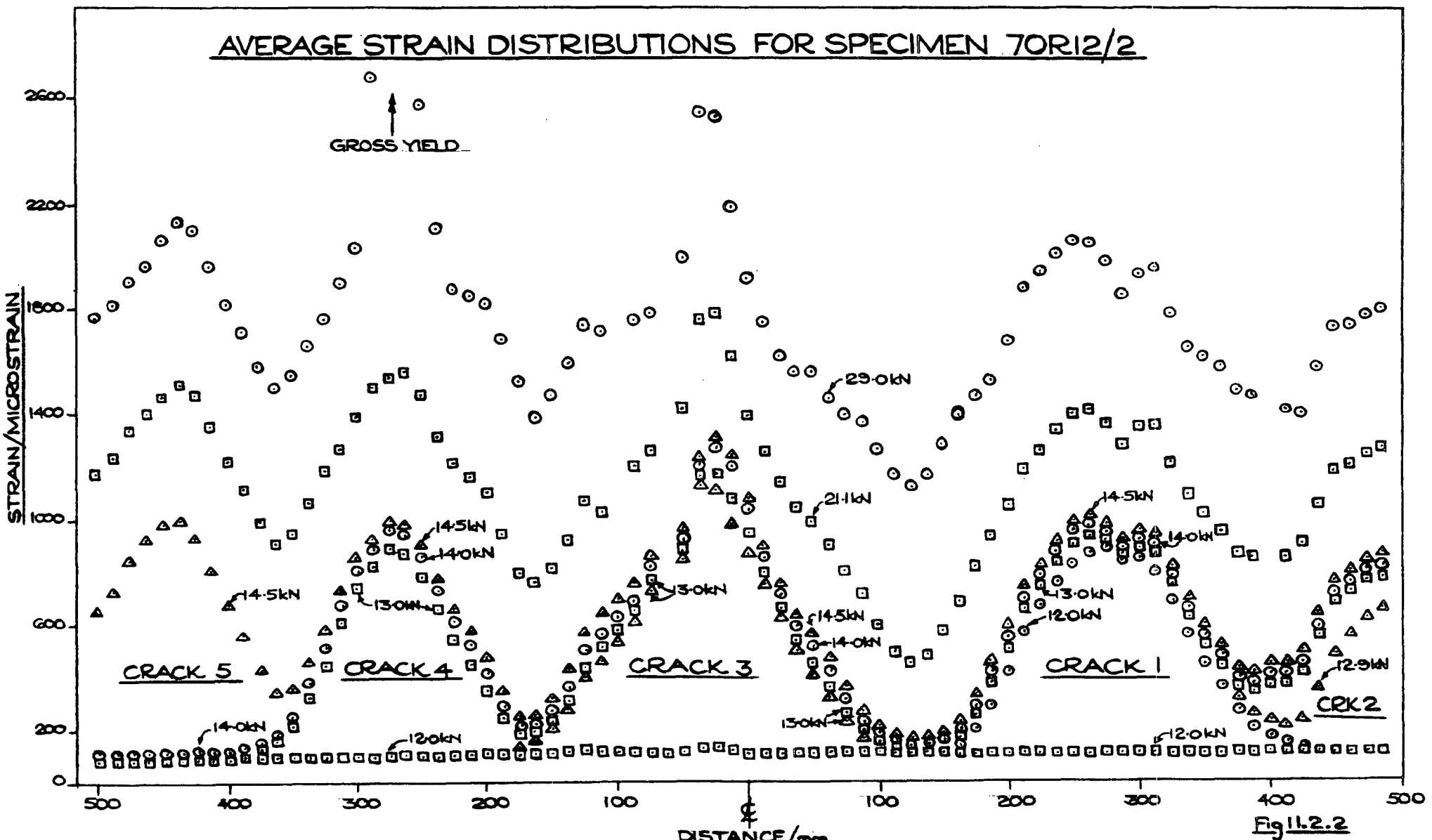
AVERAGE STRAIN DISTRIBUTIONS FOR SPECIMEN 70R12/2
GROSS YIELD
STRAIN/MICROSTRAIN
2600
2200
1800
1400
1000
600
200
0
500
400
300
200
100
100
200
300
400
500
DISTANCE/mm
CRACK 5
CRACK 4
CRACK 3
CRACK 1
CRK 2
14·5kN
14·0kN
13·0kN
12·0kN
29·0kN
21·1kN
12·9kN

Fig 11.2.2

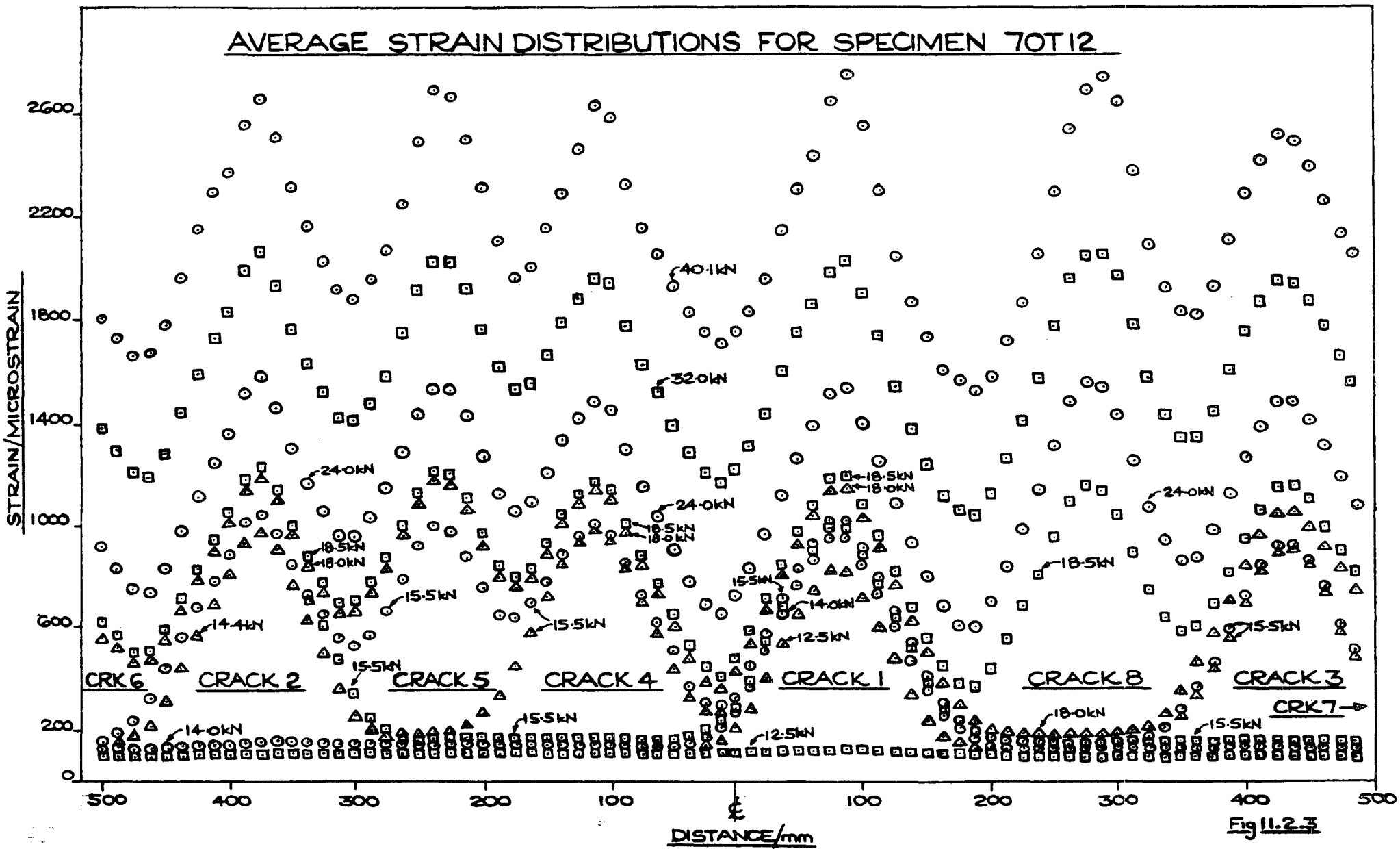
AVERAGE STRAIN DISTRIBUTIONS FOR SPECIMEN 7OT12
STRAIN/MICROSTRAIN
2600
2200
1800
1400
1000
600
200
0
500
400
300
200
100
℄
100
200
300
400
500
DISTANCE/mm
CRK6
CRACK 2
CRACK 5
CRACK 4
CRACK 1
CRACK 8
CRACK 3
CRK7
40·1kN
32·0kN
24·0kN
18·5kN
18·0kN
15·5kN
14·4kN
14·0kN
12·5kN

Fig 11.2.3

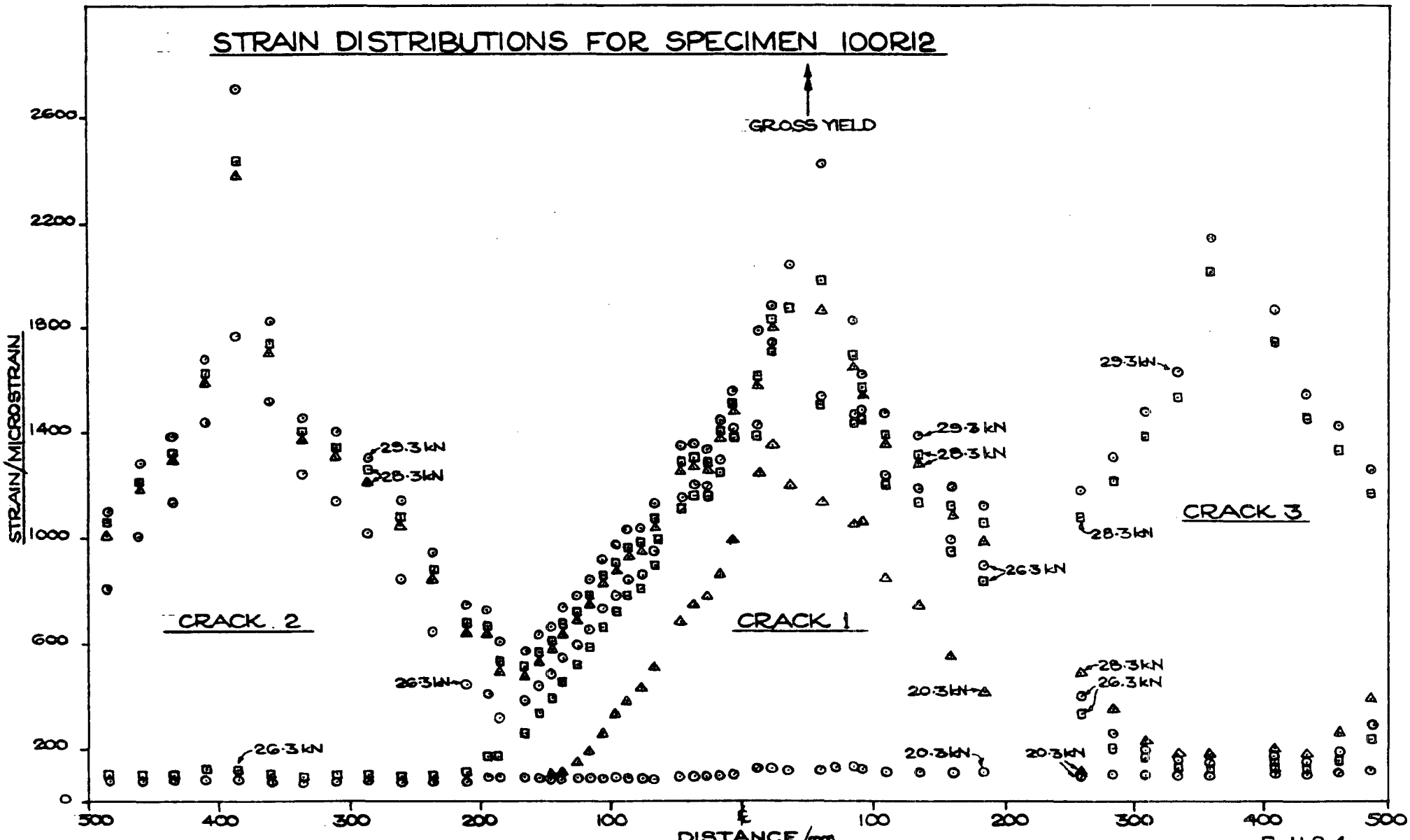
STRAIN DISTRIBUTIONS FOR SPECIMEN 100RI2
GROSS YIELD
STRAIN/MICROSTRAIN
2600
2200
1800
1400
1000
600
200
0
CRACK 2
CRACK 1
CRACK 3
29·3 kN
28·3 kN
26·3 kN
20·3 kN
500
400
300
200
100
DISTANCE/mm

Fig 11.2.4

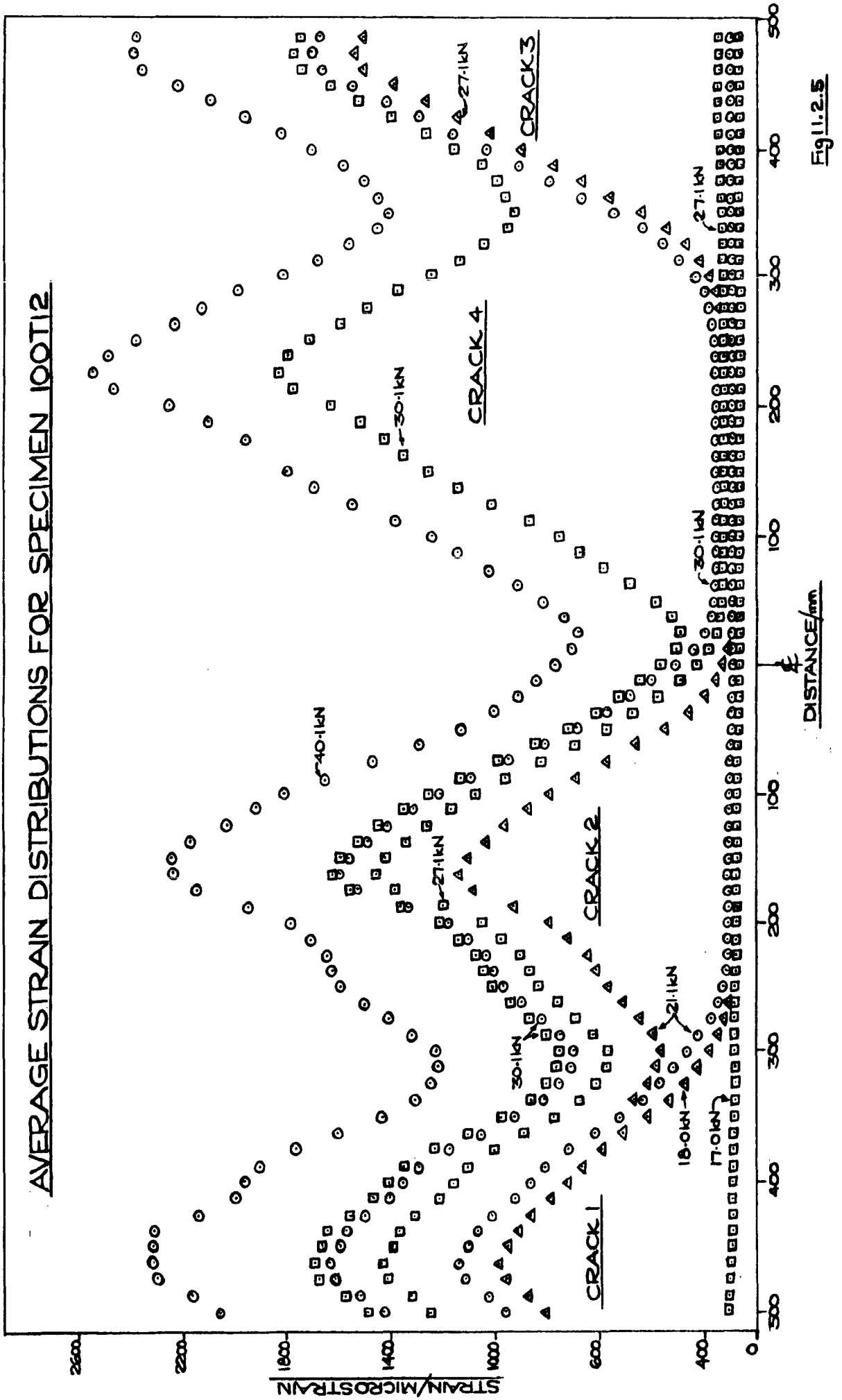
AVERAGE STRAIN DISTRIBUTIONS FOR SPECIMEN 100T12
STRAIN/MICROSTRAIN
DISTANCE/mm
CRACK 1
CRACK 2
CRACK 3
CRACK 4
17·0 kN
19·0 kN
21·1 kN
30·1 kN
40·1 kN
27·1 kN

Fig 11.2.5

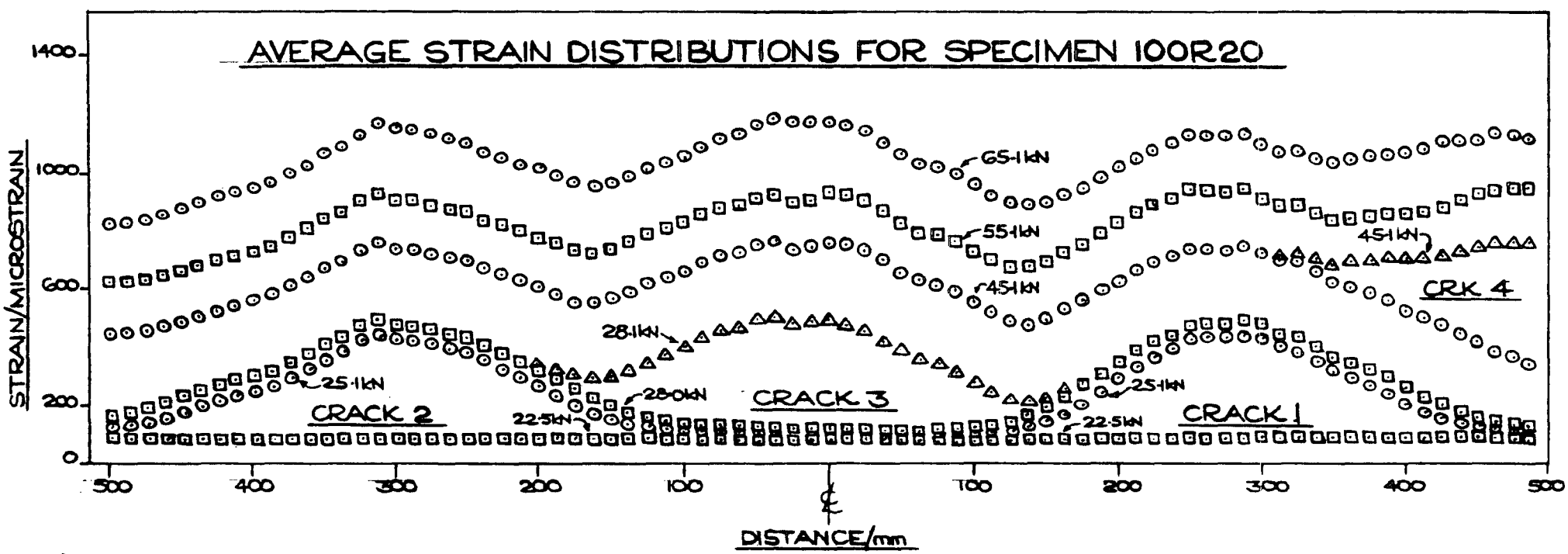
AVERAGE STRAIN DISTRIBUTIONS FOR SPECIMEN 100R20
STRAIN/MICROSTRAIN
1400
1000
600
200
0
500
400
300
200
100
℄
100
200
300
400
500
DISTANCE/mm
65·1kN
55·1kN
45·1kN
45·1kN
CRK 4
28·1kN
25·1kN
28·0kN
22·5kN
CRACK 2
CRACK 3
25·1kN
22·5kN
CRACK 1

Fig 11.2.6

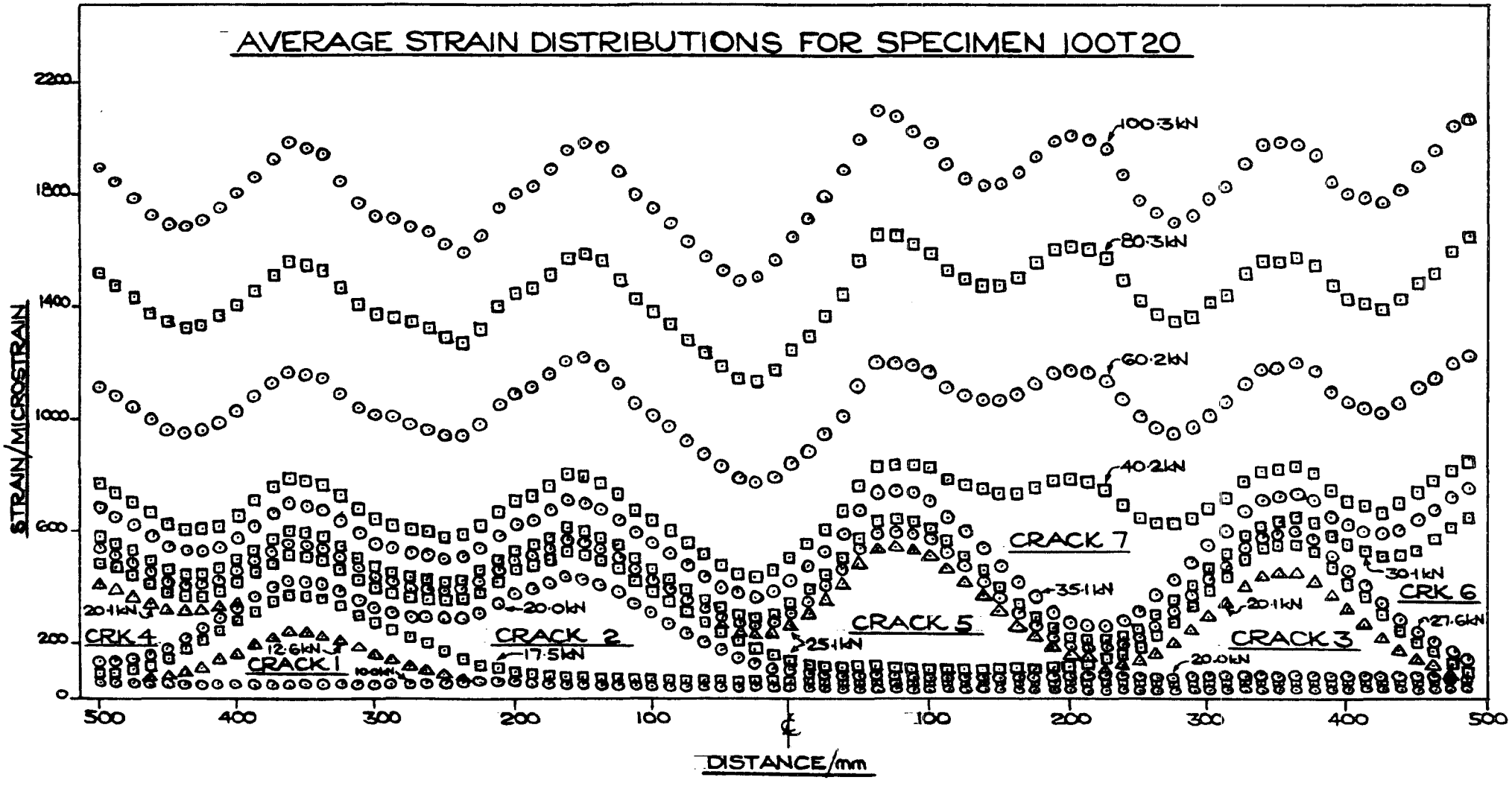
AVERAGE STRAIN DISTRIBUTIONS FOR SPECIMEN 100T20
STRAIN/MICROSTRAIN
2200
1800
1400
1000
600
200
0
500
400
300
200
100
℄
100
200
300
400
500
DISTANCE/mm
100·3kN
80·3kN
60·2kN
40·2kN
35·1kN
30·1kN
27·6kN
25·1kN
20·1kN
20·0kN
17·5kN
12·6kN
10·0kN
CRACK 7
CRACK 5
CRACK 2
CRACK 1
CRACK 3
CRK 6
CRK 4

Fig 11.2.7

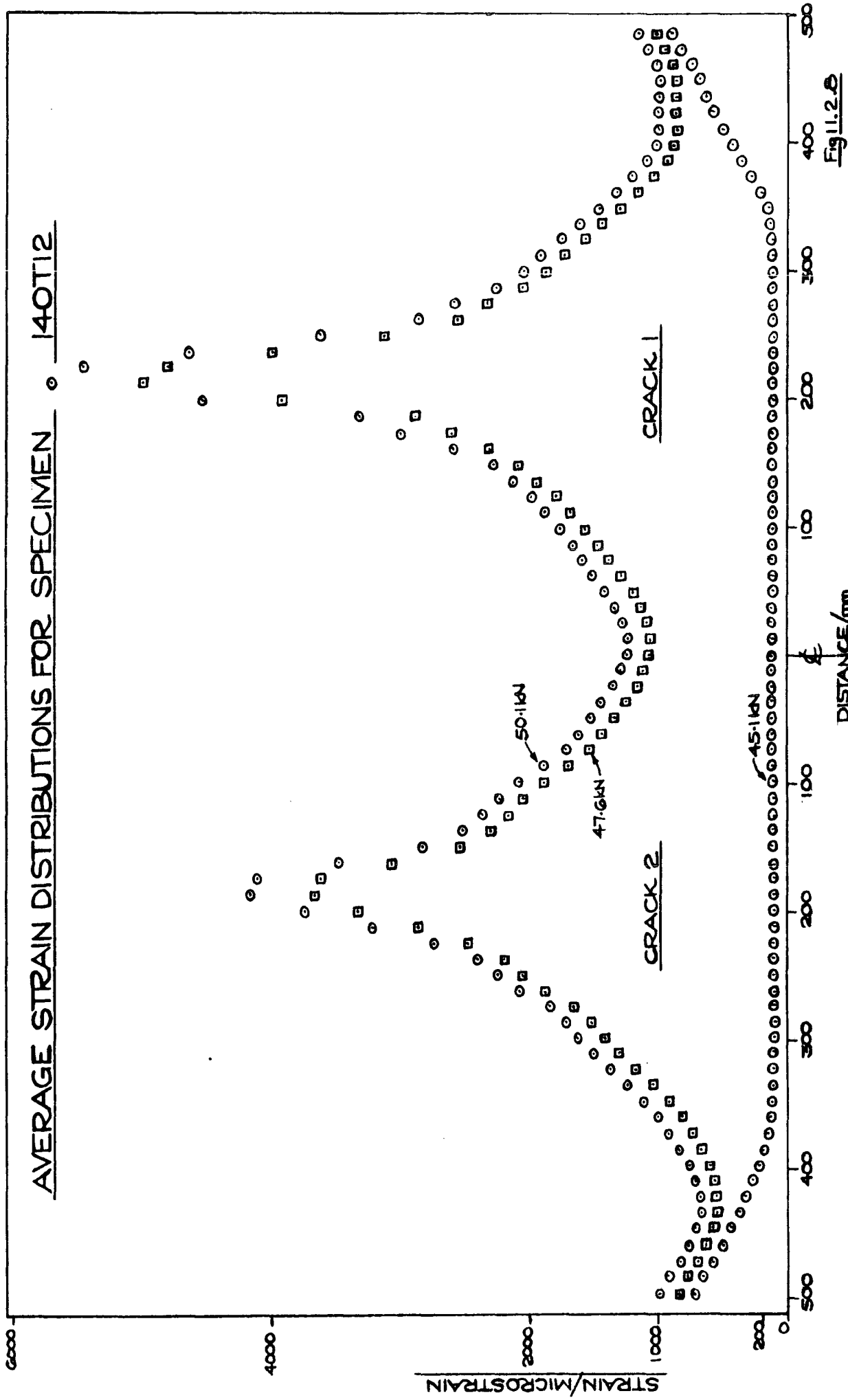
AVERAGE STRAIN DISTRIBUTIONS FOR SPECIMEN • 140T12
CRACK 1
CRACK 2
50·1kN
47·6kN
45·1kN
STRAIN/MICROSTRAIN
DISTANCE/mm
6000
4000
2000
1000
200
500
400
300
200
100
0
100
200
300
400
500

Fig 11.2.8

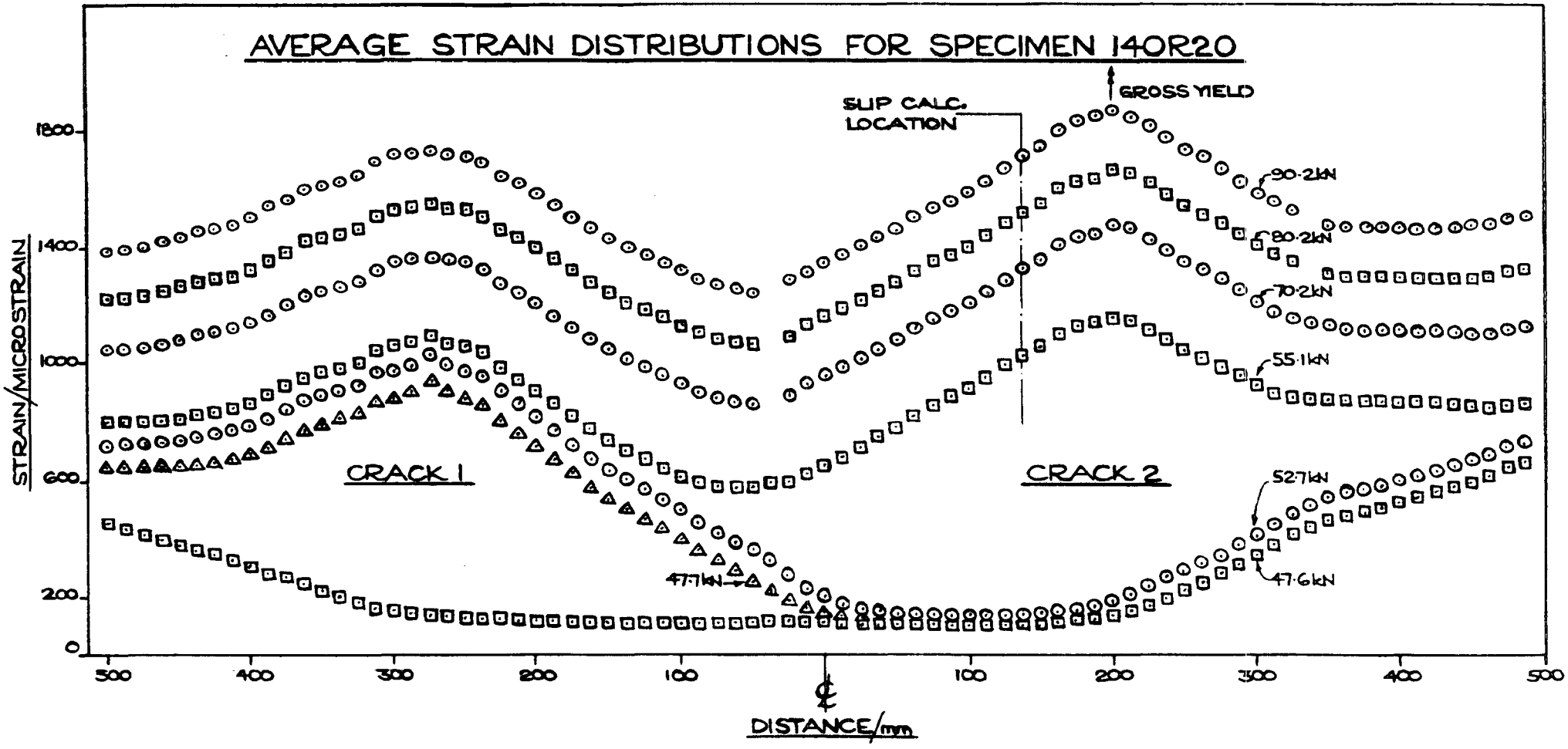
AVERAGE STRAIN DISTRIBUTIONS FOR SPECIMEN 140R20
GROSS YIELD
SLIP CALC. LOCATION
90·2kN
80·2kN
70·2kN
55·1kN
52·7kN
47·6kN
47·7kN
CRACK 1
CRACK 2
STRAIN/MICROSTRAIN
1800
1400
1000
600
200
0
500
400
300
200
100
100
200
300
400
500
℄
DISTANCE/mm

Fig 11.2.9

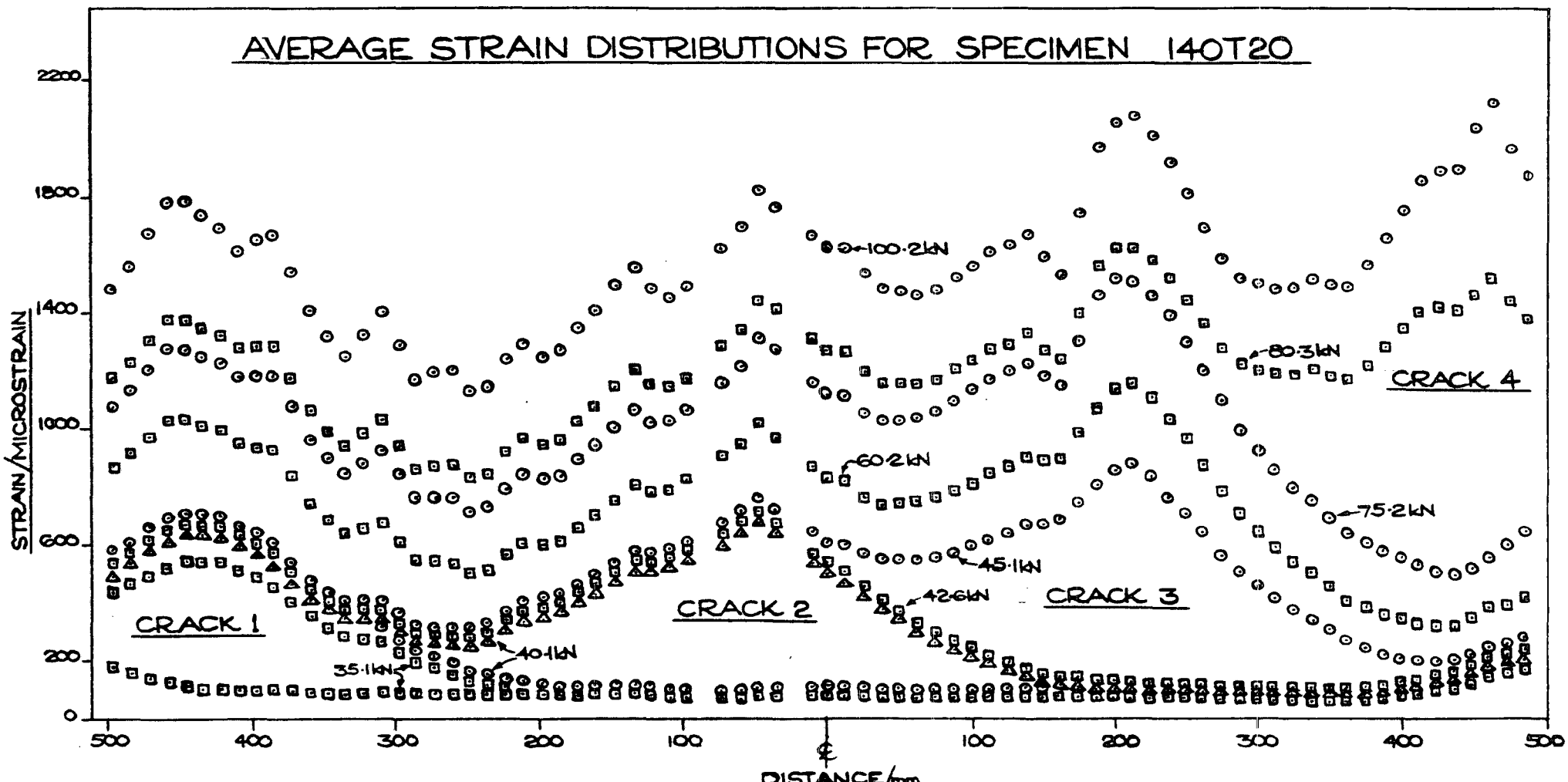
AVERAGE STRAIN DISTRIBUTIONS FOR SPECIMEN 140T20
STRAIN/MICROSTRAIN
2200
1800
1400
1000
600
200
0
500
400
300
200
100
℄
100
200
300
400
500
DISTANCE/mm
CRACK 1
CRACK 2
CRACK 3
CRACK 4
100·2kN
80·3kN
60·2kN
75·2kN
45·1kN
42·6kN
40·1kN
35·1kN

Fig 11.2.10

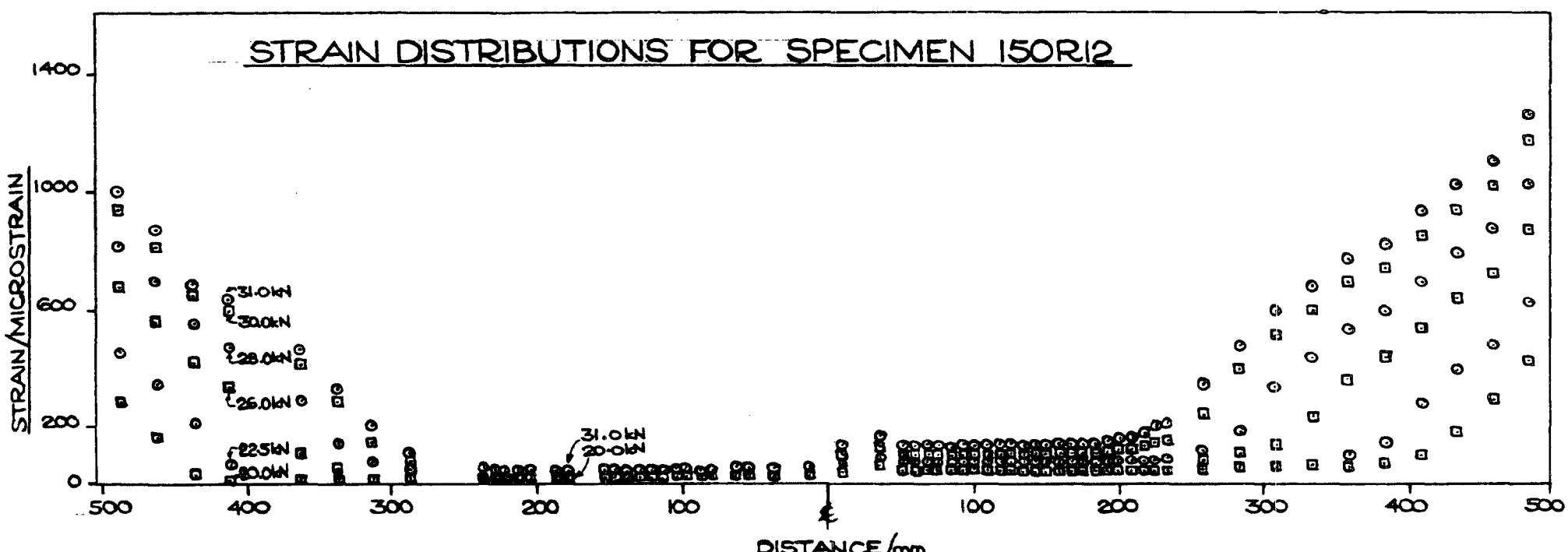
STRAIN DISTRIBUTIONS FOR SPECIMEN 150R12
STRAIN/MICROSTRAIN
1400
1000
600
200
0
31.0kN
30.0kN
28.0kN
26.0kN
22.5kN
20.0kN
31.0kN
20.0kN
500
400
300
200
100
100
200
300
400
500
DISTANCE/mm

Fig11.2.11

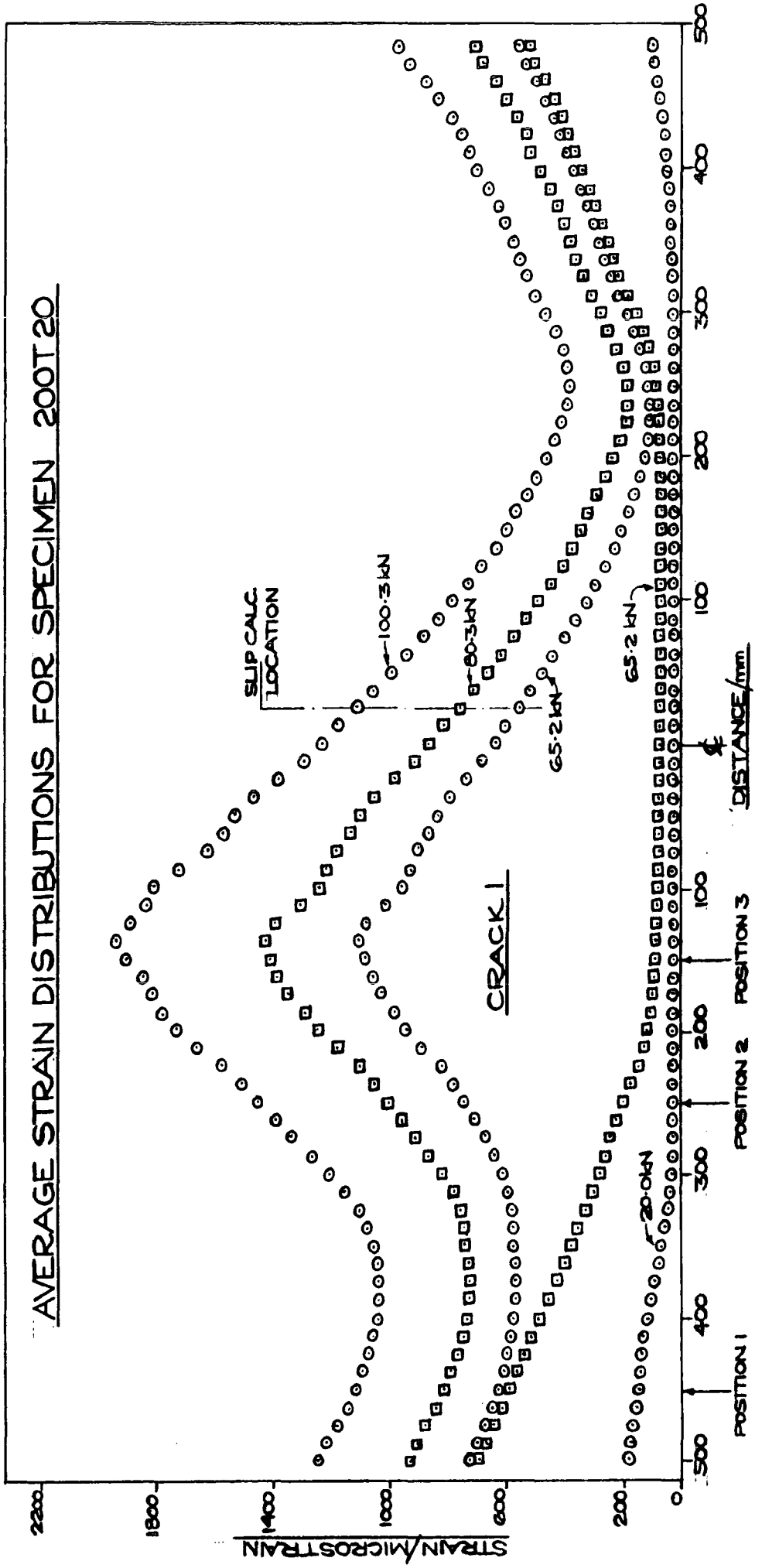
AVERAGE STRAIN DISTRIBUTIONS FOR SPECIMEN 200T20
STRAIN/MICROSTRAIN
2200
1800
1400
1000
600
200
0
500
400
300
200
100
0
100
200
300
400
500
DISTANCE/mm
POSITION 1
POSITION 2
POSITION 3
SLIP CALC. LOCATION
100·3 kN
80·3 kN
65·2 kN
65·2 kN
20 kN
CRACK 1

Fig 11.2.12

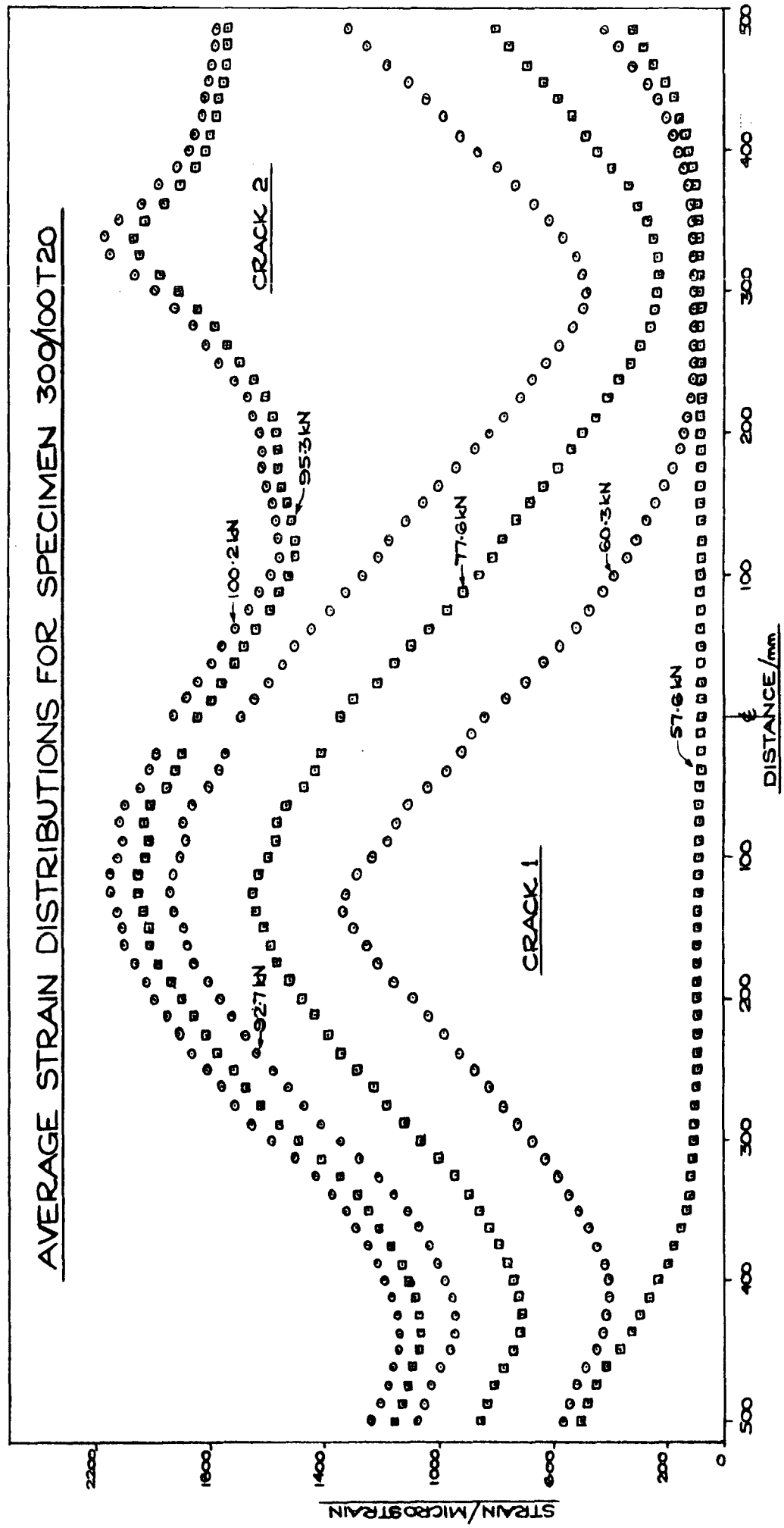
AVERAGE STRAIN DISTRIBUTIONS FOR SPECIMEN 300/100T20
CRACK 2
CRACK 1
100·2kN
95·3kN
77·6kN
60·3kN
57·6kN
92·7kN
STRAIN/MICROSTRAIN
DISTANCE/mm
2200
1800
1400
1000
600
200
0
500
400
300
200
100
100
200
300
400
500

Fig 11.2.13

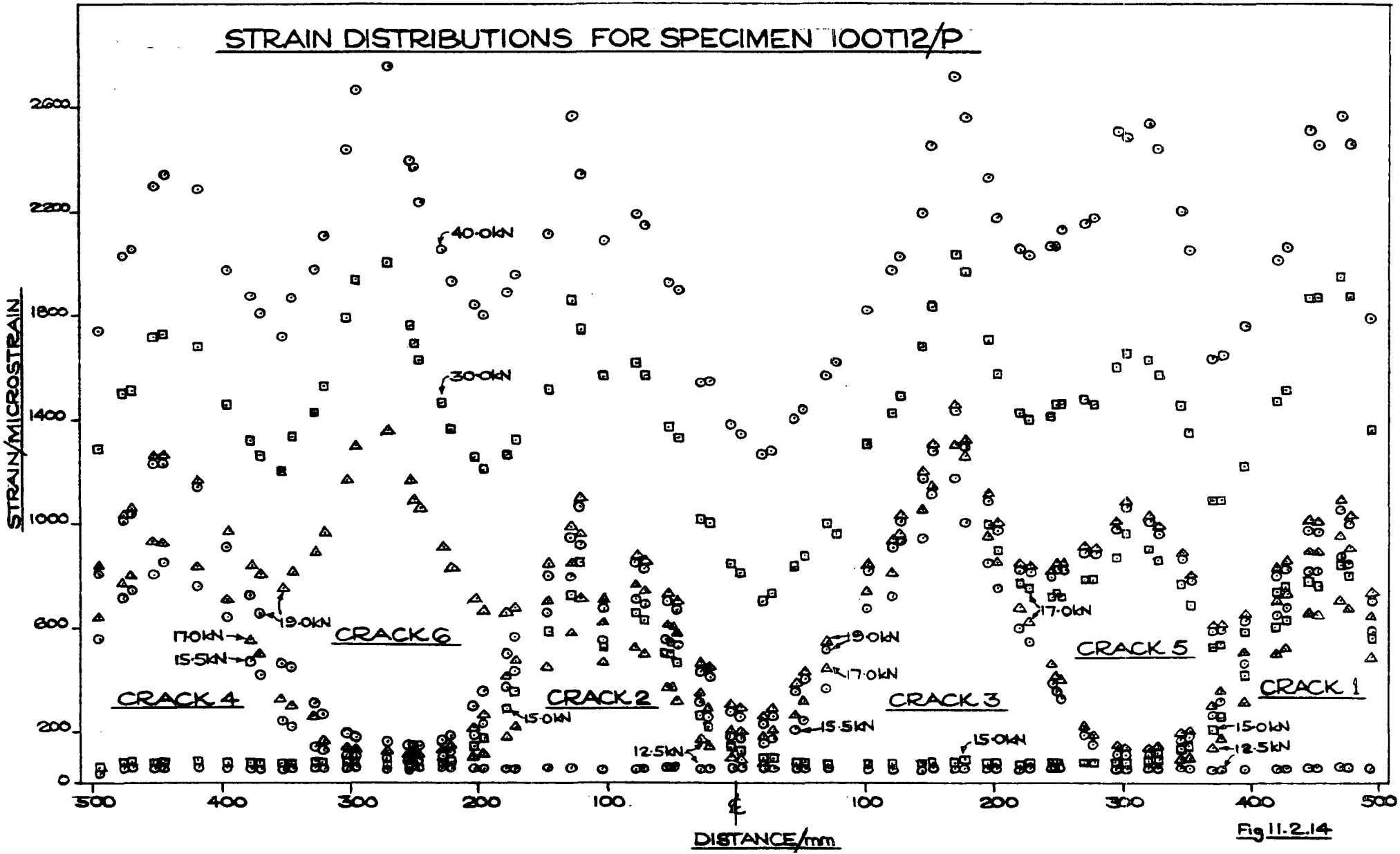
STRAIN DISTRIBUTIONS FOR SPECIMEN 100T12/P
STRAIN/MICROSTRAIN
0
200
600
1000
1400
1800
2200
2600
500
400
300
200
100
℄
100
200
300
400
500
DISTANCE/mm
40·0kN
30·0kN
19·0kN
17·0kN
15·5kN
CRACK 6
CRACK 4
15·0kN
CRACK 2
12·5kN
9·0kN
17·0kN
15·5kN
CRACK 3
15·0kN
17·0kN
CRACK 5
CRACK 1
15·0kN
12·5kN

Fig 11.2.14

SPECIMEN	% REINFORCEMENT	EMBEDMENT GAUGES/ (YES/NO)	AGE AT TEST/ (DAYS)	CUBE STRENGTH AT TEST/ (N/mm^2)	INDIRECT TENSILE STRENGTH AT TEST/ (N/mm^2)	Nº OF CRACKS	APPLIED LOAD AT FIRST CRACK/ (kN)	REINFORCEMENT STRAIN AT FIRST CRACK/ (MICROSTRAIN)	APPLIED LOAD AT LAST CRACK/ (kN)	REINFORCEMENT STRAIN AT LAST CRACK/ (MICROSTRAIN)
70R12/1	1·73	NO	28	45·5	3·1	5	12·0	105	15·5	160
70R12/2	1·65	NO	29	46·7	2·8	5	12·0	88	14·5	118
70T12	1·61	NO	28	47·3	3·0	8	12·5	105	18·5	183
100R12	0·83	NO	29	41·5	3·0	3	20·0	112	28·0	170
100T12	0·83	YES	29	45·0	2·7	4	18·0	95	30·0	157
100R20	2·68	NO	28	38·7	2·8	4	25·1	83	45·1	360
100T20	2·48	YES	28	46·7	3·1	7	12·6	55	40·2	272
140T12	0·43	NO	28	54·0	3·1	2	47·6	100	47·6	100
140R20	1·35	NO	29	42·0	3·1	2	47·7	115	55·1	190
140T20	1·33	YES	28	54·7	2·8	4	35·1	98	80·3	561
150R12	0·40	NO	29	38·1	2·8	0	—	—	—	—
200T20	0·65	YES	28	60·3	3·1	1	65·2	81	—	—
300/100T20	0·87	YES	41	48·0	3·2	2	60·3	87	95·3	564
100T12P	0·84	NO	34	35·3	1·9	6	12·5	60	19·0	155

Fig 11·3: SUMMARY OF TEST RESULTS

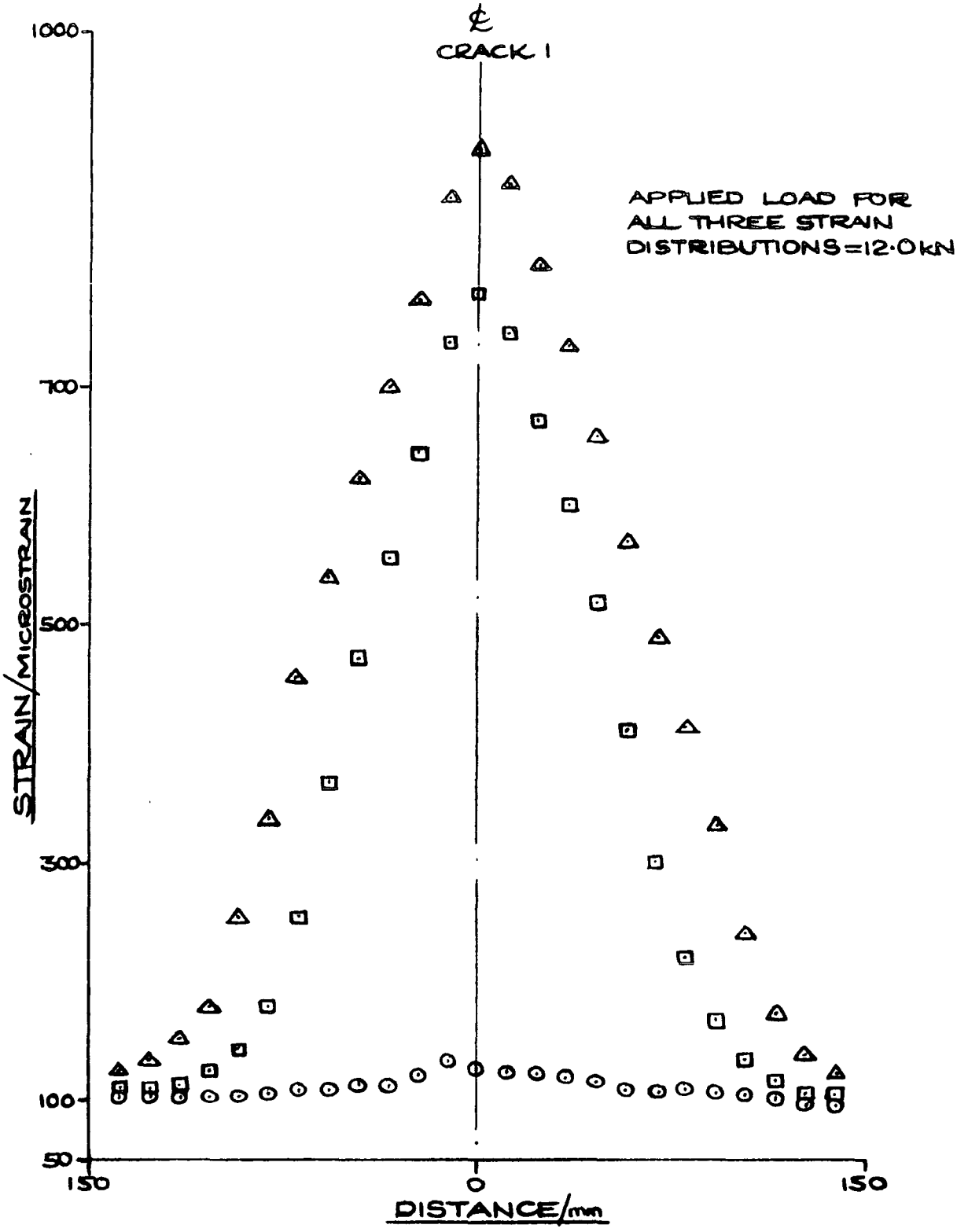

⊙ - BEFORE CRACKING
⊡ - AFTER CRACKING - BEFORE DEMEC & CRACK WIDTH READINGS
△ - 25 MINUTES LATER - AFTER DEMEC & CRACK WIDTH READINGS

Fig 11·4: SPECIMEN 70RI2/1 - CREEP DURING DEMEC READINGS

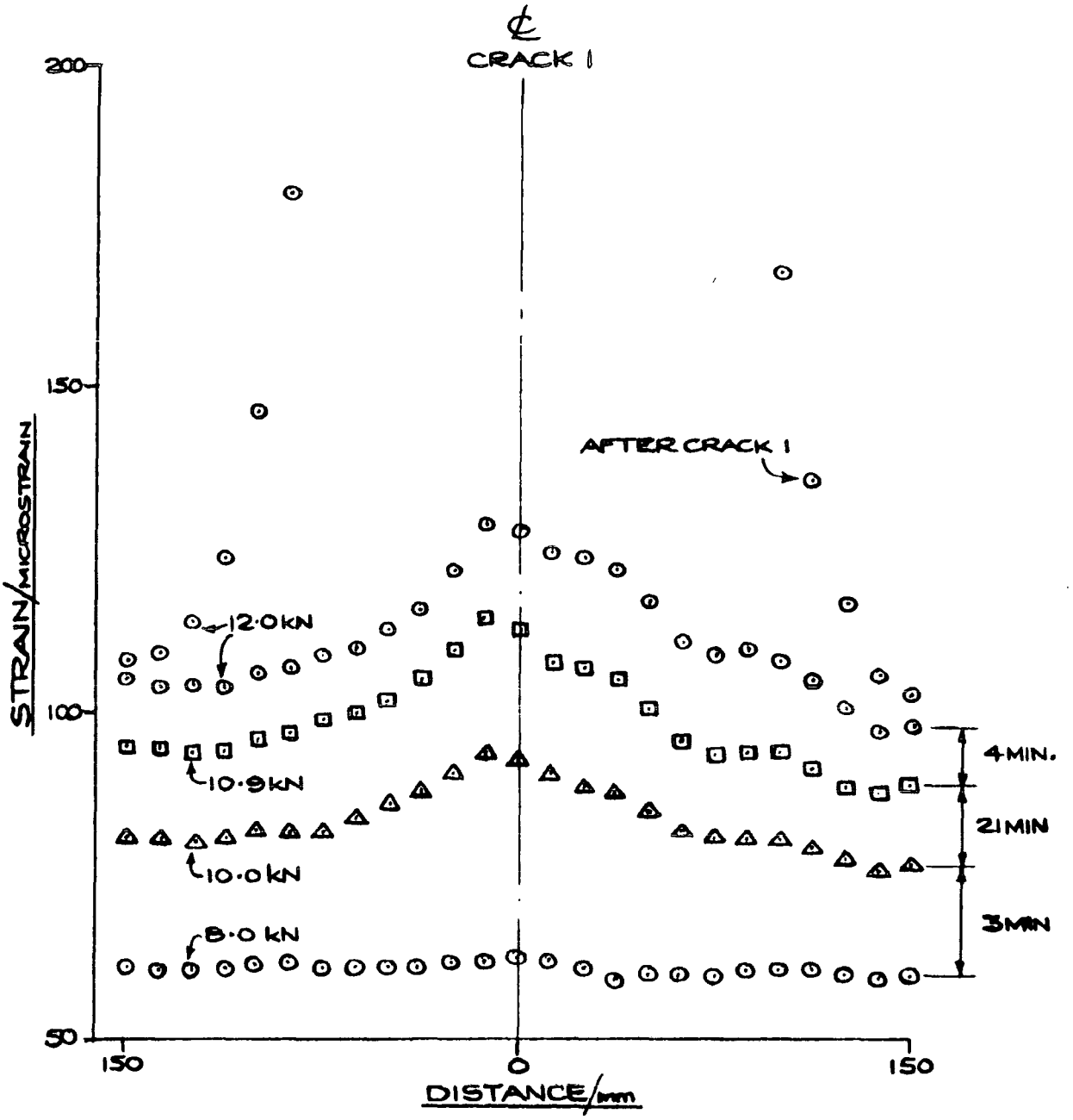

Fig11·5: SPECIMEN 70R12/1 – STRAINS PRE-CRACK 1

SPECIMEN	KEY: A / B C	A – CRACKING LOAD/kN B – ROD STRAIN BEFORE CRACK/με C – ROD STRAIN AFTER CRACK/με	E – EMBEDMENT GAUGES 150R12 – NO CRACKS					
	CRACK 1	CRACK 2	CRACK 3	CRACK 4	CRACK 5	CRACK 6	CRACK 7	CRACK 8
70R12/1	12·0 105 778	12·4 110 830	12·4 110 863	12·4 125 878	15·5 160 974			
70R12/2	12·0 88 663	12·9 – –	13·0 105 718	13·0 110 718	14·5 118 802			
70T12	12·5 105 805	14·4 135 966	15·5 155 913	15·5 165 992	15·5 177 997	15·5 – –	15·5 – –	18·5 183 1154
100R12	20·0 112 1350	26·0 127 1630	28·0 170 –					
100T12 E	18·0 95 982	21·0 105 1136	27·1 144 1538	30·0 157 1830				
100R20	25·1 83 429	25·1 82 438	28·1 115 489	45·1 360 750				
100T20 E	12·6 55 234	20·0 80 433	20·1 72 454	20·1 – –	25·1 114 547	30·1 – –	40·2 272 788	
140T12	47·6 100 4971	47·6 100 3655						
140R20	47·7 115 939	55·1 190 1168						
140T20 E	35·1 98 541	40·1 98 675	45·1 125 880	80·3 561 1524				
200T20 E	65·2 81 1098							
300/100T20 E	60·3 87 1327	95·3 564 2071						
100T12P	12·5 60 710	12·5 65 714	15·5 80 1051	15·5 84 853	17·0 137 969	19·0 155 1356		

Fig 11·6: CRACKING LOADS & STRAINS

SPECIMEN	JUST PRIOR TO EFFECTIVE FIRST CRACK			JUST PRIOR TO LAST CRACK			e_s/e_f	JUST PRIOR TO PENULTIMATE CRACK			e_{penult}/e_f
	ROD STRAIN $e_f/(\mu\varepsilon)$	CONCRETE STRESS/(N/mm²)	CONCRETE STRESS/f_c	ROD STRAIN $e_s/(\mu\varepsilon)$	CONCRETE STRESS/(N/mm²)	CONCRETE STRESS/f_c		ROD STRAIN $e_{penult}/(\mu\varepsilon)$	CONCRETE STRESS/(N/mm²)	CONCRETE STRESS/f_c	
70R12/1	105	2·09	0·68	160	2·60	0·84	1·52	—	—	—	—
70R12/2	88	2·13	0·77	118	2·53	0·92	1·34	—	—	—	—
70T12	105	2·18	0·72	183	3·13	1·04	1·74	—	—	—	—
100R12	112	1·75	0·59	170	2·43	0·81	1·52	—	—	—	—
100T12 E	105	1·86	0·69	157	2·64	0·99	1·50	—	—	—	—
100R20	83	1·99	0·72	360	2·37	0·85	4·34	115	2·09	0·75	1·39
100T20 E	80	1·54	0·50	272	2·51	0·81	3·40	114 (CRACK 5 USED – CRACK 6 DATA NOT AVAILABLE (FIG 11-6))	1·88	0·61	1·43
140T12	100	2·32	0·75	BOTH CRACKS FORMED TOGETHER			(1.00)	—	—	—	—
140R20	115	2·11	0·68	190	2·28	0·74	1·65	—	—	—	—
140T20 E	98	1·76	0·62	561	2·51	0·89	5·72	125	1·85	0·65	1·27
200T20 E	81	1·53	0·50	ONE CRACK ONLY			(1·00)	—	—	—	—
300/100T20 E	87	1·87	0·58	564	2·18	0·68	6·48	CRACK 1 IS THE PENULT. CRACK			
100T12P	60	1·13	0·60	155	1·61	0·85	2·58	—	—	—	—

E – EMBEDMENT GAUGE SPECIMEN – CRACK 2 IS THE EFFECTIVE FIRST CRACK (EXCEPT 200T20 & 300/100T20)

Fig 11·7 : ROD STRAINS & CONCRETE STRESSES

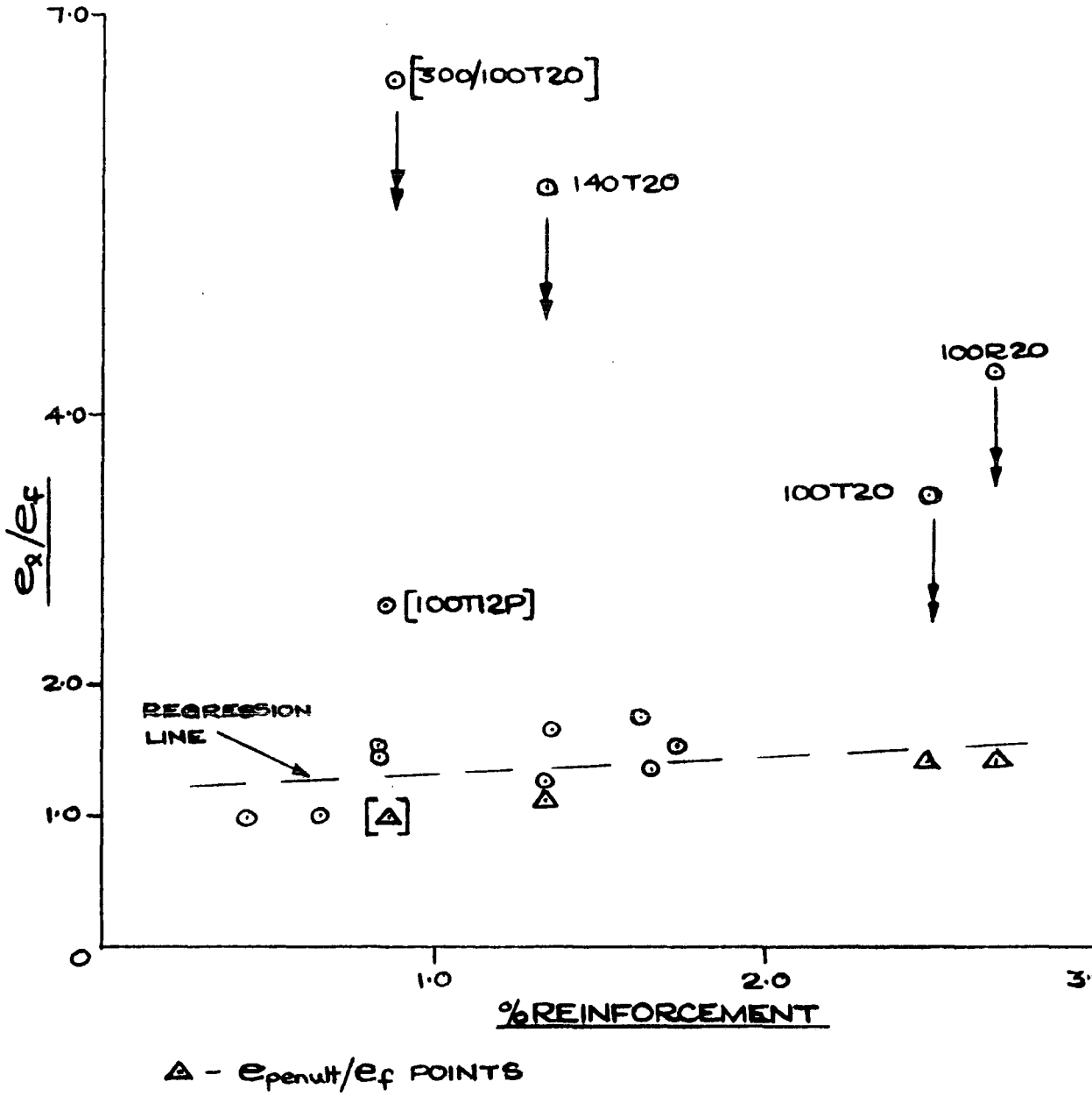

Fig 11·8: RELATIONSHIP BETWEEN e_2/e_f & %REINFORCEMENT

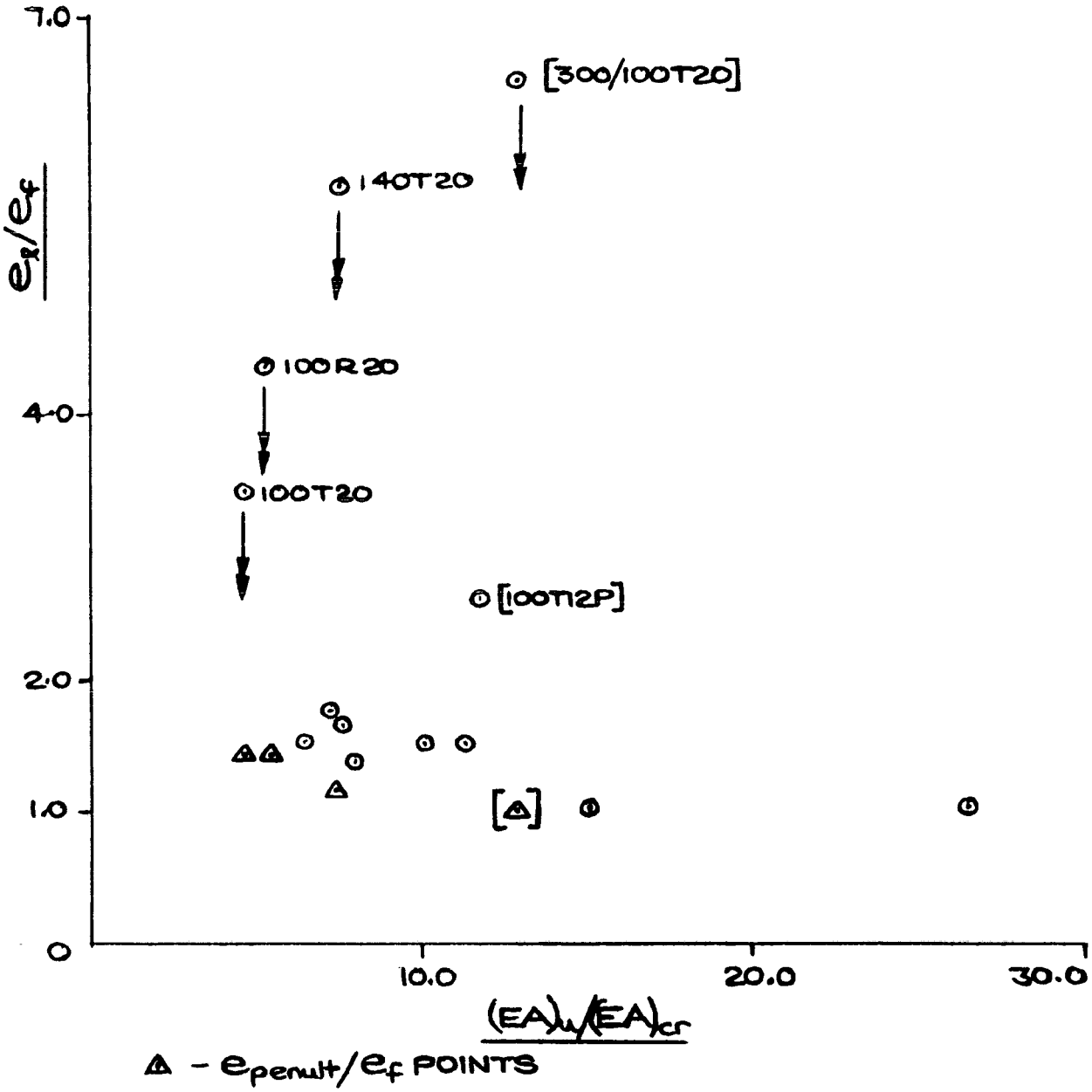

Fig11·9 : RELATIONSHIP BETWEEN e_g/e_f & $(EA)_u/(EA)_{cr}$

SPECIMEN	CRACK 1	CRACK 2	CRACK 3	CRACK 4	CRACK 5	CRACK 6	CRACK 7	CRACK 8
70R12/1	3·4 3·4 159 1·1 1·1	3·4 3·4 170 1·1 1·1	3·9 3·6 182 1·3 1·2	2·8 – 182 0·9 –	2·5 5·0 207 0·8 1·6			
70T12	4·0 4·1 167 1·3 1·4	4·3 4·5 200 1·4 1·5	4·5 – 189 1·5 –	4·4 4·4 205 1·5 1·5	4·4 4·0 206 1·5 1·3	—	—	4·7 5·0 239 1·6 1·7
100R12	3·2 3·0 268 1·1 1·0	– 3·0 302 – 1·0	2·8 – 302 0·9 –					
100T12 E	—	– 3·9 235 – 1·4	4·5 – 318 1·6 –	4·7 4·5 379 1·7 1·7				
100R20	2·7 2·1 88 1·0 0·7	– 2·2 89 – 0·8	2·0 2·0 100 0·7 0·7	—				
100T20 E	1·7 1·5 48 0·6 0·5	1·8 2·8 90 0·8 0·9	3·3 3·5 94 1·1 1·1	—	3·8 3·4 113 1·2 1·1	—	1·4 3·4 165 0·4 1·1	
140R20	1·8 3·2 194 0·6 1·0	2·5 2·2 242 0·8 0·7						
140T20 E	– 2·1 112 – 0·8	1·9 3·1 140 0·7 1·1	2·3 4·4 182 0·8 1·6	—				
200T20 E	3·3 2·7 227 1·1 0·9							

300/100T20 E	3·6 3·7 275 1·1 1·2	—						
100T12P	3·4 – 147 1·8 –	4·7 – 148 2·5 –	– 4·0 244 – 2·1	—	—	—		

Fig 11·10: BOND STRESSES & ROD STRESSES

Key:-

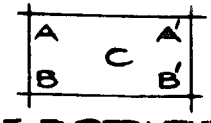

A&A': BOND STRESSES EACH SIDE OF CRACK (N/mm²)
B=A/f_t : B'=A'/f_t
C: ROD STRESS AT CRACK (N/mm²)
E: EMBEDMENT GAUGES

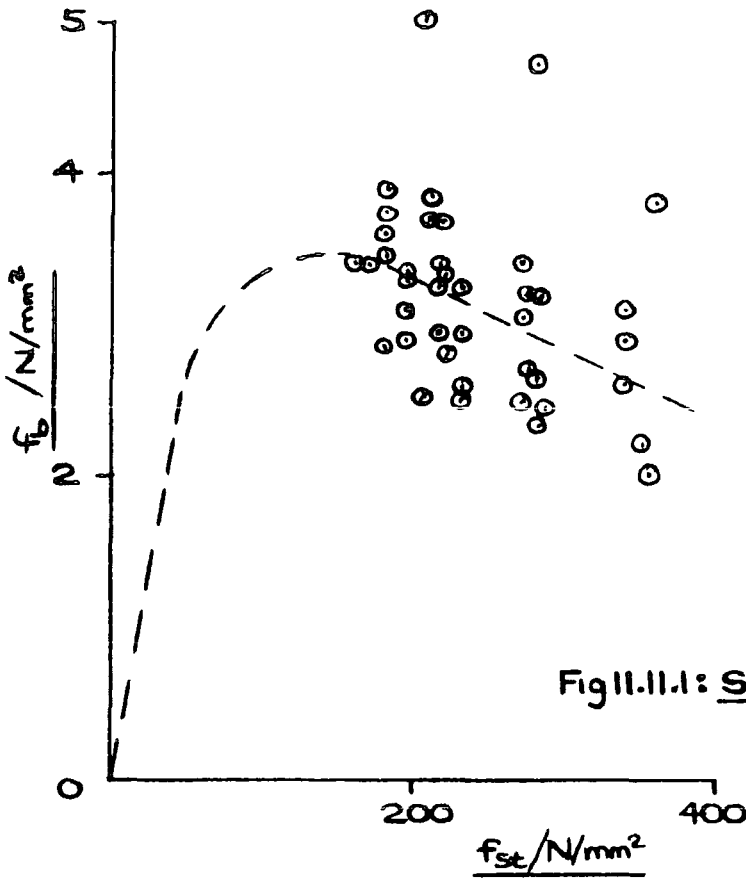

Fig 11.11.1: SPECIMEN 70R12/1

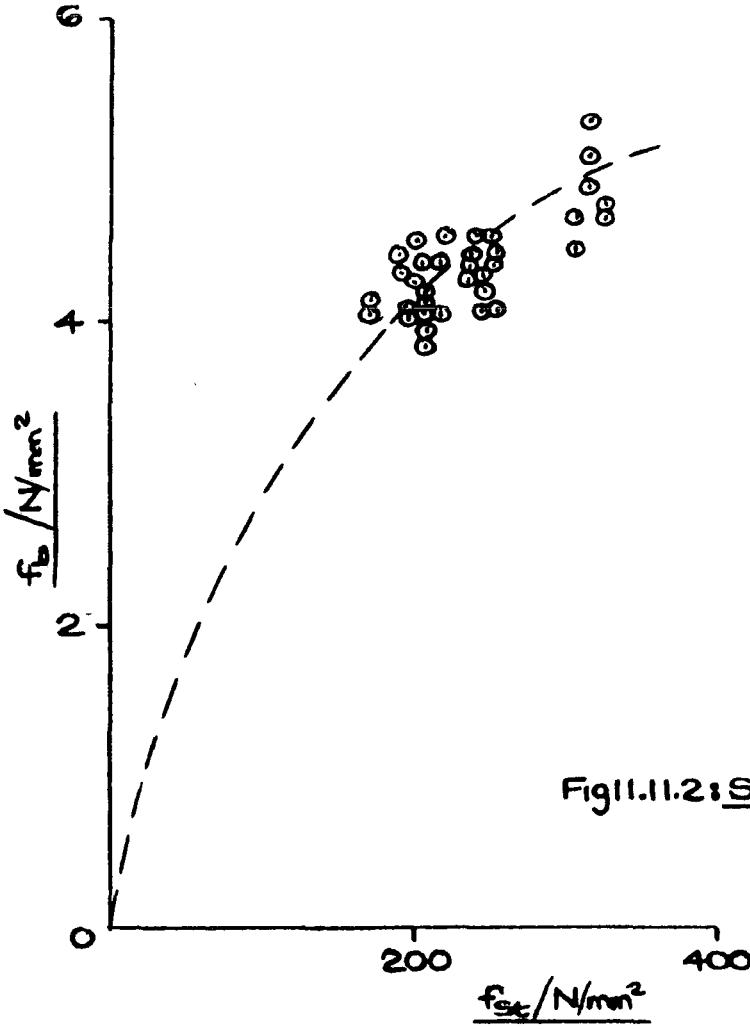

Fig 11.11.2: SPECIMEN 70T12

BOND STRESS (f_b) – ROD STRESS (f_{st}) RELATIONSHIPS

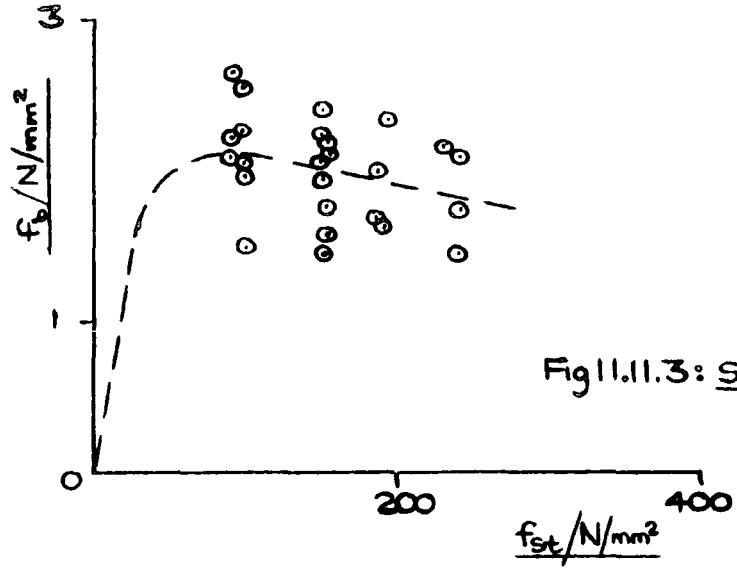

Fig 11.11.3: SPECIMEN 100R20

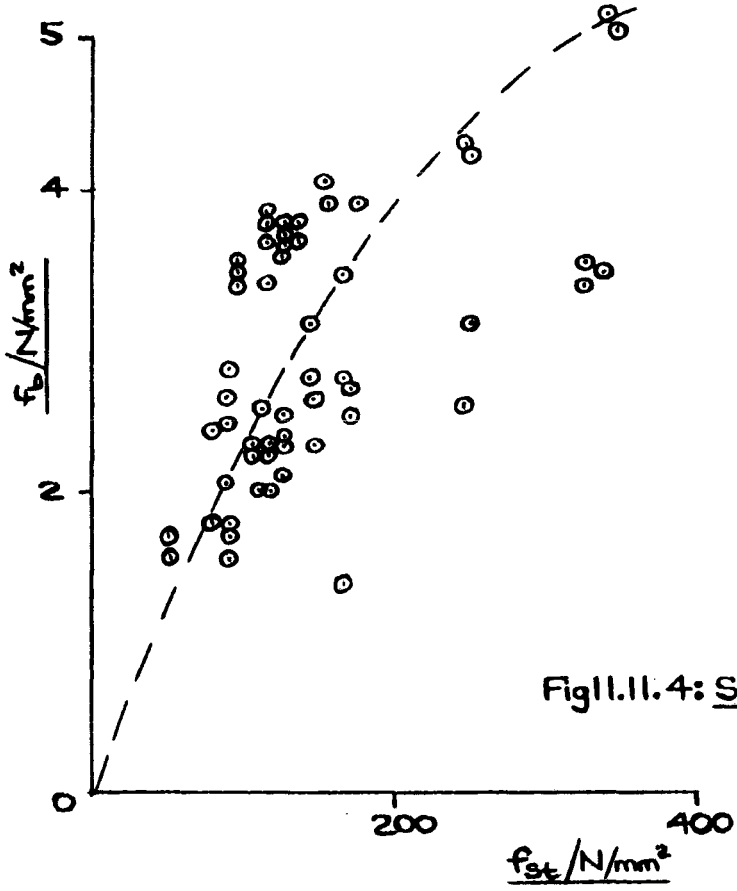

Fig 11.11.4: SPECIMEN 100T20

BOND STRESS(f_b) - ROD STRESS(f_{st}) RELATIONSHIPS

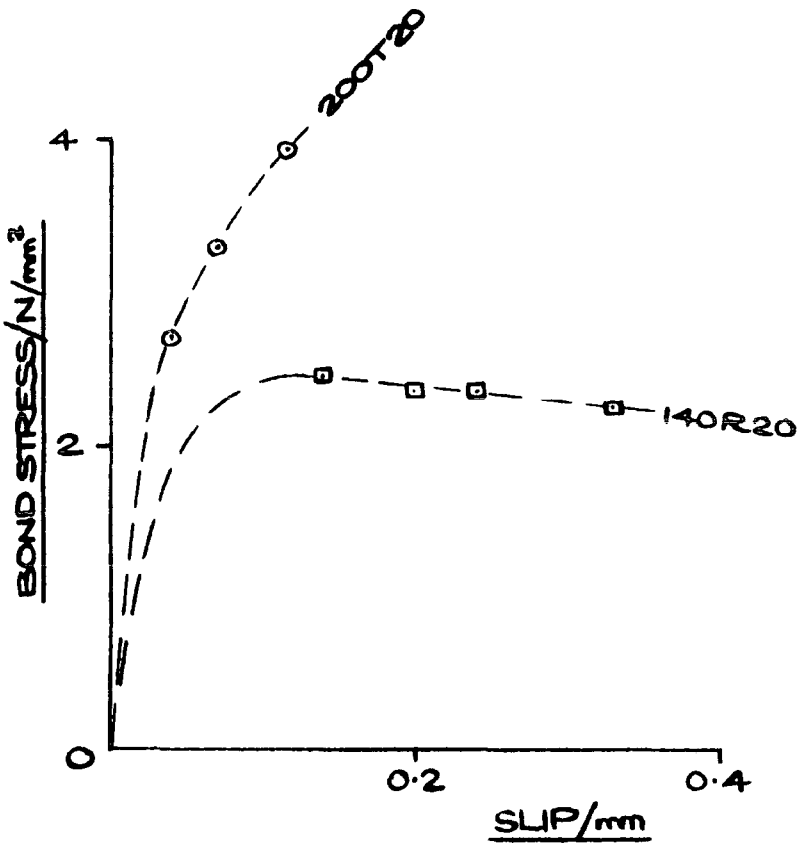

Fig 11.12: TYPICAL BOND STRESS – SLIP RELATIONSHIPS

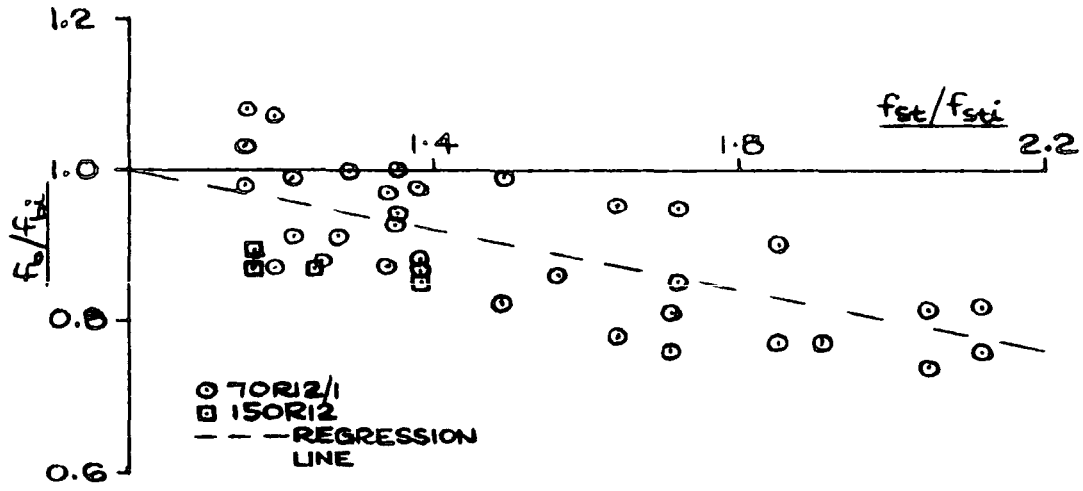

Fig 11.13.1: R12 SPECIMENS

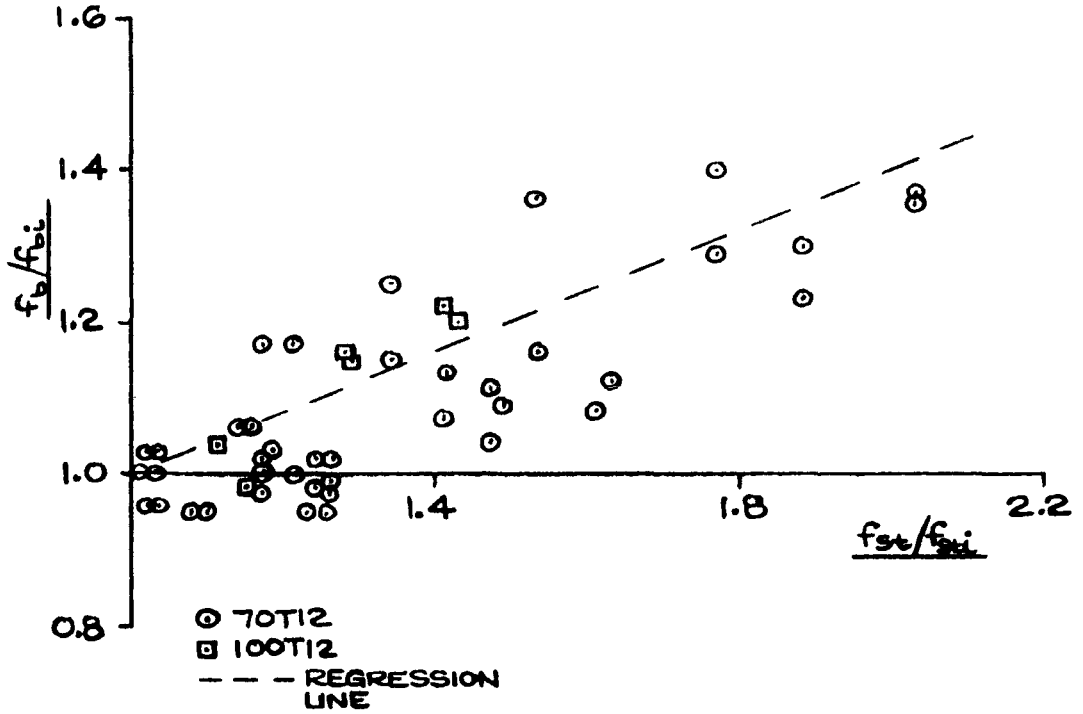

Fig 11.13.2: T12 SPECIMENS

Fig 11.13: RELATIONSHIPS BETWEEN $(f_b/f_{b,i})$ & (f_{st}/f_{sti})

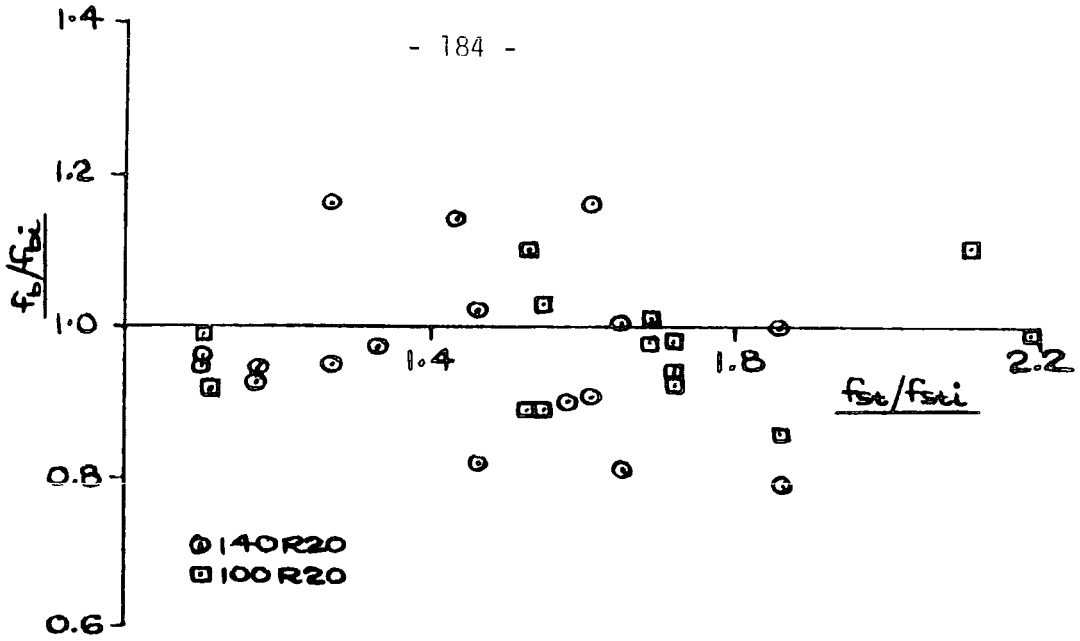

Fig 11.13.3: R20 SPECIMENS

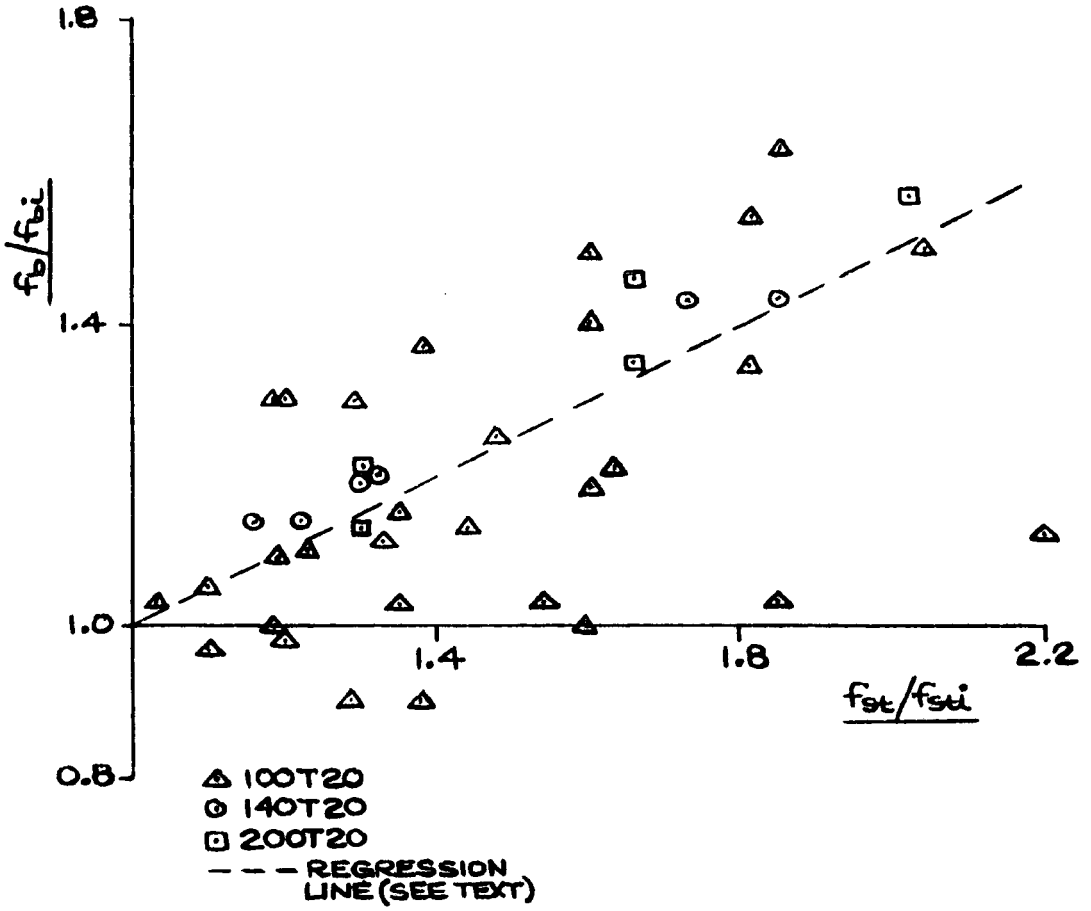

Fig 11.13.4: T20 SPECIMENS

Fig 11.13: RELATIONSHIPS BETWEEN (f_b/f_{bi}) & (f_{st}/f_{sti})

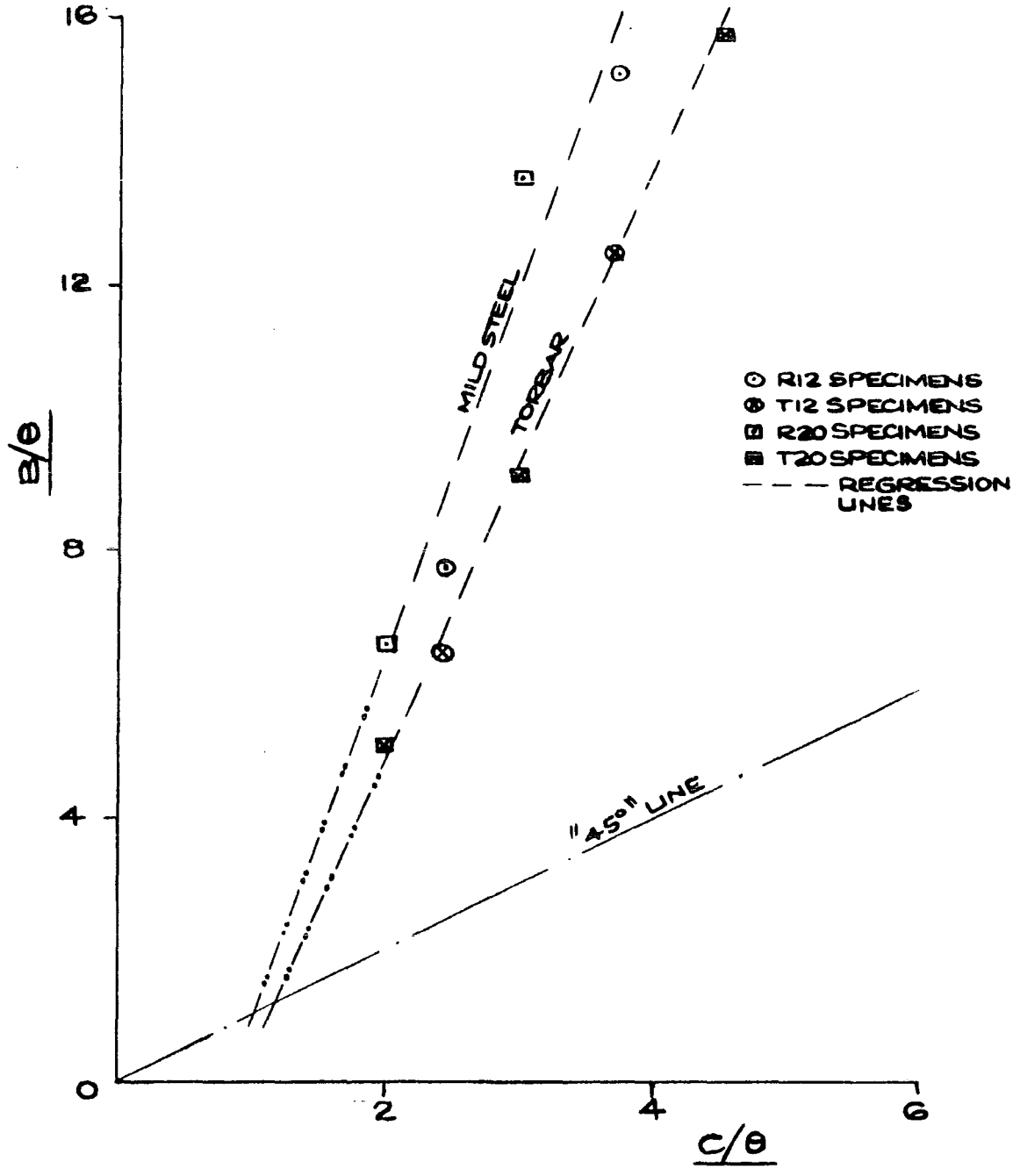

Fig 11.14: RELATIONSHIP BETWEEN B/θ & C/θ

TRANSVERSE STRAIN DISTRIBUTIONS FOR SPECIMEN 200T20

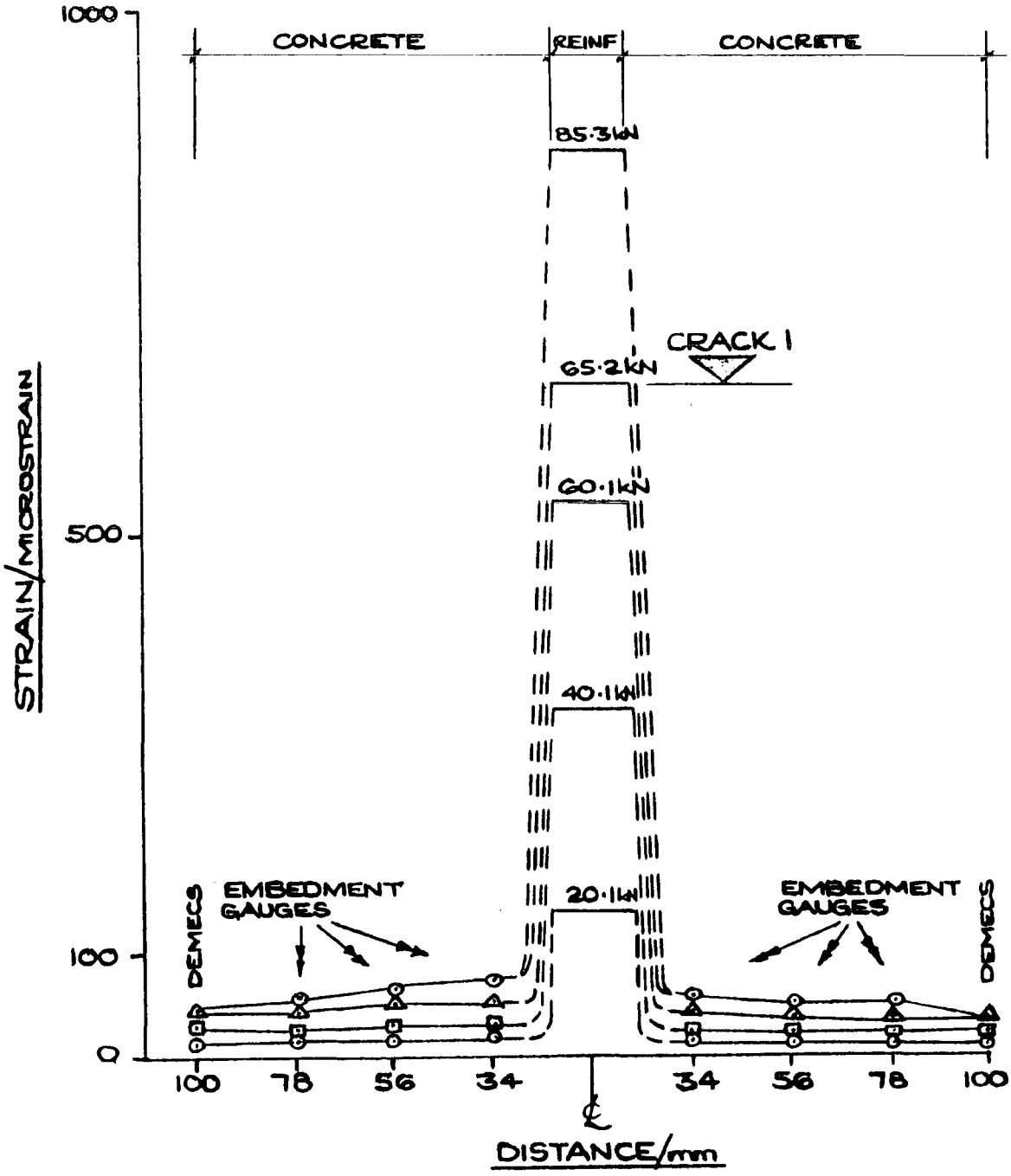

Fig 1.15.1: POSITION 1 – 300mm FROM BOTTOM END

TRANSVERSE STRAIN DISTRIBUTIONS FOR SPECIMEN 200T20

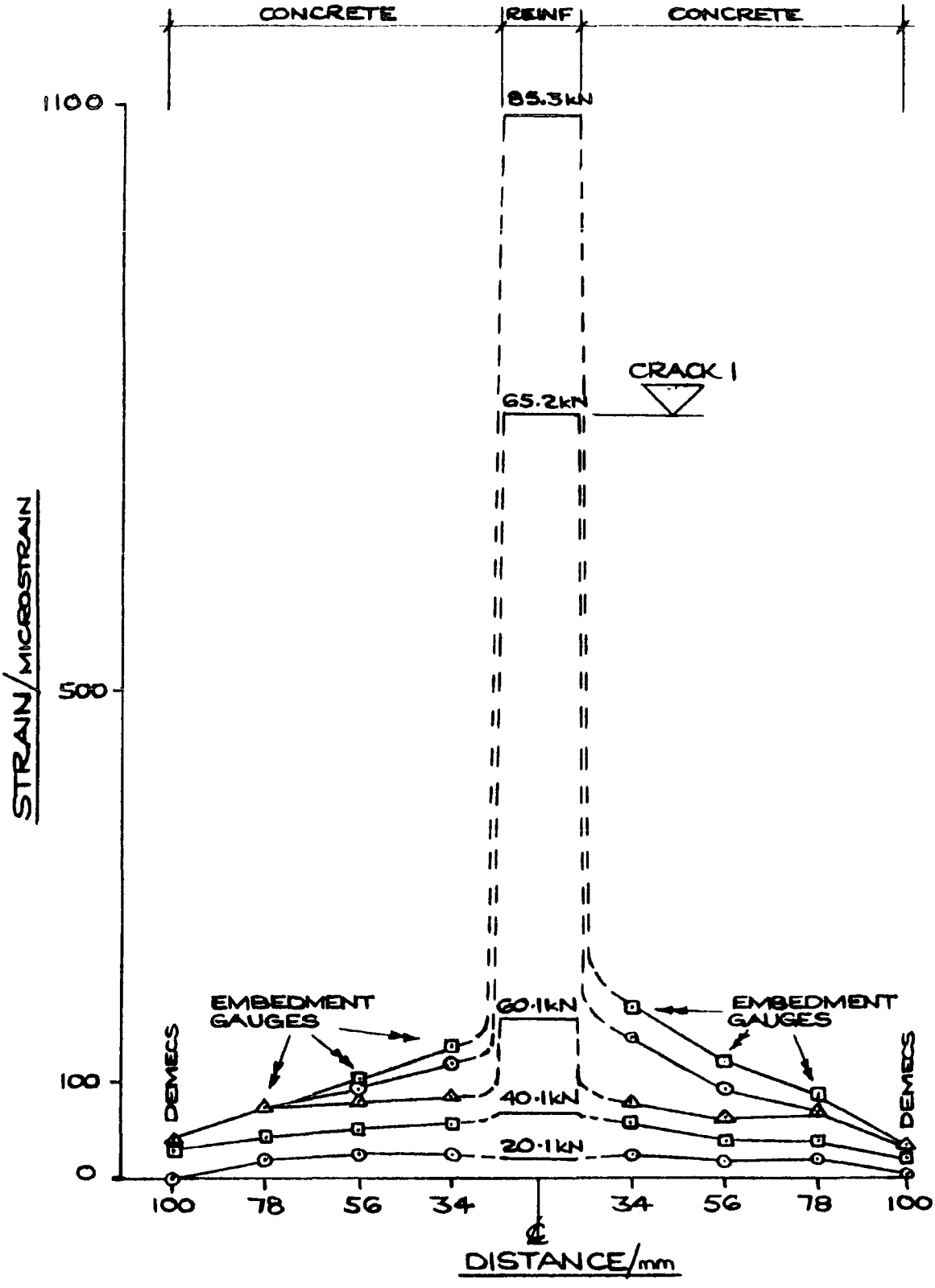

Fig11.15.2: POSITION 2 – 500mm FROM BOTTOM END

TRANSVERSE STRAIN DISTRIBUTIONS FOR SPECIMEN 200T20

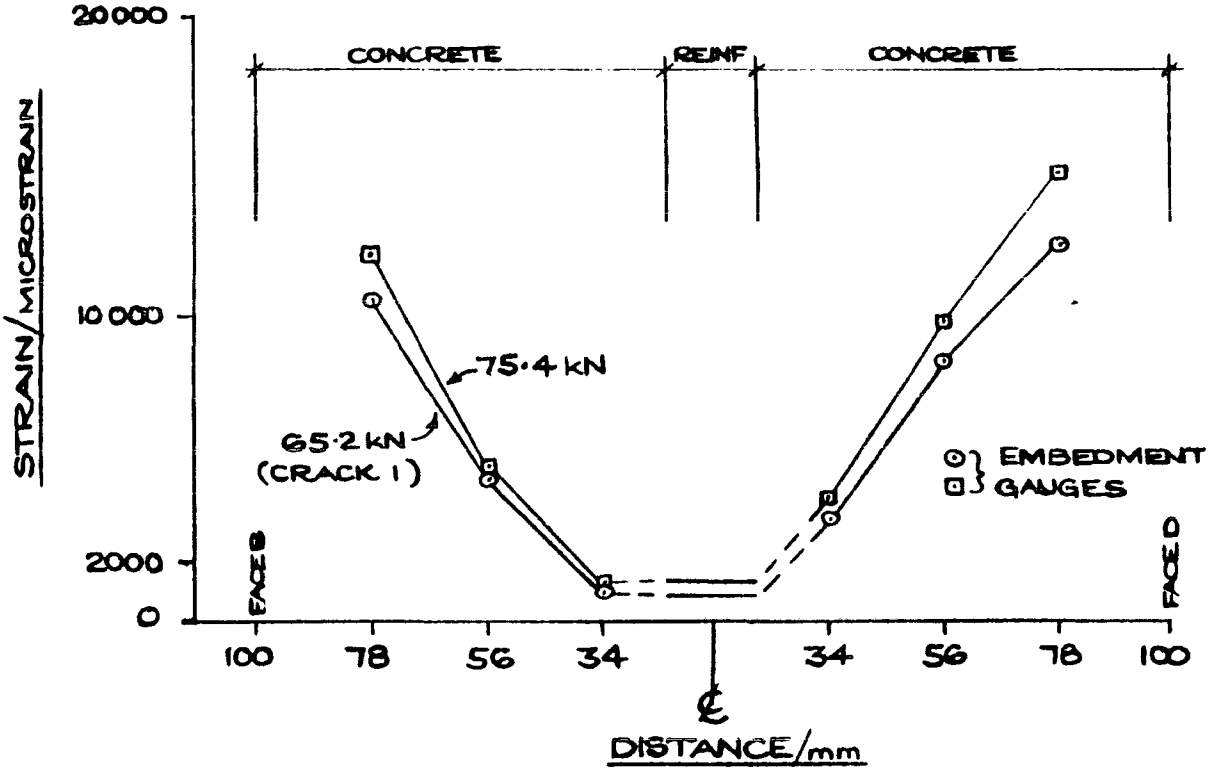

Fig 11.15.3: POSITION 3 – 600mm FROM BOTTOM END

REFERENCES

1. Kong, F.K. & Evans, R.H., "Reinforced and Prestressed Concrete" 2nd Ed. Nelson, 1980, pp. 412.

2. Maney, G.A., "Relation Between Deformations and Deflections in Reinforced Concrete Beams". Proc. ASTM, Vol. 14, Part II, 1914.

3. Swain, G.F., "Structural Engineering, Strength of Materials", McGraw-Hill, New York, 1924.

4. American Concrete Institute "Deflexions of Reinforced Concrete Flexural Members" (Report of ACI Committee 435), Journal ACI, Proc. Vol. 63, No. 6, June 1966, pp. 637-673.

5. Murashev, V.E., "Theory of Appearance and Opening of Cracks, Computation of Rigidity of Reinforced Concrete Members", Stroitelnaya Promishlenost (Moscow) No. 11. 1940.

6. Yu, W.W. & Winter, G., "Instantaneous & Long-Time Deflections of Reinforced Concrete Beams Under Working Loads", Journal ACI, Proc. Vol. 57 No. 1, July 1960, pp. 29-50.

7. American Concrete Institute, "Building Code Requirements for Reinforced Concrete" (ACI Committee 318), Detroit, 1963, pp. 144.

8. Branson, D.E., "Instantaneous and Time-Dependent Deflexions of Simple and Continuous Reinforced Concrete Beams", Report 7, Alabama Highway Research Report, Bureau of Public Roads, August 1963.

9. American Concrete Institute, "Building Code Requirements for Reinforced Concrete (ACI Committee 318), Detroit, 1977, pp. 103.

10. Comité Europeen du Béton-Federation Internationale de la Precontrainte. "Model Code for Concrete Structures", 1978.

11. Comité Européen du Béton. "Recommendations for an International Code of Practice for Reinforced Concrete", ACI/C&CA , 1965, pp.156.

12. Beeby, A.W., "Short-Term Deformations in Reinforced Concrete Members", C & CA Tech Report, 42.408, March 1968.

13. British Standards Institution, "The Structural Use of Concrete, Part 1", CP110 Part 1, London, 1972.

14. Hughes, B.P., "Limit State Theory for Reinforced Concrete Design", 3rd Ed, Pitman 1980, pp. 697.

15. ICE Research Committee "Ultimate Load Design of Concrete Structures", Proc ICE Vol 21, Feb 1962, pp. 399-442.

16. Rao P.S. & Subrahmanyam B.V, "Trisegmental Moment-Curvature Relations for Reinforced Concrete Members", Journal ACI, Proc Vol 70 No. 5, May 1973, pp. 346-351.

17. Tsimbikakis S.V., "Short-Term Deflections of Reinforced Concrete Beams", Concrete Jan 1975, pp. 34-37.

18. "Deflections of Reinforced Concrete Members", Bulletin ST-70, Portland Cement Association, 1947.

19. Myrlea T.D., "Deflection of Reinforced Concrete Members", Progress Report of ACI Committee 307, ACI Journal, Proc Vol 27, 1931, p. 351.

20. Clark L.A. & Speirs D.M., "Tension Stiffening in Reinforced Concrete Beams and Slabs under Short-Term Load", C & CA Tech Report 42.521, July 1978.

21. Scott R.H., Stevens A.T. & Black S., "The Analysis of Reinforced Concrete Beam and Column Sections", To be published in Proc Symposium on Civil and Structural Engineering Computing, London, Dec 1985.

22. Scott R.H., "The Short-Term Moment-Curvature Relationship for Reinforced Concrete Beams", Proc ICE Part 2, Vol 75, Dec 1983, pp. 725-734.

23. Mains R.M., "Measurement of the Distribution of Tensile and Bond Stresses Along Reinforcing bars", Journal ACI, Proc Vol 48 No 3, Nov 1951, pp. 225-257.

24. Nilson A.H., "Bond Stress-Slip Relations in Reinforced Concrete", Cornell University Research Report 345, Dec 1971.

25. Jiang D.H., Andonian A.T. & Shah S.P., "A New Type of Bond Test Specimen", Bond in Concrete (Ed Bartos P), Applied Science Publishers, London 1982, p. 127-139.

26. Beeby A.W., "A Study of Cracking in Reinforced Concrete Members Subjected to Pure Tension", C & CA Tech Report 42.468, June 1972.

27. Brown P.R., "The Feasibility of Internally Strain Gauging a Reinforcing Bar in Concrete for a Pure Tension Test", Final Year Undergraduate Project Report, Department of Engineering, Durham University 1981 (unpublished).

28. Scott R.H. & Gill P.A.T., "Developments in the Measurement of Reinforcement Strain Distributions in Reinforced Concrete Members", Strain, May 1982.

29. Scott R.H. & Gill P.A.T., "A Modern Data Collection System", Strain, May 1984, p. 63-68.

30. Scott R.H., Gill P.A.T. & Munro M., "A Modern Data Collection System and its Interfacing Requirements", Proc Symposium on Civil and Structural Engineering Software and Applications, London, Nov 1983, p. 297-307.

31. Scott, R.H. & Gill, P.A.T., "Long-Term Testing of Reinforced Concrete Tension Members", Proc. RILEM/ACI Symposium on Long-Term Observations of Concrete Structures, Budapest, Sept. 1984, pp. 298-307.

32. Goto, Y., "Cracks Formed in Concrete Around Deformed Tension Bars", Journal ACI Proc. Vol. 70, No. 5, May 1973, pp. 346-351.

33. Comité Euro-International du Beton, "Bond Action and Bond Behaviour of Reinforcement", Bulletin D'information, No. 151, Munich, April 1982.

34. Snowdon, L.C., "Classifying Reinforcing Bars for Bond Strength", BRE Current Paper 36/70, April 1970.

35. Scott, R.H. & Gill, P.A.T., "Measurement of Reinforcement Strains in Concrete", Proc. BSSM Conf. on Structural Integrity, Lancaster, Sept. 1984.

36. Scott, R.H. & Gill, P.A.T., "Reinforcement Strains in Reinforced Concrete Tension Members", Proc. 12th Congress IABSE, Vancouver, Sept. 1984, pp. 919-925.